INFORMATION TO USERS

This manuscript has been reproduced from the microfilm master. UMI films the text directly from the original or copy submitted. Thus, some thesis and dissertation copies are in typewriter face, while others may be from any type of computer printer.

The quality of this reproduction is dependent upon the quality of the copy submitted. Broken or indistinct print, colored or poor quality illustrations and photographs, print bleedthrough, substandard margins, and improper alignment can adversely affect reproduction.

In the unlikely event that the author did not send UMI a complete manuscript and there are missing pages, these will be noted. Also, if unauthorized copyright material had to be removed, a note will indicate the deletion.

Oversize materials (e.g., maps, drawings, charts) are reproduced by sectioning the original, beginning at the upper left-hand corner and continuing from left to right in equal sections with small overlaps.

Photographs included in the original manuscript have been reproduced xerographically in this copy. Higher quality 6" x 9" black and white photographic prints are available for any photographs or illustrations appearing in this copy for an additional charge. Contact UMI directly to order.

Bell & Howell Information and Learning
300 North Zeeb Road, Ann Arbor, MI 48106-1346 USA
800-521-0600

DYNAMIC ANALYSIS OF A MODERN URBAN BUS FOR ASSESSMENT OF RIDE QUALITY AND DYNAMIC WHEEL LOADS

Owais Mustafa Siddiqui

A Thesis

in

The Department

of

Mechanical Engineering

Presented in Partial Fulfillment of the Requirements
For the Degree of Masters of Applied Science at
Concordia University
Montreal, Quebec, Canada

September 2000

ABSTRACT

DYNAMIC ANALYSIS OF A MODERN URBAN BUS FOR ASSESSMENT OF RIDE QUALITY AND DYNAMIC WHEEL LOAD

Owais M Siddiqui

Modern urban buses with low floor and considerable over hung design are known to cause poor ride quality and excessive pavement loads. Such performance is partly due to the present status of urban roads and their rapid deterioration. On the other hand, variations in the dynamic tire forces of such vehicles are known to be a cause for acceleration of road damage and are strongly related to vibration modes of the vehicle associated with vertical and pitch motion of the sprung and unsprung masses. The high levels of tire induced road damage has prompted a growing demand for the design of heavy vehicles that are both passenger- and road-friendly.

In this investigation, a six degrees-of-freedom pitch plane model of a modern urban bus is developed to study the ride and axle load performance under deterministic as well as measured urban road excitations. The validity of the model is demonstrated by comparing the response characteristics with available measured data. The ride quality of the vehicle is assessed in relation to the proposed guidelines upon applying the recommended frequency-weighting filters. An extensive list of performance measures for dynamic wheel loads and their pavement damage potentials are discussed and used for the assessment of road-friendliness performance.

The influence of variations in design and operating variables on the ride performance of the vehicle is investigated through a comprehensive parametric study.

The variations in operating conditions include the speed, road roughness, tire inflation pressure and bus load. The parametric study on design variables includes the variations in suspension dampers and springs, geometry of the suspension and wheel base. The results of the study are discussed to highlight the contributions of these parameters on the ride quality and pavement load, and to identify most desirable design and operating conditions.

ACKNOWLEDGEMENT

The author is sincerely grateful to his supervisors, Dr. A. K. W. Ahmed and Dr. S. Rakheja for their help and guidance throughout the course of this research and during the preparation of this thesis.

The author also wishes to thank members of the faculty and staff of CONCAVE (Concordia Computer-Aided Vehicle Engineering) Research Center, Department of Mechanical Engineering, Concordia University, for their efforts and their time.

Financial support provided by my supervisors and technical support provided by local bus manufacturer and operators are gratefully acknowledged.

Many thanks to my parents and my friends for their encouragement, patience and support.

To my parents I dedicate this thesis.

TABLE OF CONTENTS

CHAPTER 3

VALIDATION OF PITCH-PLANE BUS MODEL AND PERFORMANCE MEASURES

CHAPTER 4

PARAMETRIC STUDY FOR DRIVER/PASSENGER AND ROAD FRIENDLINESS

LIST OF FIGURES

Figure Page

LIST OF TABLES

NOMENCLATURE

Symbol	Description
A_E	Effective area of the air bag
C_i	Damping coefficient
C, M, K	Mass, Damping and Stiffness matrices
DLC	Dynamic load coefficient
F_{kaf}, F_{kar}	Front and rear suspension spring force
F'_{kaf}, F'_{kar}	Front and rear static spring force
F_{caf}, F_{car}	Front and rear suspension damper force
F_{cv}, F_{cf}	Suspension damper hydraulic and friction force
F_{ktf}, F_{ktr}	Front and rear tire stiffness force
F_{ctf}, F_{ctr}	Front and rear tire damping force
F_{Tmax}	Maximum tire force in one simulation time history
F_{Fij}	Lumped friction force due to suspension bushings and joints
F_t	Tire force
H_h, H_l,	High and low pass filter transfer function
H_t, H_s	Acceleration-Velocity transition and step transfer function
IF	Impact factor
I_b, I_f, I_r	Moment of inertia of bus body, front- and rear-axle
J	Error function
N_p, N_δ	Number of pressure and deflection data points
P_o	Static pressure of the air bag
P_{atm}	Atmospheric pressure

U	Front speed of the bus
V_o	Relative velocity across the damper
W_f, W_r, W_s	Front- and rear-axle load and total vehicle load
b	Wheel base of the bus
g	Acceleration due to gravity
l_b, l_a	Horizontal lengths from bus body c.g and front- and rear-axle c.g
h_i	Vertical distance from pavement to point i
m_b, m_f, m_r	Bus body (sprung) and front- and rear-axle (unsprung) mass
p_f, p_r	Asymmetricity ratio for front and rear dampers respectively
x_b, y_b, z_b	x,y and z displacements in bus frame of reference in respective directions
x_f, y_f, z_f	x,y and z coordinate frame of reference of front-axle
x_r, y_r, z_r	x,y and z coordinate frame of reference of rear-axle
x_p, z_p	x and z coordinate of passenger from the bus c.g.
x_D, z_D	x and z coordinate of driver from the bus c.g.
z_b, z_f, z_r, z_t	Bus body, front- and rear-axle and tire vertical displacement
$\dot{z}_b, \dot{z}_f, \dot{z}_r$	Bus body, and front- and rear-axle vertical velocity
$\ddot{z}_b, \ddot{z}_f, \ddot{z}_r$	Bus body, and front- and rear-axle vertical acceleration
$\dot{z}_i$	Bounce velocity at point i
$\ddot{z}_{rms}, \ddot{\theta}_{rms}$	rms bounce and pitch acceleration
$\ddot{z}_{w,rms}, \ddot{\theta}_{w,rms}$	Weighted rms bounce and pitch acceleration
α	Angle of inclination of front damper with respect to horizontal
γ	Gas polytropic index
γ_c, γ_e	Bounce and rebound mode reduction factors for dampers

δ_f, δ_r	Instantaneous vertical deflections across front and rear air bags
δ_t	Instantaneous vertical deflection of the tire
ε	Small change in magnitude
λ_i	Eigenvalues
φ_{95}	Road Stress Factor (RSF)
μ	Coefficient of Coulomb friction
$\theta_b, \theta_f, \theta_r$	Bus body, and front- and rear-axle pitch displacement
$\dot{\theta}_b, \dot{\theta}_f, \dot{\theta}_r$	Bus body, and front- and rear-axle pitch velocity
$\ddot{\theta}_b, \ddot{\theta}_f, \ddot{\theta}_r$	Bus body, and front- and rear-axle pitch acceleration
ω_n	Natural frequency
ω_{di}	Damped natural frequency
ζ_i	Damping ratio
ψ_i	Eigenvector

CHAPTER 1

INTRODUCTION AND REVIEW OF LITERATURE

1.1 Introduction

The present status of urban roads and its rapid deterioration are partly attributed to the excessive cost associated with maintenance of the road infrastructure, and partly due to increased traffic volume and average weight of the vehicles. The axle loads of modern urban buses, such as low floor design, have increased considerably, which may cause rapid urban road deterioration. The urban buses operating on these types of deteriorated roads face complex dynamics related to the interactions of tires and the roads leading to high levels of ride vibration transmitted to the driver/passenger and high magnitudes of dynamic force transmitted to the roads. This in turn yields further deterioration of roads and further increase in ride vibration levels and dynamic tire forces. Coupled vehicle-road interactions, therefore, form a closed loop system as illustrated in Figure 1.1.

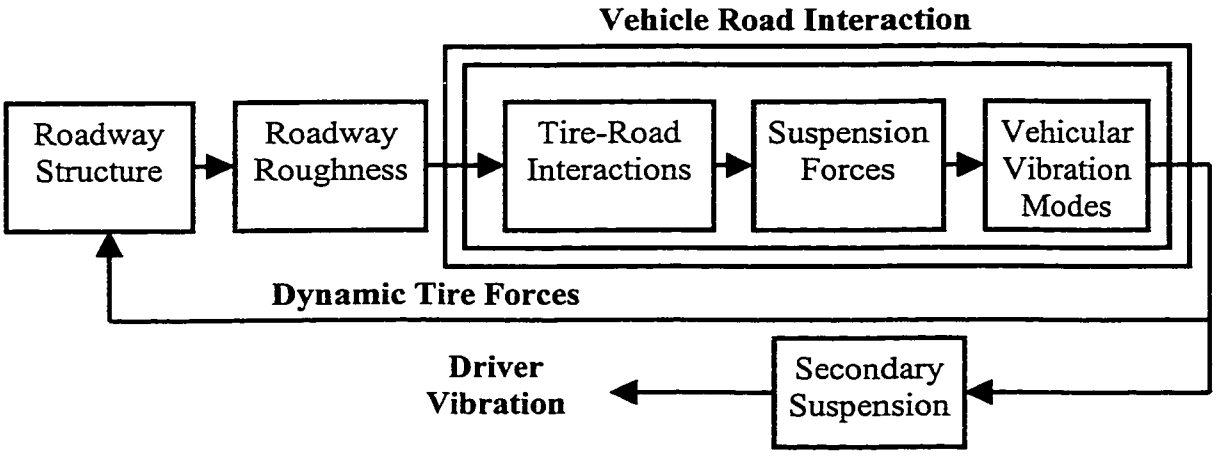

Figure 1.1: Closed-loop representation of the driver-vehicle-road system

The urban roads are more vulnerable to damage by rutting due to high average axle load of the urban buses. The average gross vehicle weight and hence the maximum axle load, of urban buses has continued to increase during the past two decades, in order to enhance passenger transportation economy. Such measures, however, have been related to increased costs associated with road damage, and health and safety risks among the drivers due to increased levels of whole body vibration. The drivers of urban buses are exposed to high levels of ride vibration for a prolonged occupational duration on a daily basis. Prolonged occupational exposure to high magnitude of whole-body ride vibration is known to affect the health, safety and productivity of the drivers in an adverse manner. The ride vibration environment of such vehicles comprises of low frequency and high magnitudes of ride vibration attributed to low natural frequency suspension and relatively rough roads, and shock motions arising from vehicle interactions with discontinuities in the road surface, such as pot-holes. Prolonged exposure to such low frequency and large amplitude ride vibrations has been related to driver bodily discomfort, physiological damage and inefficient performance. Poor performance rate of the vehicle operator has been attributed to various effects of vehicle vibration, namely: operator's slow reaction time, errors in compensatory tracking, loss of foot pressure constancy and visual acuity. The analysis and enhancement of ride vibration environment of urban buses thus forms another important design task owing to the driver's health and safety concerns related to occupational exposure to severe vibration environment. Suspension seats are widely used in the urban buses to further attenuate the vertical vibration transmitted to the driver. The low natural frequency suspension seats,

however, induce considerable shock motions due to frequent suspension bottoming under rough road excitations.

Both the ride vibration environment and dynamic tire loads of a road vehicle relate to its vibration behavior. The ride vibration and tire load performance characteristics are thus affected by many design and operating variables. While majority of the design factors is determined by the weights and dimensional regulations, the suspension and tires are designed to achieve adequate load carrying capacity, and low natural frequency within the constraints posed by available rattle space. The operating variables, such as road roughness, speed, braking and turning, operating load and tire pressure, tend to vary over a wide range in case of urban buses. The design of road and driver-friendly buses thus poses many challenges for the designer.

In view of the regulations on weights and dimensions of heavy vehicles and transportation economy, the variations in such design parameters are most likely considered to be infeasible. The driver-and road-friendliness performance of the urban bus can thus be enhanced through appropriate selection of static and dynamic properties of the suspension components and tires. Although soft suspensions are desirable, the limited rattle space and ride height also limit further reductions in suspension spring rates and thus the natural frequencies. Soft suspensions further cause reduced handling performance of the vehicles. Since the vehicular vibration response is strongly influenced by suspension damping, both the performance measures could be considerably enhanced through design of optimal dampers. Near optimal suspension parameters could be effectively realized through systematic analysis of vehicle-road interactions.

In this dissertation research, an analytical model of a modern urban bus is developed upon systematic characterization of its various components. The static and dynamic properties of suspension components and tires are evaluated through a series of laboratory experiments and the measured data are used to derive nonlinear component models on the basis of physical laws or regression analysis. A number of urban roads are characterized in terms of their surface roughness properties. The analytical model is thoroughly validated using the field measured and reported data. A comprehensive parametric sensitivity analysis is then performed to identify near optimal suspension parameters over a wide range of operating conditions.

1.2 Literature Review

The ride vibration and dynamic tire load analysis of an urban bus encompass a very wide range of subjects involving ride dynamic analysis and methods of assessment, dynamic wheel loads, pavement damage potentials of tire forces, suspension system modeling and analysis, tire characteristics, etc. A review of literature on each of these topics is carried out and presented in the following subsections in order to develop the scope of the present investigation.

1.2.1 Vehicle-Road Interactions

Pavement damage refers to degradation of the structural integrity or surface profile of a road. Since roads are designed for a finite service life and are expected to deteriorate in time, it may alternatively be defined as wear.

Rauhut et al. [1] and Pell [2] have described the primary modes of pavement failure, as listed below:

- Fatigue cracking of all types of pavements
- Rutting and reduced skid-resistance for flexible and composite pavements
- Low temperature cracking of flexible and reinforced rigid pavements
- Reflection cracking of flexible and reinforced rigid pavements
- Spalling of rigid pavements
- Faulting of jointed rigid pavements
- Punchouts and steel rupture of continuous reinforced rigid pavements

Although a precise physical mechanism related to surface cracking and permanent deformation damage has not yet been reported, the studies have shown that each failure mode is affected by many factors, such as the roadway design, construction methods, material properties of each constituent layer, traffic loading and environmental conditions. While the fatigue damage of pavements has been related to the static loads of the individual axles, the rut damage has been related to the gross weight of the vehicles Gillespie et al., [3].

From structural point of view, modern road surfaces (or pavement) may be classified as flexible, composite and rigid. A flexible pavement consists of one or more layers of asphalt supported by a granular sub grade. Composite pavement consists of a flexible surface layer supported by a stiff Portland cement concrete (PCC) base; and rigid road surface consists of a layer of PCC on a granular foundation. Rigid pavements can be further classified according to their arrangement of steel reinforcement and joints.

Apart from the environmental factors, such as temperature variations, soil properties and drainage, the pavement failure has been directly related to static and dynamic tire loads transmitted to the pavement. The magnitudes of dynamic tire loads transmitted to the roads are related to vibration modes of vehicle, which are affected by many vehicle design and operating factors. The most significant design factors include gross vehicle weight, vehicle configuration, axle loads, vehicle geometry, suspension and tire properties. The most important operating factors affecting the magnitude of dynamic tire loads include the vehicle speed, vehicle load, tire inflation pressure, road roughness etc [4,5].

Few studies have established certain analogy between the ride dynamics and tire load performance characteristics, due to their strong relationship with the vibration behavior of the vehicle [5]. Both the driver friendliness and road-friendliness measures for heavy road vehicles are thus interrelated, and depend upon common design and operating factors.

Owing to the wide range of variations in various operating factors for urban buses, it is extremely vital to investigate their influence on the performance characteristics of the vehicle design and operating factors can be effectively investigated through development and analysis of vehicle models.

The enhancement of one of these measures through selection of appropriate design variables is thus expected to yield considerable gains for the other performance measures. A study on relative contributions of each of the operating factors may provide considerable insight into design of road vehicles with improved driver and road-friendliness performance.

Urban buses impose high magnitudes of dynamic wheel loads on the city roads leading to their premature failure. The quality of roads in most urban areas has been deteriorating partly due to high cost associated with maintenance of the road infrastructure, and partly due to increased traffic volume and the average weight of urban buses. The front and rear axle loads of a fully loaded Classic bus are in the order of 60.25 kN (13,548 lbs) and 109.5 kN (24,610 lbs), respectively. The modern Low Floor buses are designed with front and rear axle loads in the order of 60.75 kN (13,600 lbs) and 115.88 kN (26,050 lbs), respectively. High axle loads coupled with tire interactions with relatively rough urban roads yield considerable magnitudes of dynamic loads transmitted to both the chassis and the road. Such dynamic interactions further yield higher levels of ride vibration transmitted to the driver and the passengers. Coupled vehicle-road interactions form a closed-loop system, where the high levels of dynamic tire loads cause further deterioration of the road structure, which causes additional increase in the ride vibration levels, and dynamic forces transmitted to the pavement and the chassis.

Although the fuel and road infrastructure maintenance costs rank among the highest [6], the dynamic tire-road interactions yield additional costs related to (i) discomfort and inefficient performance of the driver attributed to high magnitude ride vibration of the urban bus; (ii) high suspension loads transmitted to the chassis leading to reduced service life; and (iii) reduced pavement service life due to high magnitude dynamic tire forces. While a large number of studies have been reported on dynamic vehicle loads transmitted to pavements [7,8], only a few studies have attempted to relate the costs with pavement load due to associated complexities. Gibby et al. [7] assessed the costs attributed to road damage caused by urban buses and proposed the use of an

additional axle. Fekpe [9] proposed a methodology to estimate cost allocation implications of dynamic wheel loading for heavy vehicles. The study concluded that pavement costs of heavy vehicles equipped with road friendly air suspension are approximately 5% less than those equipped with steel suspension.

The vehicle-road interactions further yield high magnitudes of low frequency ride vibration, which mostly occur in the vicinity of resonant frequencies of the sprung and unsprung masses [10]. The drivers of urban buses are constantly exposed to such vibration on a daily basis, which is known to cause discomfort and fatigue among the drivers [11]. Prolonged occupational exposure to such vibration is known to impose certain potential health and safety risks among the drivers [12].

Numerous studies performed on commercial freight vehicles have established that vehicle weights and dimensions, axle loads, vehicle configuration, vehicle speed, road roughness, and suspension and tire properties, directly affect the dynamic wheel loads transmitted to the pavement [13,14,15]. A number of studies have emphasized the need to design optimal suspension to reduce the road damage [13], which can also enhance the chassis life by reducing the magnitudes of suspension forces transmitted to chassis. Modern urban buses mostly designed with air suspension, exhibit considerable dynamic vertical deflections predominant in the 1.0 -1.5 Hz frequency range [10], which may further contribute to fatigue of the road structure due to spatial repeatability of the dynamic tire forces. Such suspension designs may also yield high levels of low frequency vertical vibration at the driver's location resulting in possible bottoming of the seat-suspension.

Considering that the gross weight and axle loads of urban buses are selected in view of the provincial road laws and the transportation economy, the magnitudes of resonant forces transmitted to the pavement and the chassis are mostly affected by the tire and suspension properties. Soft suspension springs and tires are considered desirable for enhancement of road friendliness of heavy vehicles. While tires offer very light damping, their stiffness characteristics are determined by the inflation pressure. Urban buses and commercial heavy vehicles employ tires inflated at relatively high pressure, in the vicinity of 110 psi (758 kPa) in order to achieve improved fuel economy. The resulting high stiffness of such tires yields relatively high dynamic wheel loads. The suspension springs are designed to realize low sprung mass bounce mode natural frequency in order to adequately isolate the chassis from the road induced vibrations. Low suspension spring rate, although desirable for reducing the chassis and pavement load, poses increased demand for rattle space and affects the roll stability in an adverse manner. The enhancement of road and driver-friendliness of urban buses through reductions in tires and suspension spring rates alone thus appears to be infeasible.

Alternatively, dissipative properties of the vehicle suspension are also known to affect the driver and road-friendliness of heavy vehicles. High magnitude resonant response of the vehicle can be effectively reduced through appropriate selection of damping characteristics of the primary suspension. Suspension dampers are designed to provide multi-phase damping characteristics to achieve a design compromise in the response magnitudes near resonant frequencies and vibration attenuation at higher frequencies. While the studies performed by Sweatman [15] and others have identified the benefits of low frequency air suspension in reducing the pavement loads, only limited

efforts have been mounted to propose optimal suspension damping [16,17,18]. Studies on ride dynamics of such vehicles, on the other hand, have emphasized the design of optimal suspension with multi-stage and asymmetric damping to enhance the ride vibration environment or driver-friendliness of vehicles [4,16,17]. Although effectiveness of secondary suspension (suspension at the seat) has been clearly demonstrated in reducing the levels of vertical vibration, the need to enhance primary suspension design has been emphasized to minimize the frequency of seat-suspension bottoming, and transmission of longitudinal, lateral, roll and pitch vibration [19].

1.2.2 Analytical Models

The studies on ride dynamics and pavement interactions of heavy road vehicles involve development of a representative dynamic model that closely describes the vehicle behavior. Many vehicle models ranging from linear quarter vehicle models with two degree-of-freedom (DOF) to complex three-dimensional models with many DOF have been reported in literature. While majority of the models, consider the sprung and unsprung masses as rigid bodies, few models have incorporated the flexibility of the trailer structure to study contributions due to frame bending modes [20,21]

Simple one-and two-DOF models have been widely used by several investigators to study the performance potentials of different concepts in suspension systems under uncoupled vertical motions in a highly convenient manner. These models, however, cannot be utilized to analyze the ride dynamics and pavements interactions of heavy vehicles, which comprise various vibration modes associated with vertical, roll and pitch motions of the sprung and unsprung masses. Since the weights and dimensions of heavy

vehicles are mostly governed by the local regulations, the suspension and tire properties form the most important set of design variables for potential enhancement of the road and driver-friendliness performance.

The development of an analytical vehicle model thus necessitates establishment of the characteristics of static and dynamic properties of the suspensions and tires. Vehicle suspensions invariably exhibit strong nonlinearities associated with progressively hardening force-deflection characteristics of suspension springs, variable force-velocity properties of the dampers, and kinematic motions of the suspension linkages. A number of techniques have been proposed to analyze the response characteristics of nonlinear dynamic systems [22,23].

The vehicular vibration and the resulting dynamic wheel loads are influenced by various design and operating parameters in a highly complex manner. Among the various design and operating parameters, vehicle suspension properties, road roughness and speed are known to affect the road and driver friendliness of the vehicle in a very significant manner, where the driver friendliness relates to the ride vibration environment of the vehicle. The handling and directional control, ride quality and suspension rattle space performance of the vehicle, however, pose conflicting design requirements for the suspension. While lightly damped soft suspension springs are highly desirable to enhance the ride quality, the realization of adequate directional control and rattle space performance necessitates relatively hard suspension springs with adequate damping. The suspension springs are thus selected to achieve a compromise among these conflicting requirements, with relatively larger weighting placed on the rattle space and directional control performance.

The ride performance of the bus is mainly derived from the acceleration response of the driver/passenger seats [14,24]. It is reported that the fore-aft motion caused by the pitch motion of the bus body causes most discomfort to the driver/passengers. Although the roll motion is also known to cause discomfort, the magnitude of such vibration is significantly small for the urban buses, when compared with those encountered along the pitch and fore-aft axes. In order to predict the pavement load and ride performance accurately, an analytical model must incorporate the nonlinear properties of the springs in heavy vehicle suspensions, the kinematics of load sharing axles, and the sequential input of a single road profile into the various axles.

Various studies on the ride dynamics and vehicle-pavement interactions of heavy freight vehicles concluded that contributions of the roll motions are relatively insignificant [25]. The vehicle ride quality and the dynamic wheel loads are strongly related to the pitch and vertical modes of the sprung masses and vertical deflection modes of the unsprung masses. An analogy between the vehicle ride vibrations and the wheel loads has been further derived through analysis of nonlinear quarter-vehicle model [18,26]. Results of the reported studies have demonstrated that three and six DOF in-plane vehicle models can be effectively used to determine the ride performance potentials of different suspension concepts. Such simplified models, however, may not be well suited to investigate the effects of variations in the operating conditions, such as tire inflation pressure, wheel-hop phenomenon and vibration response at different locations within the bus.

Many analytical and experimental studies on ride dynamics of road vehicle have been reported in literature. The primary objectives of these studies, in general, include:

assessment of vehicle ride quality, performance evaluation of different vehicle suspensions, assessment of cargo vibrations, and evaluation of dynamic tire loads transmitted to the pavement. A number of comprehensive two-and three-dimensional vehicle models have been developed to study the ride quality and tire force characteristics of heavy freight vehicle [27,28]. There are very few studies available, which address the performance characteristics of urban buses. Boileau et al. [14] has investigated the ride vibration environment of urban bus to study the whole-body vibration exposure of the drivers through road measurements. Sujatha et. al. [24] using finite element models investigated the whole-body vibration exposure of drivers in the Indian buses. The studies on ride dynamics have invariably emphasized the significant role of the vehicle suspension, specifically the damping.

The role of vehicle suspension and tires in enhancement of road-friendliness of heavy vehicles has also been emphasized in a large number of studies. The majority of these studies, however, focuses on the restoring properties of the suspension and axle configurations [5,27], while the effects of dissipative properties of the suspension and tires have been dealt only in a limited number of studies [10,13]. These studies have invariably concluded that performance of vehicles with air suspension is considerably superior to those with steel spring suspension.

The analysis of road-and driver-friendliness of urban buses further necessitates appropriate characterization of the roughness profiles of the urban roads. The road profiles of various highways, secondary roads and dirt roads have been measured in many studies [11,29]. The roughness characteristics of urban roads, however, have not been reported in the literature. The reported studies on the highway and secondary roads have

established that roughness characteristics of these roads can be described by a stationary Gaussian random function with zero mean. The roughness profiles of certain roads in the Montreal area were recently acquired by IRSST [30]. The analysis of these roads revealed that the roughness characteristics of urban roads lie between those of a rough runway and a secondary road [18].

1.2.3 Ride dynamic analysis and methods of assessment

A recent study on assessment of vibration exposure of drivers of urban buses has established that suspension seats are vital to attenuate severe levels of low frequency vertical vibration transmitted to the driver [30]. The existence of high levels of vertical vibration in the vicinity of sprung mass resonant frequency (1 - 1.5 Hz range) coupled with low natural frequency of the suspension seat, however, may result in frequent bottoming of the suspension and thus high levels of vibration transmitted to the driver. In view of the prolonged occupational exposure and high levels of ride vibration, the need for enhancement of ride quality of such vehicles has been recognized. From the numerous studies performed on ride dynamics of freight vehicles under random road inputs, it has been concluded that the vertical and fore-aft (longitudinal) motions are significant factors in assessing the driver comfort [31,32]. The study of the driver's exposure to whole-body vehicular vibration demands development of an acceptable visco-elastic model of the human body, which is known to exhibit highly complex biodynamic behavior under vibration above 2 Hz [9]. Although heavy vehicle vibration predominates in the 1-20 Hz range, the human body is invariably represented by a rigid mass in view of the associated complex dynamics. The large amplitudes of low frequency bounce and pitch motions of

the bus body are known to cause passenger discomfort in a relatively short term. Prolonged exposure to such low frequency and large amplitude ride vibration has been associated with the operator bodily discomfort, physiological damage and inefficient performance. Poor performance rate of the vehicle operator has been attributed to various effects of vehicle vibration, namely: operator's slow reaction time, errors in compensatory tracking, loss of foot pressure constancy and reduced visual field [33,34].

The ride vibration environment of a vehicle could be expressed in terms of displacement, velocity, acceleration or jerk of the sprung mass. Many studies have shown a reasonably good correlation between the vertical acceleration and the subjective discomfort [13,35]. The acceleration response of the sprung mass has thus been widely used as a measure of the vehicle ride quality. The international standard (ISO 2631), British Standard and many other standards recommend the use of rms acceleration of the response in conjunction with the weighting filters that describe the human response to vibration [19,32,41]. Pradko and Lee [35] proposed an alternate measure based upon the energy absorbed by the occupant, which has been widely used to assess the ride quality of vehicles in the defense sector.

The ride response characteristics of heavy vehicles have been extensively investigated in view of driver/passenger comfort and safety, and potential cargo damage. While the potential cargo damage may relate to extreme impacts (impulsive motion) and high frequency vibration, the occupant comfort and safety has been related to the low frequency vibration. The occupant exposure to vibration is invariably derived from the acceleration levels measured at the occupant seat interface, while the vibration transmitted to various body segments is ignored. This is mostly attributed to the lack of

adequate measurement systems, and many physiological variabilities among the human occupants [31,35]. It has been reported that the seat and back cushion alter the nature of vibration transmitted to the seated body.

In view of lack of appropriate measurement systems to assess the vibration exposure of the body, the ride quality assessment is primarily based upon the accelerations measured at or near the driver-seat interface. The assessment of vehicle ride quality is frequently performed through field measurements conducted on specific routes. Such studies can effectively provide the relative ride rankings of different vehicles or components, while the road surface, vehicle speed, and inter- and intra-subject variations often make the analysis more complex. Alternatively a number of analytical models have been developed to assess the ride vibration response and to study the influence of various design and operating factors.

Development of an analytical vehicle model to determine its ride dynamics primarily involves characterization of the sprung and unsprung masses, suspension and tires, and road roughness. Vehicle suspension systems often exhibit nonlinearities associated with the kinematics of linkages, and progressively hardening force-deflection and variable force-velocity properties of the stiffness and damping elements, respectively [26].

A number of ride dynamics models of vehicles ranging from two-DOF quarter vehicle models to comprehensive many-DOF three-dimensional models have been reported in the literature [23]. The ride dynamics analysis of urban buses involves certain unique considerations associated with roughness characterization of urban roads, which may comprise of discontinuities due to drain covers, potholes, etc. The urban buses

operate at relatively low speeds and undergo frequent braking and turning maneuvers. Furthermore, the number of passengers and thus the operating load of urban buses may vary considerably depending upon the time of operation.

The tire-terrain interactions have been characterized by different types of linear and nonlinear tire models. The tire models, reported in the literature, can be grouped in four categories based upon the characterization of the tire-road contact, point-contact, rigid tread band, fixed foot print, and adaptive foot print models [5,7]. These models are conceived, to different degrees of complexity, to account for the tire deflection properties, geometric filtering of the rolling wheel and contact pattern with the road. In view of the complexities associated with adaptive foot print models and the lack of knowledge of tire properties, the wheel-terrain interactions in most heavy vehicle models are represented by a point contact. While some of the linear analytical models consider the force-deflection properties of the tire as bilinear and unbounded, others incorporate nonlinear tire properties influenced by the wheel-hop motion [15].

Design of suspension for a heavy vehicle involves careful selection of the suspension parameters, namely the stiffness and damping properties, to achieve a compromise between the ride, handling and control performance characteristics. A rather extensive body of literature has been published on the ride quality and cargo safety aspects of tractor-semitrailers. The performance measures related to ride quality, suspension rattle space, handling, roll stability, and directional control characteristics poses conflicting requirements on passive suspension design. Enhancement of ride quality and cargo safety necessitates soft and lightly damped suspensions. The soft vehicle suspensions, however, result in poor roll stability and directional control

performance. The suspension rattle space requirements also increases with soft suspensions. A passive vehicle suspension with constant parameters thus exhibits inherent limitations to meet the entire conflicting requirement. The overall performance measures of a heavy vehicle suspension, however, must be formulated to address a design compromise among all aspects of desirable performance characteristics. Three primary concerns that evolve from suspension design formulate the objectives for the performance analysis: (i) the level of vibration perceived by the driver/passenger, which can be related to the acceleration response at the sprung mass [6,11,36]; (ii) suspension deflections, which are indication of the working or rattle space requirements [26]; and (iii) tire deflections, which are an indication of the severity of forces transmitted to the roads [6,9].

Two DOF, quarter-vehicle models have been extensively used to gain a fundamental understanding of the effect of suspension parameters on the vehicle performance characteristics subjected to deterministic or random road disturbances. A study performed by Chalasani [37] presented comprehensive attempt to evaluate the effects of suspension stiffness and damping on the root mean square (RMS) values and frequency response characteristics of the vehicle. The study further presented the relative response characteristics of passive and ideal active suspensions using a seven DOF, three-dimensional car model, subjected to periodic and transient excitations arising from a chuck-hole-type road disturbance. [37,38].

Vehicle ride vibration and tire forces are strongly related to various vibration modes of the vehicle. Vehicle vibrations and thus the dynamic tire loads are dependent on the restoring and dissipative properties of the suspension and tires. Extensive studies

reported on ride dynamics of road vehicles, however, have concluded that suspension damping affects the vehicle vibration behavior in a significant manner [18,37]. The significance of suspension damping in reducing dynamic wheel loads has also been investigated through the response analysis of a nonlinear quarter-car model to identify the suspension damping properties most suited for reduction of tire forces [9,31,26]. Vibration absorbers mounted on vehicle axles have also been suggested for reducing the dynamic pavement loads in the vicinity of wheel hop frequencies. The study concluded that adequately tuned vibration absorbers could yield 15 to 20% reductions in the dynamic load coefficient (DLC) [39].

Majority of vehicle models, irrespective of their application, considers linear characteristics of the suspension damping. The hydraulic dampers employed in vehicles are known to exhibit multi-stage-damping characteristics, which is asymmetric in compression and rebound. The damping forces in rebound tend to be considerably larger than those in compression. The dampers yield high coefficients at low speeds and lower coefficient at higher speeds. The role of such damping characteristics in the vehicle ride response has been evaluated through analysis of simplified models using either piecewise linear formulations or local equivalent linearization technique [23,37]. Since the vehicle ride and tire-load performance is strongly related to suspension damping, it is vital to incorporate adequate damping characteristics in the vehicle model.

The ride dynamics of heavy vehicles has been extensively addressed in numerous analytical and experimental studies. The analytical investigations using two and three dimensional vehicle models of diverse degrees of complexity have mostly employed numerical integration techniques to solve the differential equations of motion. The thrust

of the work was basically in the validation of experimental measurements [5,35]. Design optimization in conjunction with time-domain analysis of vehicle models subjected to random road excitations pose considerable computational challenge, especially when the performance index comprises several components. Alternatively, the frequency domain analysis of linear equivalent vehicle models simplifies the design optimization tasks. The design optimization, however, necessitates well-defined performance objective and the formulation of a performance index. A number of studies have employed different optimization functions for the design of vehicle suspension systems [27,35]. The primary objective of such studies was to achieve an improved compromise between vibration isolation and suspension deflection, which have been identified as competing and contrary goals. Ride quality has by far been the major concern of heavy vehicle suspension design and optimization. In view of the excessive road damage caused by heavy vehicle tire forces transmitted to the pavement, it is desirable to integrate a measure of the tire forces within the performance index. There have been relatively few attempts to systematically address the tractor-semitrailer suspension optimization, while no attempt has been made for the bus suspension optimization. ElMadany [27] identified this problem and presented an optimization method to minimize the acceleration and jerk transmitted to the driver position in an attempt to enhance the vehicle ride quality.

The performance measures related to ride quality has been the subject of considerable analytical and experimental evaluations. Ride quality can be assessed in terms of preservation of health, comfort and performance. Proposed vibration tolerance criteria have related ride quality to driver's workstation design, placement of controls, visual displays, cab temperature, driver seat, and cabin noise and vibration environment

[24]. Although the ride quality related to workstation design is frequently assessed using subjective rankings. Subjective response data has been insufficient and inconsistent to derive a generally acceptable comfort criterion with respect to vibration levels. Many objective methods have been developed to assess the ride quality related to noise and vibration environment. Objective methods proposed to assess the ride vibration are based upon directly measurable physical quantities, such as velocity, acceleration and jerk. A good correlation between the mean square jerk or acceleration and the subjective human response has been reported [39]. From various objective evaluations, it has been concluded that a seated human driver is most sensitive to vibrations in the 4 to 8 Hz frequency range [40]. The International Organization for Standardization (ISO) [41] has, therefore, suggested three exposure criteria as function of exposure time and frequency, while its revised version (1997) proposed assessment based upon a single number index (frequency-weighted rms acceleration).

The ride performance of a vehicle is assessed in terms of magnitude and frequency contents of vibration transmitted to the driver's location. Human driver is known to be most fatigue sensitive to vertical and horizontal vibrations in the 4-8 Hz and 1-2Hz frequency range, respectively. The human sensitivity to rotational vibration is mostly in the 0.5-1.5 Hz frequency range [41]. The International Standard (ISO-2631/1, 1997) has outlined a procedure to assess the human exposure to whole-body type ride vibrations in terms of overall frequency-weighted rms acceleration at the driver/passenger-seat interface. The standard defines frequency-weighting W_k for vertical vibration in the 0.5-80 Hz frequency range, and W_e for pitch vibration in the 0.1-80 Hz frequency range. The frequency-weighted accelerations are computed using convolution

in conjunction with band-limiting and weighting filters, $H_b(s)$ and $H_w(s)$, defined in ISO-2631 [41].

1.2.4 Dynamic Wheel Loads and Pavement Damage Potential

High magnitudes of static and dynamic tire loads in heavy vehicles are known to accelerate the pavement fatigue and rut formation. Various aspects of the road damage caused by heavy vehicles have been addressed in the literature [9]. A number of analytical and experimental studies have been carried out to assess the dynamic tire forces, road damage potentials of heavy vehicle tire loads, and to drive reliable pavement damage assessment tools [28,32]. These studies have established that the magnitudes of dynamic tire loads are directly influenced by the vehicular vibration modes associated with the vertical and pitch motions of the sprung and unsprung masses, as observed in the studies on ride dynamics. Many studies have concluded that the dynamic tire loads are strongly dependent upon vehicle and axle configurations, inertial and geometric properties of the vehicle, speed, road roughness, and suspension and tire properties. Similar to the studies on ride dynamics, the studies on dynamic wheel loads focus on commercial freight vehicles alone. In view of number of similarities between heavy freight vehicles and buses, the reported studies are reviewed to enhance an understanding of important factor and to formulate the scope of the dissertation research.

Laboratory simulations of the service stress caused by the vehicles have been carried out by deriving synthesized random displacements based on the knowledge of road surface undulations. Laboratory evaluations of dynamic tire forces necessitate an accurate generation of road profile in the laboratory [42]. It has been shown that road

displacement can be derived from the spectral density evaluated from a single traverse along the road [5]. Hu [26,43] stressed that correct regeneration of road undulation is significant for laboratory analyses of dynamic tire forces, and suggested that a standard vehicle configuration in conjunction with realistic and consistent levels of excitation must be established to determine the suspension performance related to the tire loads.

Misoi et al. [44] investigated the road corrugation problem in view of vehicle dynamics and wheel-soil interactions. The effect of a developing road corrugation on the dynamics of a single DOF tire model was discussed based on a sinusoidal corrugation profile, and it was suggested that the poorly damped vehicles impose excessive loads on the pavements and thus should be avoided. The study further described the corrugation creation and their relation to soil properties and environmental effects such as rainfall. Pavement types, the mechanisms related to pavement deterioration and the role of environmental factors have been described in a US Department of Transportation study by Jackson [45]. The design of pavement structures, the role of traffic loads, vehicle configuration and static loads have been described by Mahoney [46]. The study proposed that the pavement design should be based on the concept of Equivalent Single Axle Load (ESAL) rather than on economics, and/or local practices and materials.

Dynamic interactions between the tire and road surface cause considerable fluctuations in the tire loads. Such fluctuations about the static load are referred to as the dynamic wheel loads (DWL) or dynamic tire forces. For continuous flexible or rigid pavements, the dynamic tire forces generated by the vehicles are generally observed to be broadband, which follow nearly Gaussian distribution [32]. A number of analytical and experimental studies have been carried out to assess the dynamic tire forces and the

associated road damage potential, and to derive reliable pavement damage assessment tools. These studies have established that the magnitudes of dynamic tire loads are directly influenced by the vehicular vibration modes, associated with the vertical and pitch motion of the sprung and unsprung masses [47], vehicle and axle configurations, inertial and geometric properties of the vehicle, speed, road roughness, and restoring and dissipative properties of suspension and tire [33,48]. The DWL's generated by heavy vehicles predominate in two distinct frequency ranges; 1.5-4 Hz, attributed to bounce, pitch and roll mode resonant frequencies of the sprung masses; and 8-15 Hz, attributed to bounce and roll mode frequencies of the unsprung masses, and 'load-sharing' pitch modes of the suspensions, and chassis flexural modes.

The frequency bands mentioned above correspond to roughness irregularities with wave lengths ranging from 6.9 m to 18.5 m and from 1.9 m to3.5 m respectively, at a speed of 100 km/h. Various experimental and theoretical studies have shown that the lower frequency sprung mass modes usually dominate the dynamic tire forces on highways, except for vehicles equipped with axle group suspension with poorly damped bogie pitch mode [47]. The natural frequencies of heavy vehicles equipped with nonlinear suspension may depend upon the amplitude of vibration and thus the roughness of the road surface. The leaf-spring suspensions with considerable interleaf friction result in lower natural frequencies under high levels of excitations. Low level excitations arising from smooth roads can result in lockup of suspension with high interleaf friction. The vehicle thus exhibits lightly damped resonant oscillations in the 3-4 Hz frequency range due to compliance of the tires. The walking beam suspensions, due to their poor pitch mode damping and air suspensions, due to their reduced spring rate in rebound,

yield high dynamic loads in the higher frequency range (8-15 Hz) associated with the resonance of the unsprung masses [47].

The dynamic wheel loads of vehicles employing multiple-axle suspension are strongly influenced by the suspension design, and load sharing mechanism. Tandem air-spring suspensions behave largely like two independent air suspensions due to slow reaction time of the pneumatic load equalization system [6]. Although a walking-beam tandem suspension yields superior load equalization during bump encountered at high speeds. While the walking beam suspension provides reasonably good static load equalization, it is prone to "tandem-hop" vibration at high speeds, resulting in relatively high dynamic loads [9]. The influence of axle spacing on the pavement wear depends on the degree to which the response under one axle is affected by the response induced by a nearby axle. Rigid pavements distribute loads over distances that are of the same order as the common axle spacing. The axle spacing is thus a factor in determining rigid pavement fatigue. The influence of axle spacing on the potential damage of flexible pavements, however, is insignificant since the stresses are more localized in the wear course of a flexible pavement. It has been established that axle spacing has only insignificant influence on the rutting [36].

The response characteristics of the road materials and structures are sensitive to vehicle speed and thus to the roughness profile of the road interacting with the tires. Recent studies have shown that spatially repeatable dynamic loads result in rapid wear of most severely loaded locations of the pavements [9,39,48]. Higher speeds reduce the time duration of the application of the wheel load on a given pavement location, which may result in reduced fatigue and rutting of the visco-elastic material in flexible pavements

[47]. As the speed increases, the peak strain under a constant moving load diminishes in amplitude and occurs behind the point of application of the load [40,41]. The dominant frequencies of dynamic tire forces, however, may vary significantly with vehicle speed due to the phenomenon known as 'wheel-base filtering' [41,47]. Although the excitations caused by the road surface roughness comprise various frequency components, the geometric effects can result in relative attenuation or amplification of certain frequency components [26]. These geometric effects depend on the spacing between axles and the vehicle speed.

The vibration of heavy trucks, transmitted through the tires to the pavement, is a major cause of pavement damage. In recent years, cross-ply tires have largely been replaced by radial-ply tires, and average inflation pressures have increased from 550 kpa to 690 - 769 kpa [6]. Furthermore, wide-base single tires with enhanced load capacities are replacing the dual tires, particularly for the triaxle group suspensions. The engineering community has expressed serious concern that such changes in tires and inflation pressure may cause increased pavement damage, particularly the rutting [49]. The wide-base single tires have the potential to do more damage to the pavement due to a relatively smaller contact area. On the basis of asphalt strain measurements, Huhatala [50] reported that wide-base single tires are likely to cause 3.5 to 7 times more damage than the dual tires. Bonaquist [51] reported that wide single tires generate pavement strains approximately twice as large as those of the dual tires under identical loads. They also generate twice the rutting damage and four times the fatigue damage. Furthermore, wide single tires are likely to cause up to 10 times more damage than dual tires on relatively thin asphalt pavements that fail by fatigue cracking. For thicker pavements,

where permanent deformation is the main mode of failure, wide single tires are likely to cause 1.5 to 2 times more damage than dual tires. For rigid pavements, wide single tires are likely to cause a relatively small increase in fatigue damage [30].

An increase in tire inflation pressure may cause increased road damage due to reduced contact area and higher stiffness. The distribution of high pressure over the contact patch affects the stresses and strains near the surface of the pavement, while the corresponding response of the lower layers depends mainly on the overall load [6,52]. From the strain measurements performed on asphalt pavements, it was reported that a 40% increase in the tire pressure could increase fatigue damage by 26%.

A parameter often used to characterize the magnitude of dynamic tire forces is the dynamic load coefficient (DLC), defined as the ratio of root mean square (rms) tire force to the mean tire force [9]. Under normal operating conditions, heavy vehicles typically yield DLC ranging from 0.05 to 0.3. Many studies have reported that the DLC increases with increase in road roughness, speed, tire inflation pressure and suspension stiffness [5,47], while the influence of roll stiffness, lateral suspension spread, track width, and cornering and longitudinal stiffness of tires on the DLC is found to be relatively insignificant [5].

The properties of vehicle suspensions and tires have been identified as the most important elements in the design process, when pavement life is to be taken into account [43,53]. Many experimental studies have established that the properties of heavy vehicle suspensions strongly affect the magnitudes of the dynamic loads transmitted to the road surfaces [28]. A reliable methodology to assess the pavement failure, however, does not yet exist due to the complex dynamics associated with the wheel-road interactions and

the pavement structure. Although considerable efforts have been made to derive effective assessment tools the agreement between theory and experiment is often unsatisfactory [54]. Concerns on the validity of the fourth power law, variations in the vehicle configurations, and climatic effects are some of the complicating factors that can result in underestimating the pavement fatigue by a factor of 100 [54,55]. The damage caused by dynamic wheel loads is thus considered to be an area of high uncertainty [15]. It has thus been proposed, that various vehicle configuration should be classified based on the magnitudes of tire forces, represented by the dynamic load coefficients in order to assess their road damage potentials.

Kulakowski et al. [5] studied the effects of various design and operating factors on the road damage potentials of heavy vehicles and concluded that the magnitudes of dynamic wheel loads generated are strongly affected by speed and road roughness and moderately affected by the static wheel load. Tire inflation pressure has no significant effect on dynamic wheel loads. It was also found that the dynamic performance of the truck was not strongly affected by the type of tires, while the wide-base tires generated 10 to 12 percent lower DLCs than both the standard radial and low profile dual tires. Based on the values of the Eisenmann's road stress factor, however, the wide-base tires are expected to cause twice as much pavement damage as dual tires.

The heavy vehicle frames, exhibit bending modes in the 6 to 9 Hz frequency range, which may further contribute to the ride dynamics and dynamic wheel load performance of the vehicle. The motion imposed on the axles by frame bending, however, is relatively small when compared with the motions of the sprung and unsprung masses. The majority of the studies have thus concluded that the contributions due to

frame bending modes to the overall dynamic behavior are insignificant [35,56]. The lumped-parameter models of the vehicles are thus considered adequate for such analysis.

From the review of reported studies on vehicle ride quality and dynamic wheel load performance; it can be further established that both these measures are directly related to vibration modes of the vehicle. The studies on ride quality have invariably concluded that vibration characteristics of vehicles are strongly influenced by suspension damping. The significance of suspension damping has also been addressed in few studies on the dynamic wheel loads. In view of the analogy between the two measures, and significant influence of restoring and dissipative properties of the suspension, it is vital to explore the influence of such parameters on the dynamic wheel load variations and ride quality of the vehicles. The above two measures, however, are complex functions of coupled bounce, pitch and roll vibration modes of the sprung and unsprung masses [8]. The study of vehicle suspension may thus necessitate development and analysis of comprehensive three-dimensional vehicle models. Since vertical vibration modes of the vehicle are known to contribute most significantly to both the measures, preliminary analysis can be performed through development and analysis of simplified pitch plane models of the bus suspension.

1.3 Scope of the Thesis

From the review of the literature, it is concluded that the ride dynamic environment and dynamic wheel loads of urban buses are strongly related to the suspension properties. Furthermore, the road and driver friendliness characteristics of urban buses have been explored in very few studies. In view of the driver's health and

safety implications, and road damaging potentials, it is vital to enhance the performance of urban bus through effective suspension design. It is also essential to quantify the influence of various operating factors, such as speed, road roughness and tire inflation pressure, on the driver- and road- friendliness performance measures.

The overall objective of this thesis research is thus formulated to contribute towards enhancement of road-friendliness and driver-friendliness of the urban bus. The specific objective of this dissertation is to develop effective analytical model of a modern urban bus and perform analysis to identify near optimal suspension damping in order to reduce the magnitudes of dynamic wheel loads transmitted to the pavement.

It is recognized that the driver- and road- friendliness performance of a vehicle are known to be related to many design and operating factors, such as weights, dimensions, axle loads, suspension and tire properties, road roughness and speed. Since the vehicle dimensions and axle loads are related by the provincial road laws, this dissertation research investigates the role of suspension and tire properties, road roughness, and some of the operating factors, which are somewhat unique for urban buses. These include the operating load, which may vary considerably from empty to full passenger load, and tire inflation pressure, which may vary from 85 psi to 120 psi.

The validity of a vehicle model strongly relies upon the accurate characterization of its components, integration of the components and adequate description of representative urban road excitations. Although suspensions with air suspension springs and hydraulic dampers have been in use for more than three decades, appropriate models applicable over a wide range of operating conditions, such as those encountered in urban buses, have not been reported. Furthermore, roughness characteristics of urban roads

have not been defined. The specific objectives of this dissertation research are thus formulated as follows:

1. Develop a mathematical model of low-floor urban bus to investigate its ride vibration and dynamic wheel load characteristics.
2. Analyze the nonlinear force-deflection and force-velocity characteristics of suspension components, and the component models that could be applied over a wide range of operating conditions.
3. Analyze the roughness characteristics of urban roads from the measured data, and evaluate the vehicle response under specified operating conditions.
4. Examine the validity of the analytical model in relation to road measured ride vibration and wheel load, data, and perform necessary refinements.
5. Explore the analogy between the dynamic wheel loads and ride quality performance characteristics of the urban bus under specified operating conditions.
6. Formulate performance measures to assess the driver- and road- friendliness characteristics of the urban bus.
7. Perform a comprehensive parametric sensitivity analysis to quantify the effects of variations in operating conditions and suspension design parameters.

1.4 Layout of the Thesis

In Chapter 2, the design of the suspension system of the candidate bus is discussed. A six degrees-of-freedom in-plane model of the urban bus is developed and the associated assumptions are described. The equations of motion for the vehicle model are formulated upon appropriate considerations of the component models, Coulomb

friction forces and suspension geometry. The measured elevations of different roads in Montreal are analyzed to derive the roughness spectra of urban roads.

In Chapter 3, the model parameters are identified from the measured data and manufacturer's specifications. A linear vehicle model is derived about the operating point and eigenvalue analysis is performed to derive the free vibration response of the vehicle. The nonlinear vehicle model is analyzed under random road excitations, and its response characteristics are compared with the road-measured data to demonstrate the model validity. Performance measures are defined and formulated to assess both driver- and road- friendliness of the vehicle.

In Chapter 4, The results of a thorough parametric sensitivity analysis are presented in terms of the performance measures. The analysis are performed for variations in four operational parameters, including: road roughness, tire inflation pressure, operating load and speed; and various design parameters related to the force-deflection, force-velocity and geometry of the suspension components. The influence of variations in these design and operating parameters on the potential performance enhancement are discussed. The conclusions drawn and the recommendations for future work are finally presented in chapter 5.

CHAPTER 2

DEVELOPMENT OF THE URBAN BUS MODEL

2.1 Introduction

While the variations in dynamic wheel loads of commercial freight vehicles have been extensively investigated, only few studies have reported ride and dynamic wheel load characteristics for urban or highway buses [16,17]. These studies have clearly established that variations in dynamic wheel forces transmitted to the pavement and ride vibration transmitted to the driver/passengers of a vehicle are strongly influenced by various design and operating factor [4]. The operating factors, such as road roughness, speed and gross vehicle weight, and design factors related to axle loads, axle configuration, and static and dynamic properties of suspension and tires, are known to contribute most significantly to both the dynamic wheel load and ride quality performance. The role of vehicle suspension and tires in enhancement of road-friendliness of heavy vehicles has thus been emphasized in a large number of studies. Majority of these studies, however, focuses on the restoring properties of the suspension and axle configurations [4,16], while the effects of dissipative properties of the suspension and tires have been dealt only in a limited number of studies [13]. These studies have invariably concluded that performance of vehicles with air suspension is considerably superior to those with steel spring suspension.

From the review of reported studies on vehicle ride quality and dynamic wheel load performance, it can be further established that both these measures are directly

related to vibration modes of the vehicle. The studies on ride quality have invariably concluded that vibration characteristics of vehicles are strongly influenced by suspension damping. In view of the analogy between the two measures, and significant influence of restoring and dissipative properties of the suspension, it is vital to explore the influence of such parameters on the dynamic wheel load variations and ride quality of the vehicles. The above two measures, however, are a complex function of coupled bounce, pitch and roll vibration modes of the sprung and unsprung masses [4]. The study of vehicle suspension may thus necessitate development and analysis of comprehensive three-dimensional models. In straight driving conditions, however, the roll dynamics is expected to have negligible contribution from both measures of interest. For the purpose of this investigation, a simplified pitch plane model of modern urban bus is considered. Special emphasis is placed on the modeling of vehicle components such as tire, suspension spring and dampers.

2.2 Development of the Pitch Plane Model of an Urban Bus

There is a wide range of bus configurations that are used for urban public transportation throughout North America. The low floor design of bus is increasingly being used for urban transportation, while the older design (Classic) is still in use. From the design specifications of different buses it is apparent that all buses exhibit comparable weights and dimensional characteristics, while the axles exhibit certain similarities in terms of suspension components, geometric layout and linkages. The geometric and inertial properties of different buses may differ slightly. The primary differences among

the various axles include the use of anti-roll bar in some axle suspensions, and variations in spring and damper tracks, axle loads, and properties of springs, dampers and tires.

In this study, a generic pitch-plane model is developed, which could be applied for various models of buses. The specific features of the model, however, are based on the low floor urban bus referred to as LFS. Figures 2.1 and 2.2 illustrate the schematics of the front- and rear-axle suspension configurations in the pitch plane. As illustrated in Figure 2.1, the front axle suspension consists of two air bags on each side of the track, placed 0.4064m apart in the longitudinal direction. One damper is mounted with an inclination of 3 degrees with respect to the vertical axis. The rear suspension, shown in Figure 2.2 consists of two air springs on each track placed 1.391m apart in the longitudinal direction. Two dampers are used with each suspension unit, where each damper is placed in close proximity to the air spring and are mounted without any inclination. Based on the front and rear axle configuration, a generic model in the pitch plane is developed that can represent a wide range of urban buses.

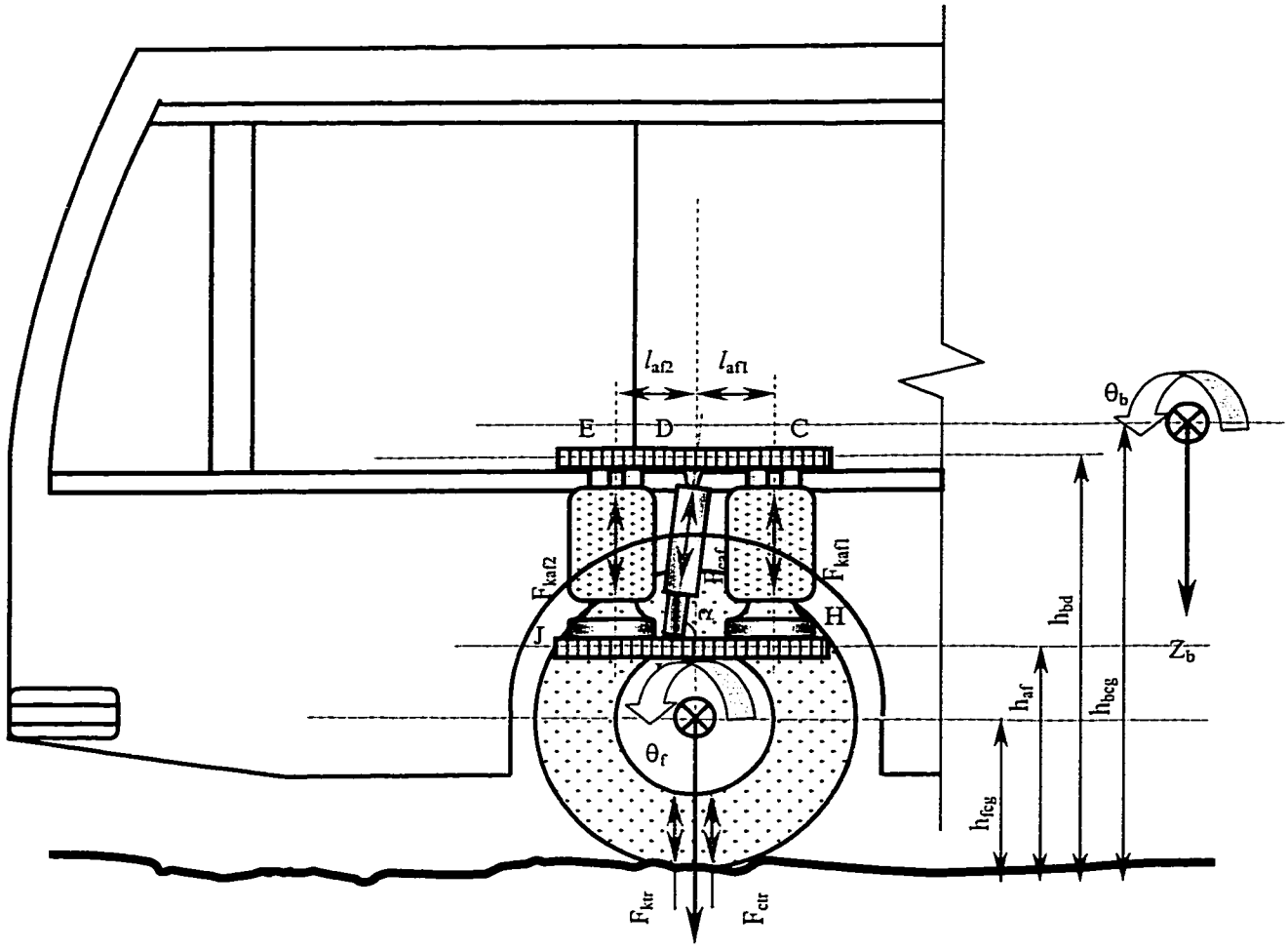

Figure 2.1: Schematic of front-axle suspension components

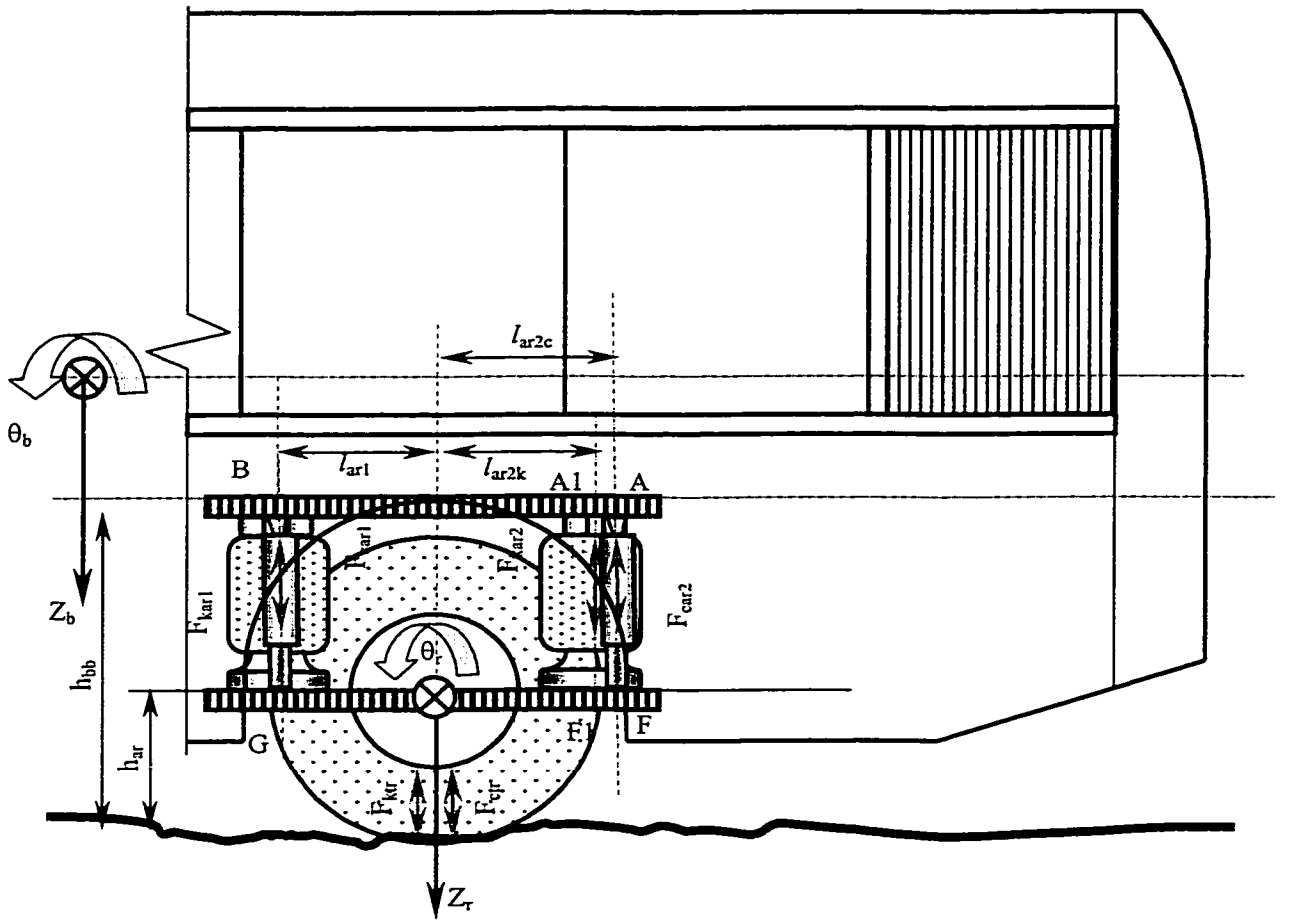

Figure 2.2: Schematic of rear-axle suspension components

Figure 2.3 illustrates the pitch plane model of the vehicle, comprising the lumped sprung and unsprung masses, air springs, inclined shock absorbers and tires. The sprung mass m_b represents the lumped mass due to body, chassis and passengers. Unsprung masses m_f and m_r represent the masses due to front and rear axle and wheel assemblies, respectively. The suspension components, air springs and dampers are represented by

two-point force generating elements assumed to generate forces along the respective axis, which are nonlinear functions of respective axial deflections and velocities.

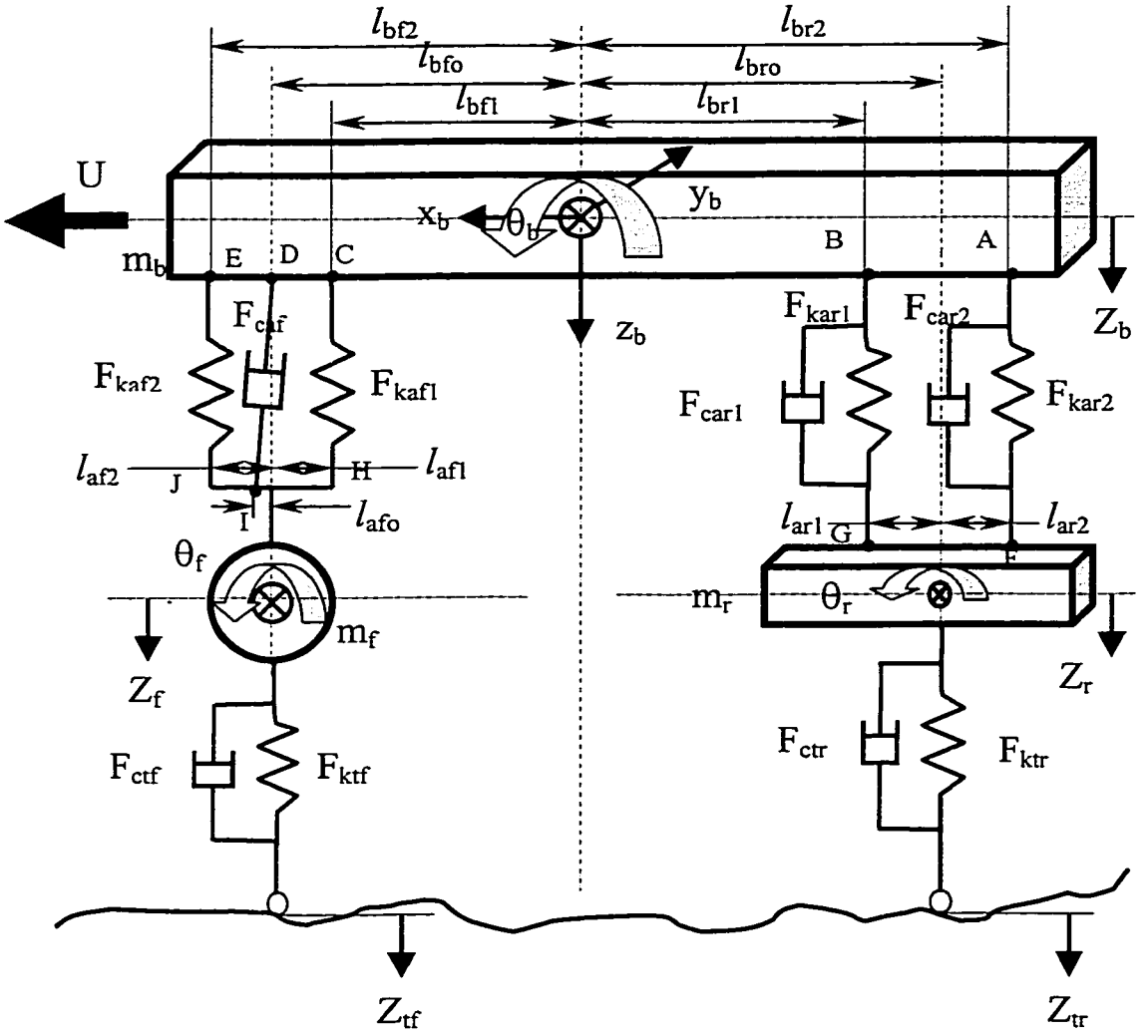

Figure 2.3: Schematic of six-DOF in-plane model of the bus

2.3 Equation of Motion

Assuming negligible contributions due to roll and lateral dynamics of the vehicle on the ride and pavement load response, the low floor (LFS) vehicle is represented by a six-degrees-of-freedom (DOF) system in the pitch plane, as shown in Figure 2.3. Assuming constant forward speed, the motion of the spring mass is considered along the vertical and pitch axes, The motion of unsprung masses due to single axles are, in general, considered as single-DOF along the vertical axis [26]. The layout of suspension springs and dampers in the urban bus design, however, may cause certain pitch moments about the axle center. The magnitudes of such moments may be considerable under pitch oscillations of the sprung mass that could be caused by road irregularities and application of braking. The unsprung masses due to front- and rear-axles are thus considered to posses two-DOF motion along the vertical and pitch directions. The flexibility due to bus body and chassis structure is assumed to be negligible for simplicity although practically, bus frame bending occurs near 6 Hz, but the displacement magnitude of this vibration is very small. The sprung mass is thus represented by a rigid mass. The validity of this simplification, however, may be questioned for modern lightweight design of the chassis, which may exhibit considerable deflection of the chassis [20,21]. The tire-road interactions are characterized by a nonlinear point-contact spring incorporating loss of tire-road contact and nonlinear force-deflection characteristics as a function of inflation pressure. The forces developed by suspension components are derived from the component models described in later subsections. The equations of motion for the pitch plane model, derived using D'Alembert's principle, are summarized below:

Bounce motion of the sprung mass:

$$m_b\ddot{z}_b - F_{kar1} - F'_{kar1} - F_{kar2} - F'_{kar2} - F_{kaf1} - F'_{kaf1} - F_{kaf2} - F'_{kaf2} - F_{car1} - F_{car2} - F_{caf}\sin\alpha + m_b g = 0 \quad (2.1)$$

Pitch motion of the sprung mass:

$$I_b\ddot{\theta}_b + F_{kar1}\ell_{br1} + F'_{kar1}\ell_{br1} + F_{kar2}\ell_{br2k} + F'_{kar2}\ell_{br2k} - F_{kaf1}\ell_{bf1} - F'_{kaf1}\ell_{bf1} - F_{kaf2}\ell_{bf2} - F'_{kaf2}\ell_{bf2} + F_{car1}\ell_{br1} + F_{car2}\ell_{br2c} - F_{caf}\ell_{bfo}\sin\alpha + F_{caf}(h_{bcg} - h_{bd}).\cos\alpha = 0 \quad (2.2)$$

Bounce motion of the front unsprung mass:

$$m_f\ddot{z}_f + F_{kaf1} + F'_{kaf1} + F_{kaf2} + F'_{kaf2} - F_{ktf} - F'_{ktf} - F_{ctf} + F_{caf}\sin\alpha + m_f g = 0 \quad (2.3)$$

Pitch motion of the front unsprung mass:

$$I_f\ddot{\theta}_f - F_{kaf1}\ell_{af1} - F'_{kaf1}\ell_{af1} + F_{kaf2}\ell_{af2} + F'_{kaf2}\ell_{af2} + F_{caf}(h_{af} - h_{fcg}).\cos\alpha + F_{caf}\ell_{afo}.\sin\alpha = 0 \quad (2.4)$$

Bounce motion of the rear unsprung mass:

$$m_r\ddot{z}_r + F_{kar1} + F'_{kar1} + F_{kar2} + F'_{kar2} + F_{car1} + F_{car2} - F_{ktr} - F'_{ktr} - F_{ctr} + m_r g = 0 \quad (2.5)$$

Pitch motion of the rear unsprung mass:

$$I_r\ddot{\theta}_r + F_{kar1}\ell_{ar1} + F'_{kar1}\ell_{ar1} - F_{kar2}\ell_{ar2k} - F'_{kar2}\ell_{ar2k} + F_{car1}\ell_{ar1} - F_{car2}\ell_{ar2c} \quad (2.6)$$

Where, z_b and θ_b are the vertical and pitch displacement coordinates, respectively, of the center of gravity (c.g) of the sprung mass. α, m_b, m_f and m_r are the front-axle damper inclination with respect to the vertical axis, m_b is the lumped mass of the bus, m_f and m_r are the lumped masses of front and rear axles. The pitch motion of the sprung mass is assumed to occur about its pitch oscillation center, which is assumed to coincide with the cg. z_f and θ_f are vertical and pitch displacement coordinates of the front-axle

unsprung mass, respectively. z_r and θ_r are vertical and pitch displacements of the rear-axle unsprung mass, respectively. The pitch deflections of unsprung masses are considered to occur with respect to their respective mass centers.

F_{kaf1}, F_{kaf2}, F_{kar1} and F_{kar2} are nonlinear suspension forces developed by the front and rear air springs, respectively, as a function of their relative deflections and static ride height. Owing to the use of height control valves, the air bags are assumed to maintain constant ride height irrespective of the operating axle load. The subscripts '1' and '2' denote the forces due to air springs located near and far from bus body c.g., respectively. The static forces developed by suspension springs are denoted by F'_{kaf1}, F'_{kaf2}, F'_{kar1} and F'_{kar2} which are related to sprung weight supported by the axle and the design ride height. F_{caf}, F_{car1} and F_{car2} are nonlinear forces developed by the front- and rear-axle suspension dampers, respectively, as functions of relative velocities along the respective shock absorber axes. The angle α_f describes the inclination of the shock absorbers with respect to the vertical axis. 'g' represents the acceleration due to gravity, and I_b, I_f and I_r are pitch mass moments of inertia due to sprung and unsprung (front and rear) masses, respectively. The constants l_{af0}, l_{af1}, l_{af2}, l_{ar1}, l_{ar2k}, l_{ar2c}, l_{bf0}, l_{bf1}, l_{bf2}, l_{br0}, l_{br1} and l_{br2} define the coordinates of the spring and damper mounts, as shown in Figure 2.3. F_{ctf} and F_{ctr} denote the damping forces developed by front- and rear-axle tires respectively, and F_{ktf} and F_{ktr} are the respective restoring forces.

2.3.1 Suspension Forces

The suspension forces developed by air springs and dampers are derived from the nonlinear component models presented in section 2.4. The integration of the component

models within the pitch-plane models of the vehicle, however, involves appropriate considerations of kinematic and dynamic motions of the sprung and unsprung masses. The total force developed by a damper comprises components due to gas spring, seal friction and hydraulic forces. Since the gas spring force is considerably smaller than those due to the hydraulic flows and seal friction, the force developed by a damper F_c can be expressed as:

$$F_c = F_{cv} + F_{cf} \tag{2.7}$$

Where, F_{cv} and F_{cf} are components of forces attributed to hydraulic flows through the valves or orifices, and the seal friction, respectively. Assuming ideal characteristics, the seal friction force is expressed as

$$F_{cf} = F_{cfo}\,\mathrm{sgn}(V_o) \tag{2.8}$$

The force F_{cfo} is the magnitude of friction force and V_o, is the relative velocity across the damper. The sgn function is used to ensure the phase relationship between the force and the velocity, such that, sgn(·) = 1 for (·) > 1, and sgn(·) = -1 for (·) < 1. The relative velocity across a damper is derived from the coordinates of the damper attachment points. Referring to Figure 2.3, the velocities across the front (V_f) and rear (V_{r1} and V_{r2}) dampers can be evaluated from:

$$V_f = (\dot{Z}_I - \dot{Z}_D).\sin\alpha,\ V_{r1} = (\dot{Z}_G - \dot{Z}_B),\quad V_{r2} = (\dot{Z}_F - \dot{Z}_A) \tag{2.9}$$

Assuming small motions, the vertical velocities at the attachment points between the sprung and unsprung masses can be derived from the vertical and pitch velocities of the sprung and unsprung masses, such that:

$$\dot{Z}_B = \dot{Z}_b - \ell_{br1}\dot{\theta}_b,\ \dot{Z}_A = \dot{Z}_b - \ell_{br2c}\dot{\theta}_b \text{ and } \dot{Z}_D = \dot{Z}_b + \ell_{bfo}\dot{\theta}_b$$

$$\dot{Z}_G = \dot{Z}_r + \ell_{ar1}\dot{\theta}_r,\ \dot{Z}_F = \dot{Z}_r - \ell_{ar2c}\dot{\theta}_r \text{ and } \dot{Z}_I = \dot{Z}_f + \ell_{afo}\dot{\theta}_f \tag{2.10}$$

The instantaneous inclination angle α is related to the coordinate of the attachment points, and given by:

$$\alpha = \tan^{-1}\left[\frac{\ell_f - (Z_b + \ell_{bfo}\theta_b) + Z_f + \ell_{af}\theta_f}{\ell_{afo}}\right] \tag{2.11}$$

Where l_f is the static height derived from the ride height and geometry. In view of relatively small inclination, the variations in α are expected to be very small and thus may be neglected.

Equations 2.7 to 2.11, together with the component models presented in section 2.4, describe the dynamic forces generated by the dampers in the pitch plane of the bus. The static and dynamic forces generated by air springs are also derived from component models, presented in section 2.4. The static force developed by the air springs is directly related to the component of the sprung weight supported by each air spring. The static components of forces due to front and rear air springs, F'_{kaf1}, F'_{kaf2}, F'_{kar1} and F'_{kar2}, can be formulated from the static equilibrium, illustrated in Figure 2.4.

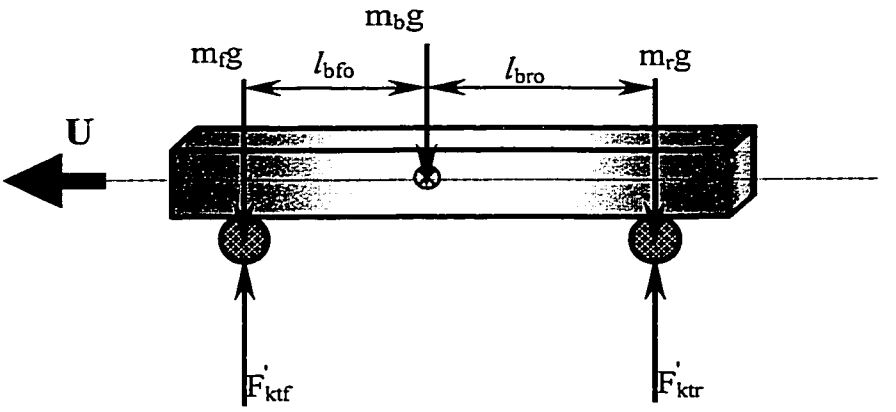

Figure 2.4 Static equilibrium of the whole bus

The static weight supported by the front- and rear-axle tires can be expressed as:

$$F'_{ktf} = \left(\frac{\ell_{bro}}{\ell_{bro} + \ell_{bfo}}\right) m_b g + m_f g$$

$$F'_{ktr} = \left(\frac{\ell_{bfo}}{\ell_{bro} + \ell_{bfo}}\right) m_b g + m_r g \qquad (2.12)$$

The static forces due to suspension springs, F'_{kaf1}, F'_{kaf2}, F'_{kar1} and F'_{kar2} can then be derived from the static tire forces upon consideration of the static equilibrium of the front usprung mass, shown in Figure 2.5:

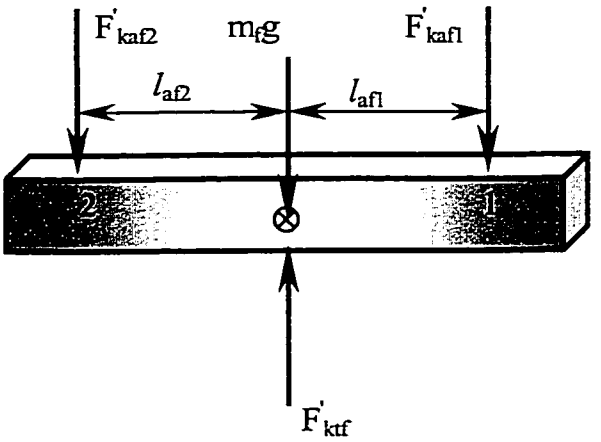

Figure 2.5: Static equilibrium of front-axle unsprung mass

$$F'_{kaf1} = \left(\frac{\ell_{af2}}{\ell_{af1} + \ell_{af2}}\right)\left[\left(\frac{\ell_{bro}}{\ell_{bfo} + \ell_{bro}}\right) m_b g\right]$$

$$F'_{kaf2} = \left(\frac{\ell_{af1}}{\ell_{af1} + \ell_{af2}}\right)\left[\left(\frac{\ell_{bro}}{\ell_{bfo} + \ell_{bro}}\right) m_b g\right]$$

$$F'_{kar1} = \left(\frac{\ell_{ar2k}}{\ell_{ar1} + \ell_{ar2k}}\right)\left[\left(\frac{\ell_{bfo}}{\ell_{bfo} + \ell_{bro}}\right)m_b g\right]$$

$$F'_{kar2} = \left(\frac{\ell_{ar1}}{\ell_{ar1} + \ell_{ar2k}}\right)\left[\left(\frac{\ell_{bfo}}{\ell_{bfo} + \ell_{bro}}\right)m_b g\right] \quad (2.13)$$

The air springs are assumed to maintain constant ride height, given by δ'_{f1}, δ'_{f2}, δ'_{r1} and δ'_{r2} under the static equilibrium, irrespective of the sprung and unsprung weights. The dynamic forces developed by the air springs are then related to the instantaneous relative displacements across the spring. The dynamic restoring forces are dependent on the instantaneous air pressure and effective piston area, which are related to instantaneous height of air bag. The instantaneous heights of front and rear air bags δ_{f1}, δ_{f2}, δ_{r1} and δ_{r2} are computed from the vertical motions of the attachment points, given by:

$$\delta_{f1} = Z_f - l_{af1}\theta_{f1} - Z_b - l_{bf1}\theta_{b1} + \delta'_{f1}$$

$$\delta_{f2} = Z_f + l_{af2}\theta_f - Z_b - l_{bf2}\theta_b + \delta'_{f2}$$

$$\delta_{r1} = Z_r + l_{ar1}\theta_r - Z_b + l_{br1}\theta_b + \delta'_{r1}$$

$$\delta_{r2} = Z_r - l_{ar2k}\theta_r - Z_b + l_{br2k}\theta_b + \delta'_{r2} \quad (2.14)$$

Let δ_i be the instantaneous height of air spring i, and P_i be the instantaneous absolute pressure within the spring. The restoring force is then expressed as a function of the effective area A_E:

$$F_a(\delta_i) = (P_i - P_{atm}).A_E.(\delta_i) \quad (2.15)$$

Where P_{atm} is the atmospheric pressure and A_E is the effective area of the piston, which is a nonlinear function of the instantaneous height [42]. The instantaneous air pressure can be derived from the gas laws, assuming a polytropic process such that:

$$P_i(\delta_i) = \frac{P_{oi}^{'} V_A^{\gamma}}{\left[V_o - A_E(\delta_i - \delta_i^{'})\right]^{\gamma}} \tag{2.16}$$

Where γ is the polytropic constant and δ'_i is the static height. On the basis of data obtained from laboratory tests performed at CONCAVE, it has been shown that variations in effective area can be expressed by a regression function in change in height, δ'_i ($\delta'_i = \delta'_i - \delta'_i$) [19].

$$A_E = k_o + \sum_{j=1}^{m} k_j \delta^j \tag{2.17}$$

Where m is the order of the polynomial, and k_o, k_j (j = 1,2,3...m) are regression coefficients. V_A is the air volume corresponding to static height and P_{oi} is the static pressure, which is related to the static spring load:

$$P_{oi} = \frac{F_{ki}^{'}}{A_E(\delta_i^{'})} + P_{atm} \tag{2.18}$$

Where F'_{ki} is the static spring force. Suspension systems with its linkages and bushings exhibit considerable magnitudes of friction forces. The total dynamic force developed by air spring F_{kar1}, F_{kar2}, F_{kaf1} and F_{kaf2} also include lumped values of friction forces arising from suspension bushings and joints.

$$F_{kaij} = F_{aij} + F_{Fij}; \qquad i = f, r \text{ and } j = 1,2 \tag{2.19}$$

Where F_{aij} is the force developed by the spring and F_{Fij} is the lumped friction force, which may be expressed in terms of the friction coefficient, 'μ':

$$F_{Fij} = \mu F_{kaij}^{'} \text{sign}(V_o) \tag{2.20}$$

Equation 2.12 to 2.20 together with the effective area model, presented in section 2.4, completely describe the static and dynamic forces developed by the air springs.

2.3.2 Tire Forces

The static and dynamic components of vertical forces developed by front- and rear-axle tires are dependent upon the tire deflection and static force-deflection characteristics of the tires [19]. The static force-deflection characteristics of tires are further dependent upon tire design, inflation pressure and static load. The urban buses invariably use radial tires. The inflation pressure and static load, however, may vary considerably due to variation in passengers load and driver's preferences. Although the urban bus manufacturers and operators recommend a nominal inflation pressure of 110psi, considerable variations in inflation pressure have been reported by the operators. Since the tire stiffness and thus the dynamic loads transmitted to the pavements are strongly related to tire inflation pressure [5], it is extremely vital to derive vertical forces as a function of inflation pressure. The tire model should also incorporate variations in static load in view of expected variations in number of passengers during service. The static and dynamic characteristics of tires are established from the laboratory-measured data, as a function of static load and inflation pressure [5,29]. The test methodology employed in these studies, and test results and component models are presented in section 2.4.

The static force-deflection characteristics of the tires are also strongly related to the static load applied. The variation in number of passengers during service is the key factor, which gives rise to the variations in the static load of the bus.

The static deflections of front- and rear-axle tires, δ'_{tf} and δ'_{tr} are evaluated from the static tire loads, described in equation 2.12, and the force deflection characteristics of the tire. The total forces developed by tires are related to the total deflection and the stiffness characteristics. The total force diminishes to zero in the event of loss of contact with the road. The total tire deflections, δ_{tf} and δ_{tr} can be expressed as:

$$\delta_{tf} = Z_{tf} + \delta'_{tf} - Z_f$$

$$\delta_{tr} = Z_{tr} + \delta'_{tr} - Z_r \qquad (2.21)$$

The dynamic vertical forces developed by the tires, F_{tf} and F_{tr} are expressed as a function of inflation pressure (P), deflection and velocity, using the component model presented in section 2.4.

2.4 The Component Models

The ride and tire load performance characteristics of urban buses are directly related to static and dynamic properties of the suspension components and tires, which are known to be strongly nonlinear functions of various design and operating factors. The effectiveness of the analytical model thus relies upon accurate analytical characterization of static and dynamic properties of these components. Furthermore, the component characterization and models must demonstrate their validity over the range of operating conditions. Urban buses invariably employ air springs and shock absorbers with multi-stage damping characteristics associated with hydraulic flows through bleed and blow-off valves. The forces generated by such components are strongly nonlinear functions of their design, and displacements and velocities of the sprung and unsprung masses. The

forces generated by the vehicle tires are also dependent upon the static loads and inflation pressure.

As it was discussed in the literature review, that urban buses encounter wide range of variations in their operating conditions and that the component characteristics have not been adequately quantified over wide range of operating conditions. A series of systematic laboratory tests and data analysis were recently carried out at CONCAVE research center in order to establish the characteristics of primary suspension components of different urban buses [14,30]. The test results acquired from these tests performed on air springs, dampers and tires are utilized to develop accurate nonlinear component models, which are incorporated in the proposed pitch plane model of the bus. The component models are developed based upon the physical laws and regression analysis, which are described in the following sections.

2.4.1 Air Bag (Air spring)

The urban bus suspension consisted of flexible air bags mounted between the chassis and the arm links attached to the axles, as shown in Figures 2.1 and 2.2. The restoring force developed by the air medium is a complex function of the air pressure, effective piston area, air volume and the instantaneous height. Unlike the commercial freight vehicles, the suspension and tire loads of urban buses may vary considerably due to variations in the number of passengers being transported. The front axle load of an LFS model may vary from 40kN under unloaded, to approximately 61kN fully loaded conditions, while the rear axle load may vary from 81kN to approximately 116kN. It is therefore, necessary to characterize the air springs for a wide range of load conditions.

A series of laboratory tests were performed to acquire pressure-deflection and force-deflection characteristics of air springs in front- and rear-axle suspension under different static loads. The tests were performed under constant spring heights of 31.50 cm and 25.15cm for the front and rear-axle suspension springs respectively. Figures 2.6 and 2.7 illustrate the force-deflection and pressure-deflection characteristics of the front-axle air springs under preloads of 8.76 kN and 10.05kN, while the static design height is held at 31.5 cm. The spring deflection in the figures is expressed in terms of total height. The effective piston area is derived from the measured pressure and force data, assuming uniform cross-section. Figure 2.8 illustrates the variations in effective area as a function of the bag height.

Figures 2.9 to 2.11 illustrate the pressure-deflection, force-deflection and effective area variations of the rear-axle suspension springs. The results show considerable variations in the effective area with the bag height. The effective area decreases significantly as the bag undergoes an extension, while it increases under compressive motion.

The front-axle air springs yield lower spring rates near static ride height and the spring rate decreases further under extension. The spring rate tends to increase gradually. The results show that the effective area remains almost constant in the vicinity of static ride height and increases under extreme deflection in compression. The effective area decreases sharply during extension when the ride height exceeds approximately 37cm.

The force-deflection characteristics of the rear-axle air spring, shown in Figure 2.9, also reveals similar trends, i.e. low spring rate near static ride height and during extension, and progressively hardening spring rate during compression. The effective

area, shown in Figure 2.11, remains nearly constant in the vicinity of static ride height and during compression, and it decreases rapidly when ride height exceeds 37cm.

From the measured data, it was further concluded that the mean effective area of the air spring is a function of deflection alone [26]. A regression analysis was performed to express effective area as a polynomial function of deflection δ:

The mean effective area of the air spring is a function of deflection alone. The expression for the area in terms of deflection is a polynomial in deflection 'z'.

$$A_E(z) = k_o + \sum_{j=1}^{m} k_j z^j \tag{2.22}$$

Where, z is the deflection of the air bag, m is the order of the polynomial, k_o, k_j, (j=1,2...m) are the constant coefficients. These coefficients can be estimated by minimizing the error function J that is defined in terms of effective area $A_E(z)$.

$$J = \frac{1}{N}\sum_{i=1}^{N}[A_E(z_i) - A_{ET}(z_i)]^2 \tag{2.23}$$

Where N is the number of observation points, A_{ET} is the measured mean effective area of the air springs and J is the mean squared error.

Equations 2.22 and 2.23 are solved to derive the constant coefficients. The error minimization is performed using polynomial of order 6, which yields a minimum mean squared error. The coefficients of the polynomial and the mean squared error for different air springs are presented in Table 2.1. The effective areas, $A_E(z)$, computed from equation 2.22 for the two springs, are compared with the measured values, as shown in Figures 2.12 and 2.13. From the results, it is evident that the effective area estimated from the polynomial function correlates very well with the mean measured data

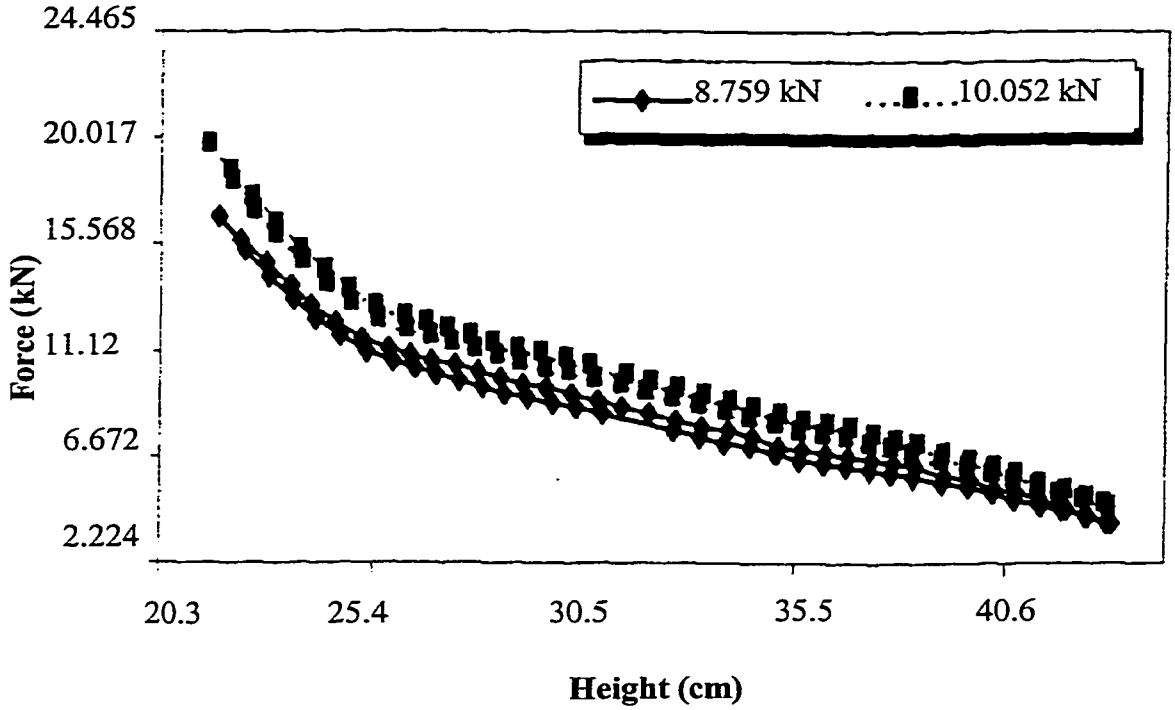

Figure 2.6: Force-displacement characteristics of a front-axle air spring (Desig height = 31.49 cm) [26]

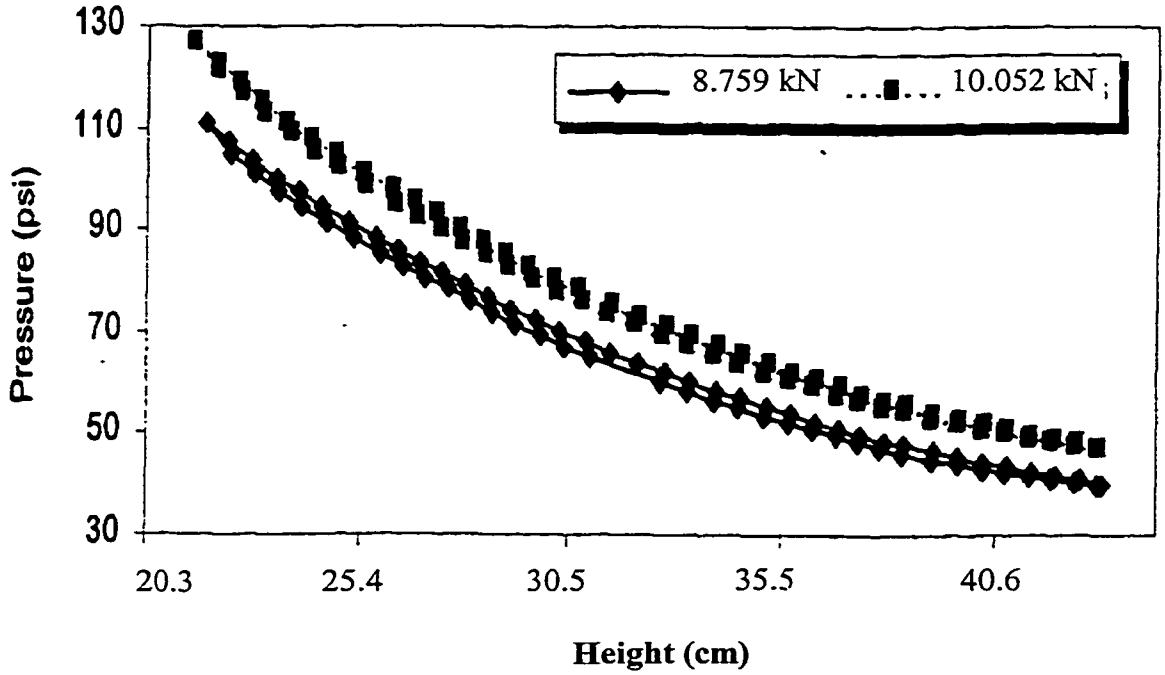

Figure 2.7: Pressure-displacement characteristics of a front-axle air spring (Design height = 31.49 cm) [26]

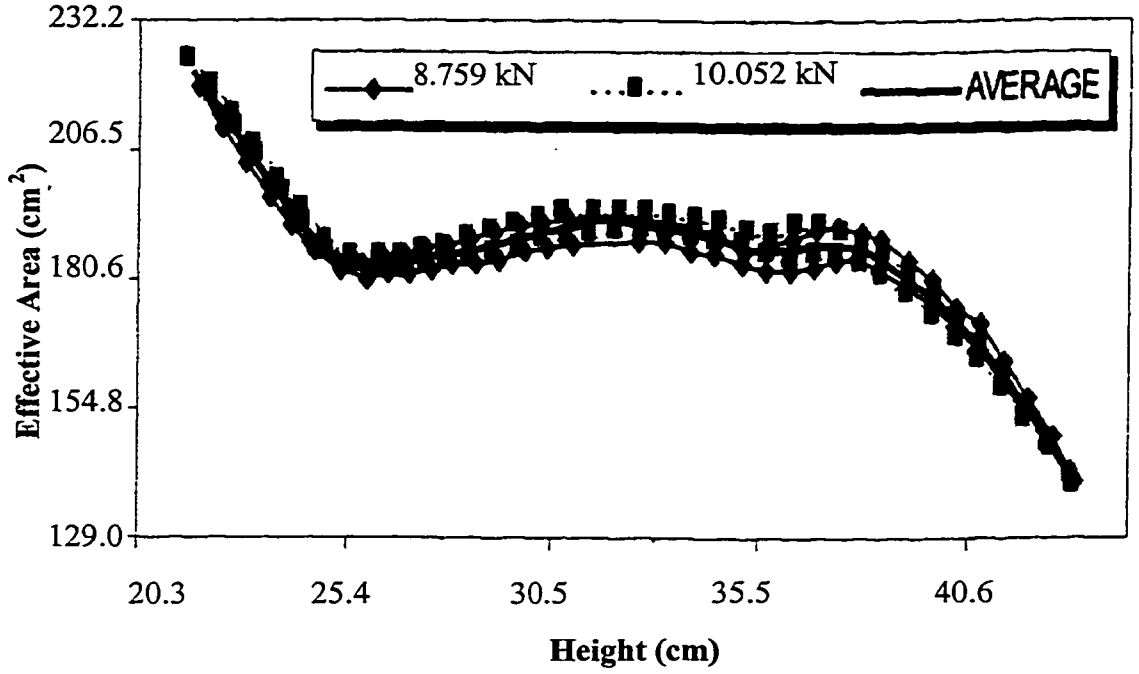

Figure 2.8: Effective area-displacement characteristics of a front-axle air spring (Design height = 31.49 cm) [26]

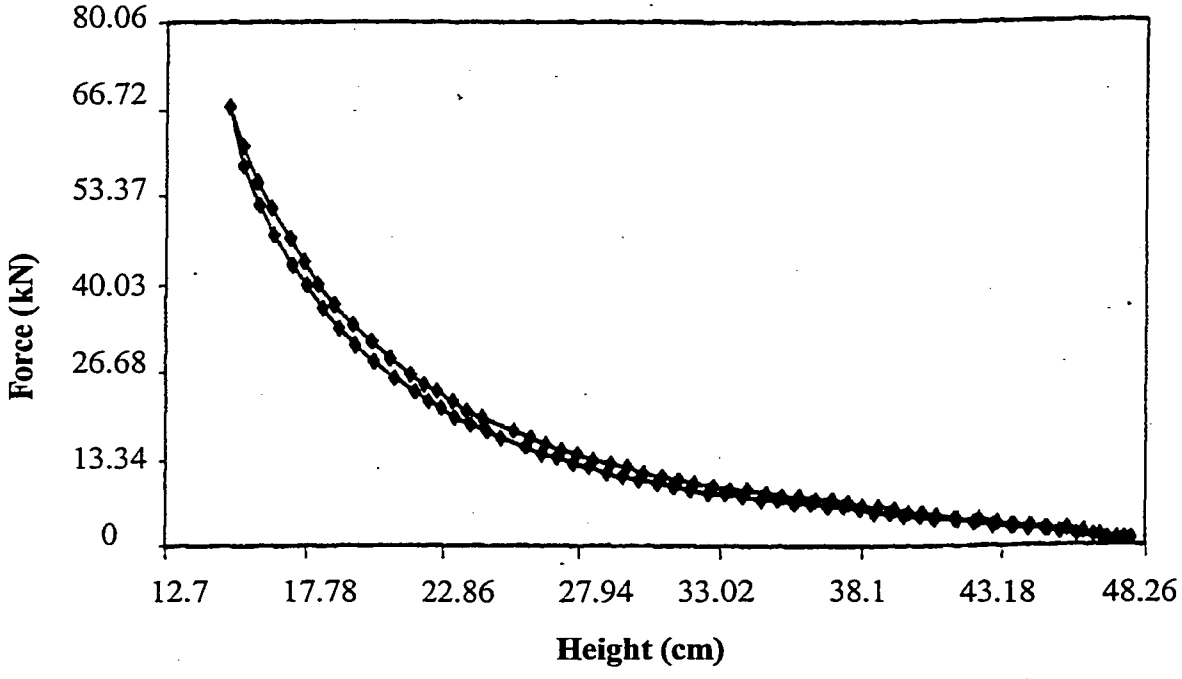

Figure 2.9: Force-displacement characteristics of a rear-axle air spring (Design height = 25.15 cm, Preload = 18.031 kN) [26]

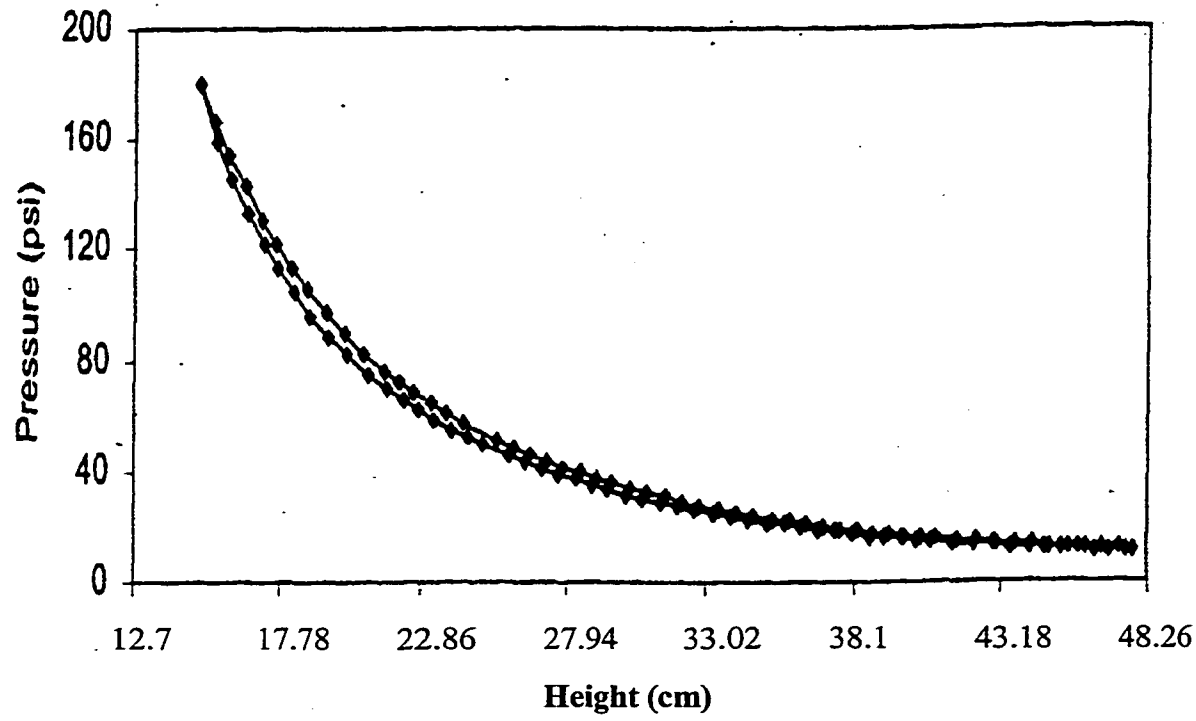

Figure 2.10: Pressure-displacement characteristics of a rear-axle air spring (Design height = 25.15 cm, Preload = 18.031 kN) [26]

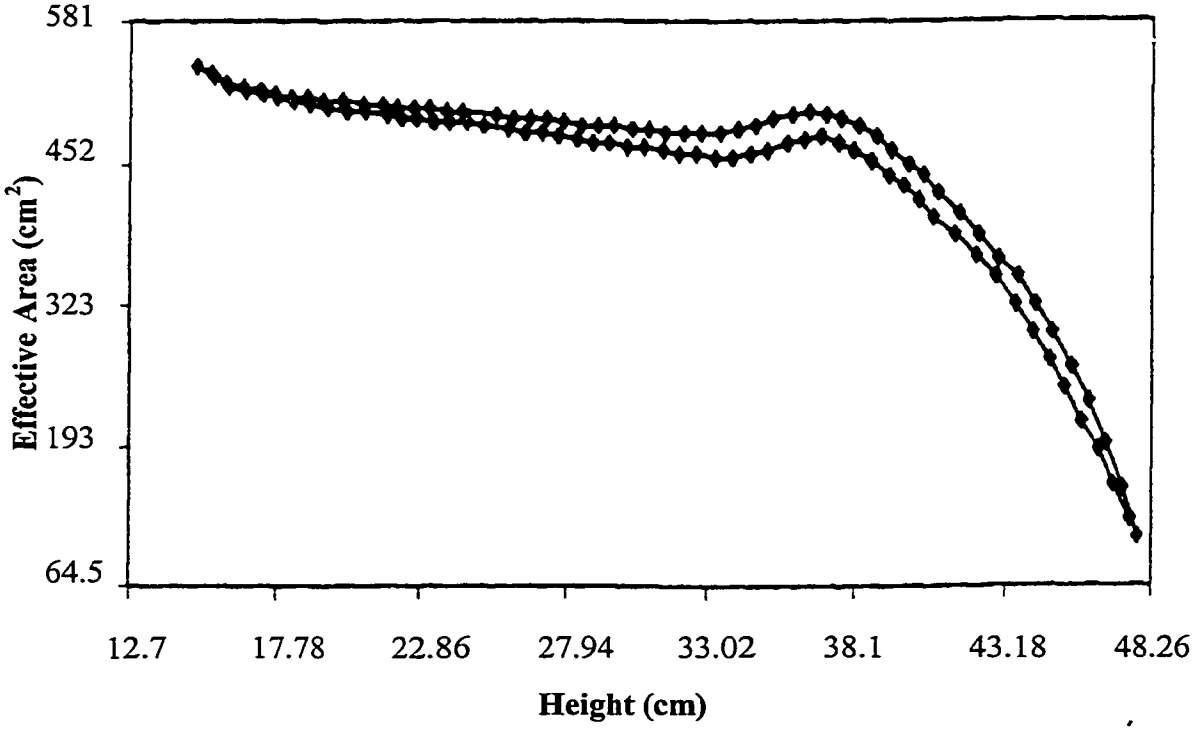

Figure 2.11: Effective area-displacement characteristics of a rear-axle air spring (Design height = 25.15 cm, Preload = 18.031 kN) [26]

Analytical model of the air spring is next developed based on the experimental data for limited preloads. The static and dynamic force exerted by the bus body on the air bags is balanced by the restoring force developed by the air column inside the air bags. The relationship between the applied and developed restoring force is given in terms of instantaneous pressure and effective area

$$F(\delta_i) = (P_i - P_{atm})\, A_E\, (\delta) \tag{2.24}$$

Where, P_i is the absolute air pressure, P_{atm} is the atmospheric pressure and A_E is the effective area as a function of deflection δ. The instantaneous pressure and effective area are nonlinearly dependent on the bag height, as observed from the measured data. The instantaneous gas pressure may be related to the static charge pressure and the spring deflection using the gas law. Assuming a polytropic process, the instantaneous pressure may be derived as;

$$P_i = \frac{P_{oi} \nu^{\gamma}}{(\nu_o - A_E \delta_i)^{\gamma}} \tag{2.25}$$

Where, P_o is the absolute pressure corresponding to static height, ν_o is the static volume and γ is the polytropic constant. Equations 2.24 and 2.25 are solved to drive the spring force relationship as a function of spring deflection for different values of γ, ranging from 1.0 to 1.4. The results revealed good correlation between the model results and the measured data for $\gamma = 1.1$.

Table 2.1: Coefficients of sixth order polynomial for effective area of the air bags [26]

Spring	Coefficients							J
	k_0	k_1	k_2	k_3	k_4	k_5	k_6	
Front-axle	29.8	-0.4295003	-0.3941464	0.0676160	0.0420375	0.0026782	-0.0009389	0.0838
Rear-axle	75.92	1.6079682	-0.0233256	-0.149985	0.0043246	0.0078929	0.0005359	0.5019

The pressure-deflection and force-deflection characteristics for the air springs are derived using equations 2.25 and 2.22. For the best-suited value of the polytropic constant $\gamma = 1.1$ the results show good correlation with the measured data, as shown in Figures 2.14 and 2.15. The results suggest that the proposed model yield a reasonably good estimation of force-deflection characteristics of the air springs under different preloads.

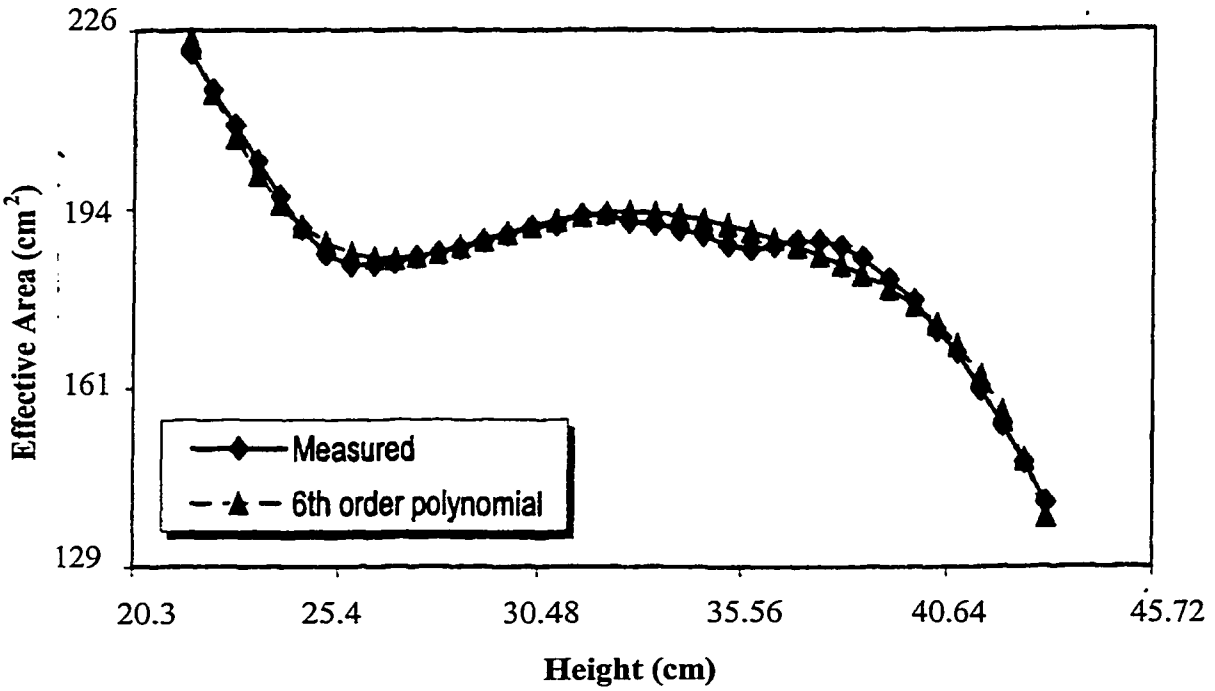

Figure 2.12: Comparison of mean effective area of a front-axle air spring derived from the measured data and that from the polynomial function [26].

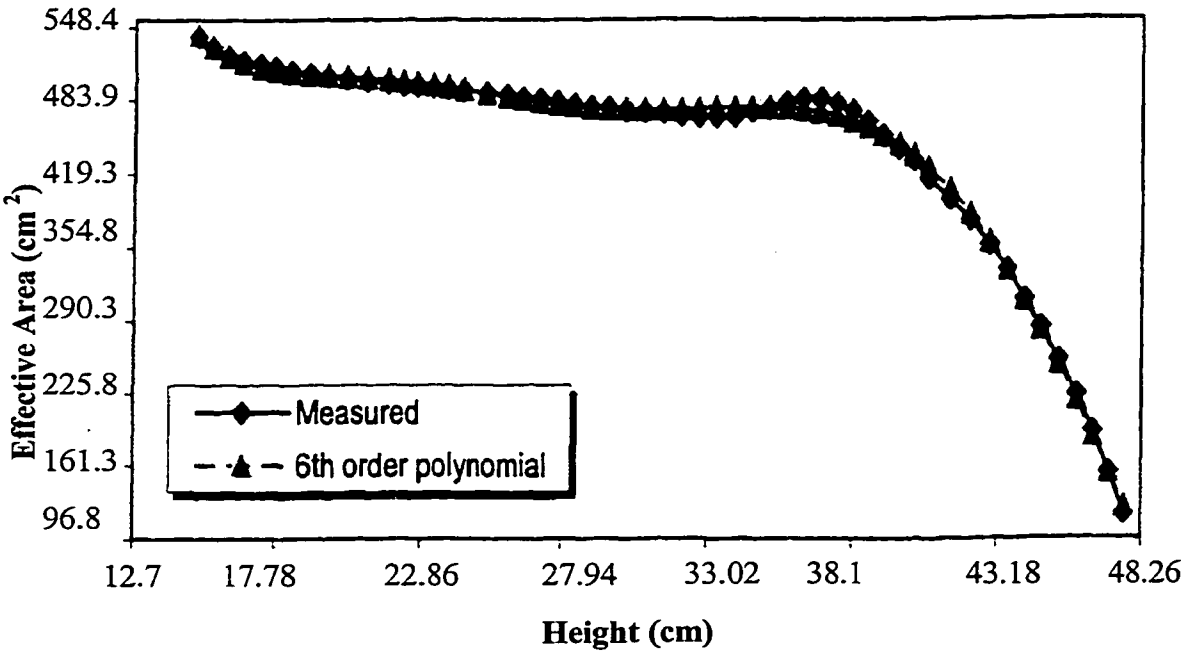

Figure 2.13: Comparison of mean effective area of rear-axle air spring derived from the measured data and that from the polynomial function [26].

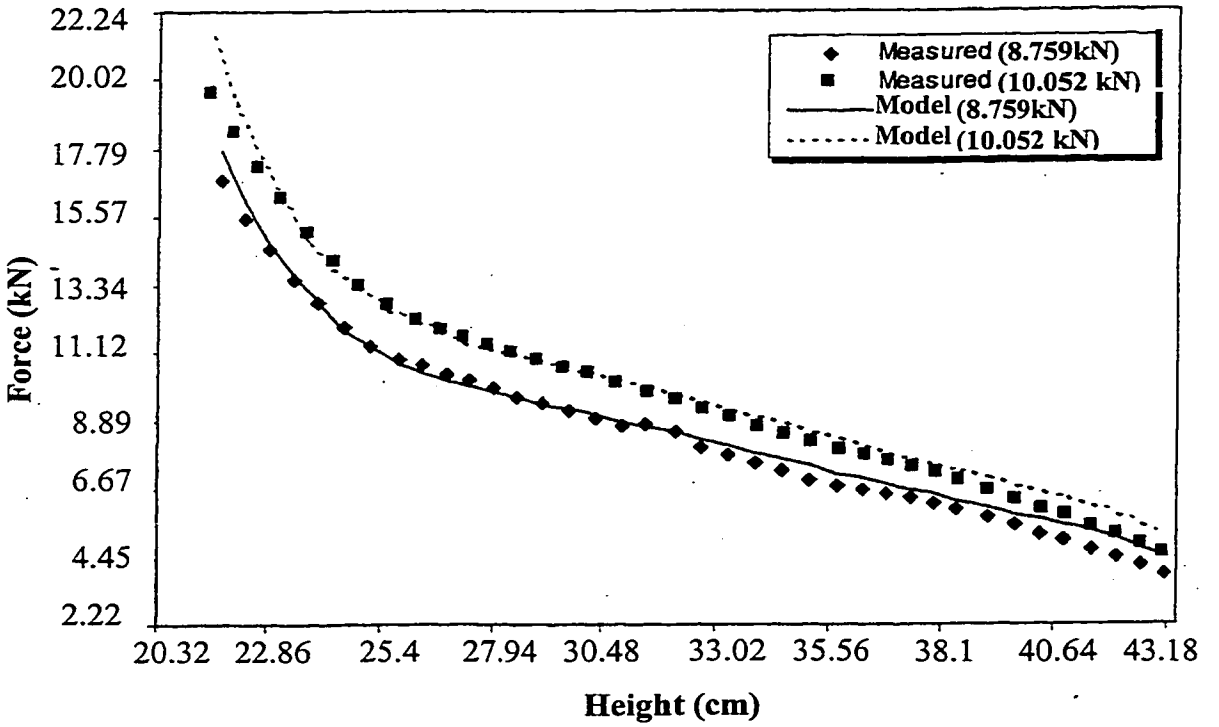

Figure 2.14: Comparison of mean force derived from the measured data and that from the analytical model for front-axle air spring [26].

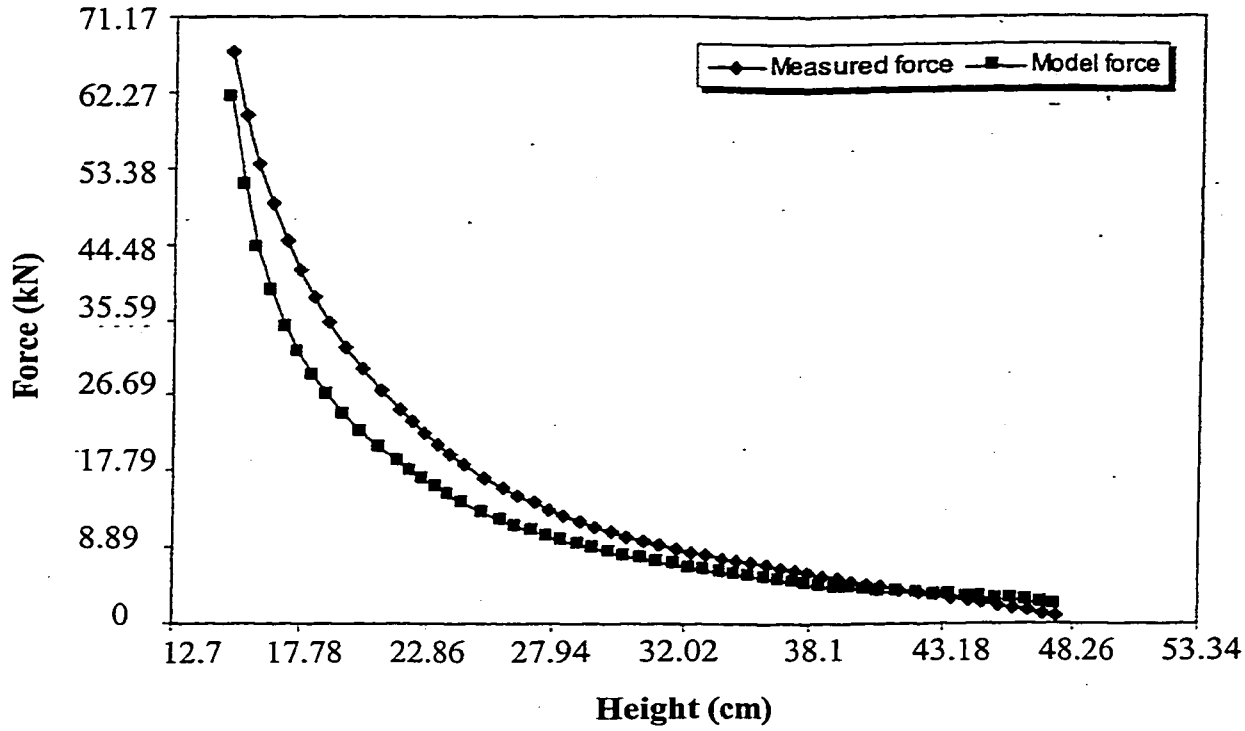

Figure 2.15: Comparison of mean force derived from the measured data and that from the analytical model for rear-axle air spring [26].

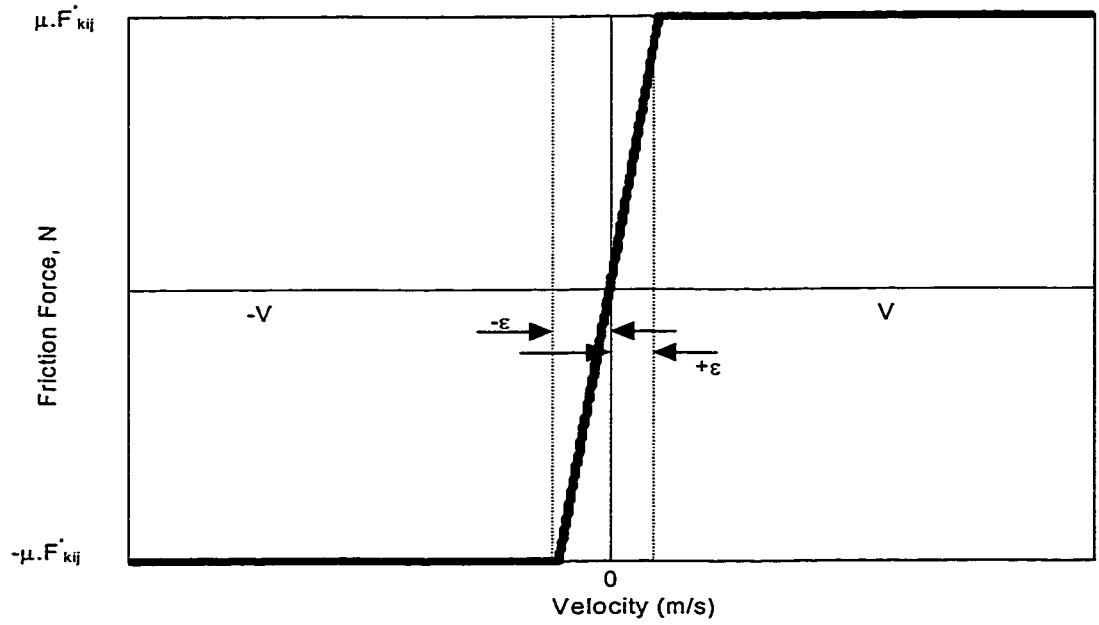

Figure 2.16: Coulomb friction model for friction force due to bushings and linkages

The coulomb friction force due to bushings and linkages is considered to posses friction force characteristics of solid friction. A small viscous band, however, is introduced, as shown in Figure 2.16, in order to reduce the contributions due to discontinuity near zero velocity. The friction force is thus expressed as:

$$F_{Fij} = \mu F'_{kij} \mathrm{Sgn}(V_o) \qquad \text{for } |V_o| > \varepsilon$$

$$F_{Fij} = \frac{\mu F'_{kij}}{\varepsilon}.V \qquad \text{for } |V_o| < \varepsilon \tag{2.26}$$

2.4.2 Damper Model

The dampers employed in vehicle suspension, invariably, exhibit multi-stage-damping properties, which are asymmetric in compression and rebound [22]. The dampers in general yield considerably higher damping forces in rebound, and relatively high damping coefficient at low velocities. The damping coefficients are reduced considerably at higher velocities in order to achieve improved vibration isolation. Laboratory tests were performed to characterize the force-velocity characteristics of dampers employed in the front- and rear-axle suspensions. Figures 2.17 and 2.18 illustrate the measured force-velocity characteristics of front- and rear-axle suspension dampers, respectively. An analysis of the mean force data shows single stage damping in compression and two-stage damping in rebound. The damping force in rebound is considerably larger than that in compression for both dampers. Upon neglecting the hysteresis, the mean force-velocity characteristics are expressed by the following piecewise linear model:

$$F_{cfv} = C_{1f} V_f \quad ; \qquad V_f \geq 0$$

$$F_{cfv} = C_{2f} V_f \; ; \qquad V_{fe} \le V_f \le 0$$

$$F_{cfv} = C_{2f} V_{fe} + C_{3f}(V_f - V_{fe}); \qquad V_f \le V_{fe} \tag{2.27}$$

and

$$F_{crv} = C_{1r} V_r \; ; \qquad V_r \ge 0$$

$$F_{crv} = C_{2r} V_r \; ; \qquad V_{re} \le V_r \le 0$$

$$F_{crv} = C_{2r} V_{re} + C_{3r}(V_r - V_{re}); \qquad V_r \le V_{re} \tag{2.28}$$

Where C_{1f} and C_{1r} are the compression mode damping coefficients of front- and rear-axle suspension dampers, respectively. C_{2f} and C_{2r} are the low speed rebound mode damping coefficients of the front- and rear-axle suspension dampers. C_{3f} and C_{3r} are high-speed rebound damping coefficient. V_{ef} and V_{er} represent the transition velocities, where low speed damping coefficients assume the high-speed coefficient values, respectively. These coefficients, identified from the mean measured data, are presented in Table 2.2. The table also summarizes the magnitudes of seal friction forces identified from the measured force-displacement characteristics [37,43]

The hydraulic forces derived from above equations for the two dampers are compared with the mean measured damping characteristics as shown in Figures 2.17 and 2.18, to demonstrate the validity of the proposed piecewise linear model. The results show that the proposed model can effectively describe the mean force-velocity characteristics of the dampers, while neglecting the hysteretic effects. .

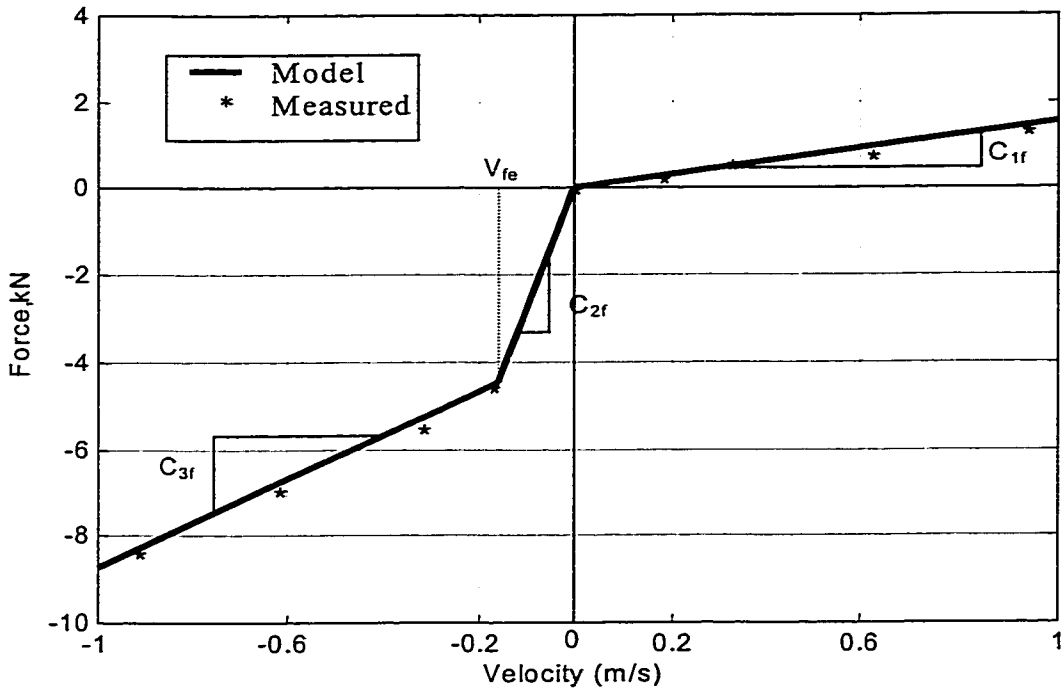

Figure 2.17: Comparison of force-velocity characteristics of the front-axle suspension damper derived from measured data and the proposed model

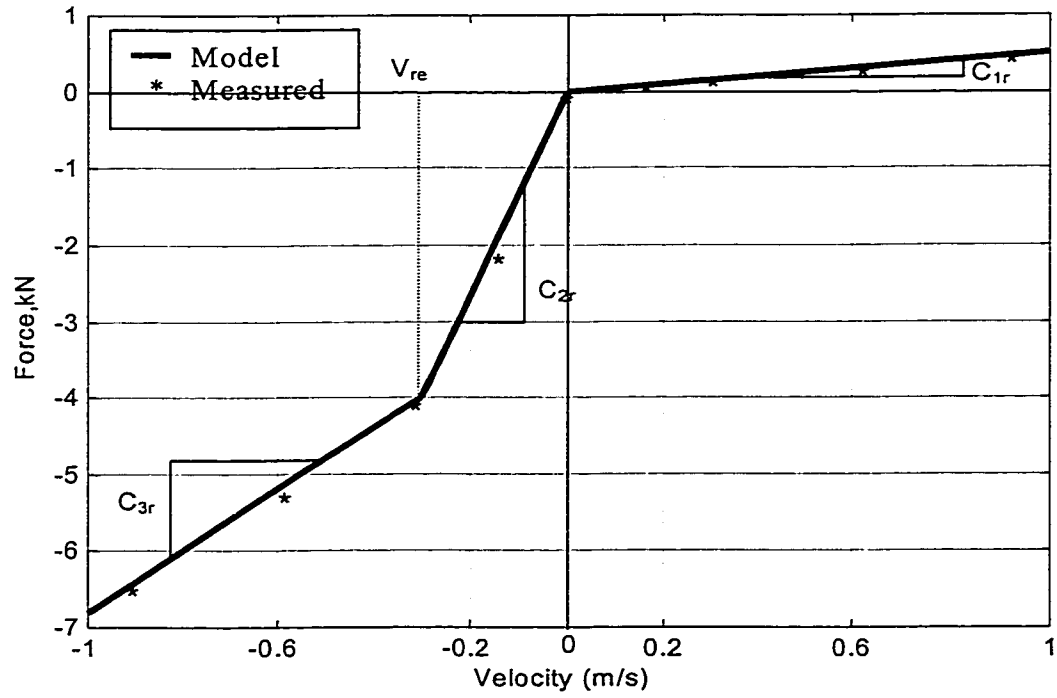

Figure 2.18: Comparison of force-velocity characteristics of the rear-axle suspension damper derived from measured data and the proposed model

2.4.3 Tire Model

As discussed earlier, the stiffness and damping characteristics of tires are related to their design, inflation pressure and static load. In view of wide variations in the inflation pressure and static load, encountered in urban buses, a tire model is derived using the measured force-deflection data acquired from laboratory tests and tire manufacturers. Figure 2.19 illustrates the measured force-deflection properties of a typical bus tire over a wide range of inflation pressure. The results show that the stiffness properties of tires increase with increase in inflation pressure and tire deflection.

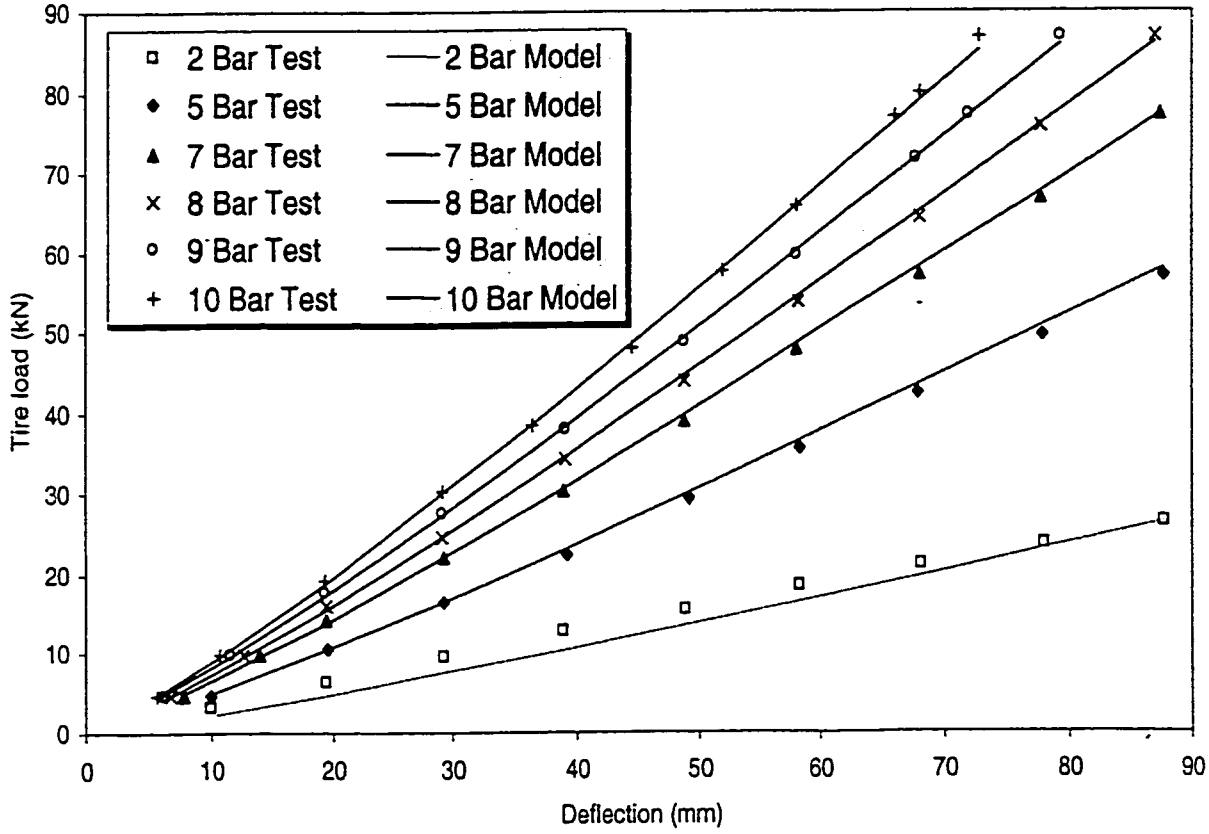

Figure 2.19: Comparison of force-deflection characteristics derived from the regression model with the measured data. (Tire: Michelin 305/70R22.5 XDA TL 152/148 L) [26].

A regression analysis was performed to identify a tire force-deflection model as a function of the inflation pressure. A regression function of the following form was considered [26]

$$F_t(P,\delta_t) = F'_t.P^a.\ \delta^b{}_t\ ;\quad \delta_t \geq 0; \tag{2.29}$$

Where $F_t(P,\delta_t)$ is the tire force as a function of inflation pressure P and deflection δ_t. F'_t, a and b are constant coefficients identified from the measured data and through minimization of the cost function, given by:

$$J = \frac{1}{N_p N_\delta} \sum_{i=1}^{N_p} \sum_{i=1}^{N_\delta} \left[F_t(P_i, \delta_{tij}) - F_{tij}\right]^2 \tag{2.30}$$

Where N_p and N_δ are numbers of pressure and deflection data points available from the measured data, respectively. F_{tij} is the measured force of the tire corresponding to the ith pressure and the jth deflection point. The error function, J, is minimized using Gauss-Newton method to derive the coefficients of the regression model.

2.5 Bus Parameters

The bus parameters taken in this dissertation research for analyses consist of inertial parameters, suspension component parameters, and geometric parameters of the bus and suspension system. Moments of inertia are calculated using the parameters supplied by the manufacturer of the candidate bus. The data for suspension components such as dampers, air springs and tires, obtained through laboratory testing is available at CONCAVE research center. The geometric data and physical constants related to the candidate bus have been provided by the bus manufacturer Nova Bus Corporation.

Parameter	Empty bus	Half load	Full load
Bus Body Mass (m_b) (Kg)	10532	13116	15632
Bus Body Moment of Inertia (I_b) (Kg-m^2)	124194.8	150024.2	175034.9
Front Axle Mass (m_f) (Kg)	700	700	700
Front Axle Moment of Inertia (I_f)(Kg-m^2)	23.87	23.87	23.87
Rear Axle Mass (m_r) (Kg)	1250	1250	1250
Rear Axle Moment of Inertia (I_r) (Kg-m^2)	37.68	37.68	37.68
Tire spring constant, K_t (N/m)	921607	921607	921607
Tire damping constant, C_t (Ns/m)	800	800	800
Acceleration due to gravity, g (m/s^2)	9.80655	9.80655	9.80655
Atmospheric pressure, P (pa)	101325	101325	101325
Front damper friction force, F_{ff}(N)	87.5	87.5	87.5
Rear damper friction force, F_{rf} (N)	60	60	60
Joint friction coefficient, F_{fkaf}, F_{fkar}	0.01	0.01	0.01
Polytropic Index of air inside air bag, γ	1.1	1.1	1.1
Rear-Front spring to rear axle c.g, l_{arl} (m)	0.6955	0.6955	0.6955
Rear-Rear spring to rear axle c.g, l_{ar2k} (m)	0.6955	0.6955	0.6955
Rear-Rear damper to rear axle c.g, l_{ar2c} (m)	0.7209	0.7209	0.7209
Front damper to front axle c.g. l_{af0} (m)	0.0381	0.0381	0.0381
Front-Rear spring to front axle c.g. l_{afl} (m)	0.2032	0.2032	0.2032
Front-Front spring to front axle c.g. l_{af2} (m)	0.2032	0.2032	0.2032
Rear axle c.g. to bus body c.g. l_{br0} (m)	2.11	2.286	2.401
Rear-Front spring to bus c.g. l_{brl} (m)	1.414	1.59	0.1705
Rear-Rear spring to bus c.g. l_{br2k} (m)	2.806	2.982	3.097
Rear-Rear damper to bus c.g. l_{br2c} (m)	2.8314	3.0074	3.1224
Front damper to bus body c.g. l_{bf0} (m)	4.09	3.914	3.799
Front-Rear spring to bus body c.g. l_{bfl} (m)	3.988	3.8124	3.697
Front-Front spring to bus body c.g. l_{bf2} (m)	4.192	4.016	3.901
Rear spring upper joint to ground h_{bd} (m)	1.065	1.065	1.065
Front Lower joint from ground h_{af} (m)	0.605	0.605	0.605
Ground to bus body c.g. h_{bcg} (m)	1.173	1.173	1.173
Ground to front axle c.g. h_{fcg} (m)	0.465	0.465	0.465
Wheel base, b (m)	6.2	6.2	6.2

Table 2.2: Bus data provided by Nova Bus Corporation

2.6 Road Profile Characterization

The dynamic characteristics of the road vehicle, and thus the dynamic wheel loads and ride quality are strongly related to the road profile. The roads are known to randomly exhibit randomly distributed roughness. A number of studies have established that road roughness closely follows a Gaussian distribution, and proposed spatial spectral density functions to characterize the mean roughness profiles of various roads. The power spectral density (PSD) of the roughness of two different Montreal City roads is illustrated in Figure 2.20 among the available six road roughness data for Montreal City roads. There has been a multitude of devices for measuring pavement roughness, being broadly grouped into profilometer-type and response-type [5].

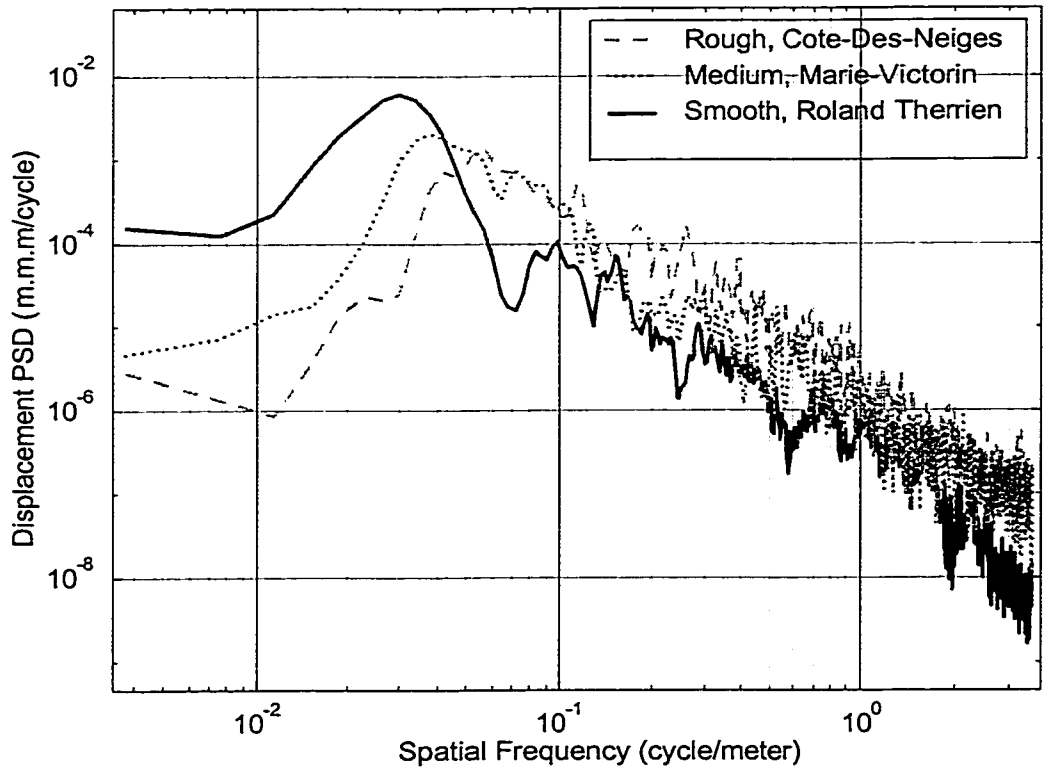

Figure 2.20: Displacement power spectral density of smooth, medium and rough Montreal roads

Also there has been a variety of indices for summarizing and reporting pavement roughness. Damien [53] reported the roughness profiles of various Ontario roads, ranging from extremely smooth to very rough roads. In this model three different roads are analyzed, referred to as smooth, medium rough and rough roads. From the PSD plots above it is clear that Cote-Des-Neiges is the roughest road of all the six roads considered in the analysis. The smooth road is Roland Therrien (South) whereas Marie Victorin is medium rough, which is in between the two extremes of rough and smooth roads.

2.7 Summary

The bus data is provided by the bus manufacturer Nova Bus Corporation and is tabulated in Table 2.2. The components of the bus are modeled as non-linear components. Experimental data related to the components is available and the analytical models are derived. The analytical model for the whole bus system consisting of two axles and a bus body with driver/passenger load is formulated and the equations of motions are accordingly derived. The road roughness of six different roads is characterized in terms of PSD. In the six road profiles three are taken for further study on the basis of roughness and characterized as smooth, rough and medium rough roads. This road profile serves for the dynamic analysis of the bus using random input taken from any of these road profiles.

CHAPTER 3

VALIDATION OF PITCH-PLANE BUS MODEL AND PERFORMANCE MEASURES

3.1 Introduction

Analytical simulation for realistic performance analysis of any system necessitates good characterization of each component, accurate model parameters, and true description of external excitations to the system. In the development of the analytical model, however, number of assumptions are made to simplify the problem and estimation of some parameters and component characteristics are inevitable. It is therefore, an important task to validate the developed model, which is vital to gain confidence in reliability of the analytical investigation using computer based tools. Attempts are made in this section to validate the pitch plane urban bus model developed in chapter 2. The validity of the candidate bus pitch-plane model, relies upon accurate identification of various inertial and geometric parameters, static and dynamic characteristics of component and road roughness. The inertial and geometric properties of the candidate bus are identified and taken from the data supplied by the bus manufacturer and users. The tire and suspension components are most important bus components for dynamic analysis. The tires and suspension properties are established by laboratory experiments and component modeling is presented in chapter 2. While the roughness characteristics of highways and secondary roads have been extensively measured and analyzed [51,53] the roughness properties of urban roads have not been reported. The roughness data of

different secondary roads are thus taken from the data available at CONCAVE research center for different segments of Montreal city roads. Road roughness are characterized based on displacement data in terms of smooth, medium and rough roads and are used as analytical input to the six degree of freedom pitch-plane model of the bus. The roughness displacement time history data of six Montreal roads are thus analyzed to derive representative road spectra based upon the PSD of vertical input displacement as presented in chapter 2.

The validation is carried out in several stages. A free vibration analysis of the pitch plane model is first carried out for both undamped and damped conditions. The natural frequencies and damping ratios are established for both empty and fully loaded conditions. Time history responses are then obtained for sinusoidal inputs of different amplitudes and frequencies corresponding to different forward speeds. These results are primarily obtained for in depth understanding of the bus dynamics and response in terms of bounce and pitch motions for qualitative validation.

Attempts are then made for quantitative validation of pitch plane model with experimental results available from full-scale bus tested on Montreal roads. Experiments were recently carried out by CONCAVE research center with a full-scale modern urban bus. The test results are analyzed to establish PSD of vertical responses at the driver and passenger seats, and magnitude of tire loads. Simulation results from pitch plane model for smooth and rough road for different speeds are compared with the experimental results to demonstrate the effectiveness of the pitch-plane model. Results are compared in terms of responses at driver and selected passenger locations. Comparisons are also made in terms of PSD of tire forces on different roads and load conditions. This chapter finally

describes various performance measures that are used in subsequent performance evaluation and parametric study of urban bus driver- and road-friendliness.

3.2 Identification of Model Parameters

The validation of the pitch-plane model developed in Chapter 2 is carried out against road test of a medium urban bus over selected Montreal roads. The design drawings available for the bus thus utilized to identify the dimensional and inertial parameters required to analyze the pitch-plane model of the bus. The mass and inertial parameters were estimated from the axle load data, corresponding to empty and fully loaded bus. The overall pitch moments of inertia of the sprung and unsprung masses are estimated from moments of inertia of the passengers, sprung mass, axles and tires. The pitch moment of inertia due to a passenger is estimated assuming uniform rectangular solid shell, while the sprung mass is also assumed to consist of a rectangular solid shell. The pitch moment of inertia of each sprung mass is estimated by considering the axle as a uniform cylinder with two uniform circular plates. Figure 3.1.a illustrates the principle of estimating the pitch moment of inertia for the sprung mass.

$$I_{c.g} = I_{g.c} + my^2 \tag{3.1}$$

$$I_{c.g} = I_{g.c} + mz^2 \tag{3.2}$$

where, $I_{c.g}$ and $I_{g.c}$ are moment of inertia about the center of gravity of the bus and moment of inertia about the centroidal axis of each side. Where the pitch moment for each side is determined by assuming rectangular section. The pitch moment with respect to the bus c.g. is determined using parallel axis theorem. Similarly, the pitch moment of

inertia for the axles (unsprung mass) are determined using Figures 3.1.b and 3.1.c by combining the inertia of each component about the c.g. of the axle.

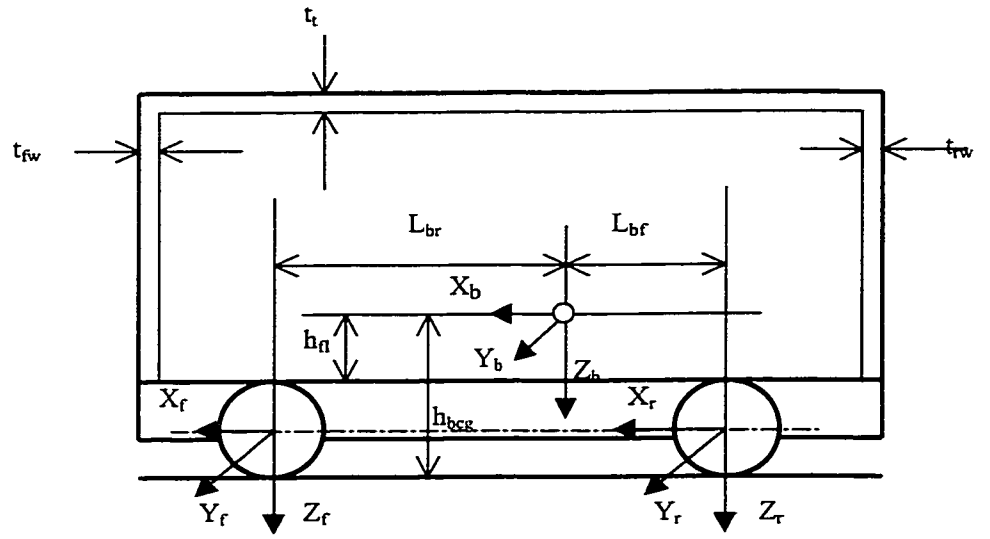

Figure 3.1.a: Sprung mass, bus body

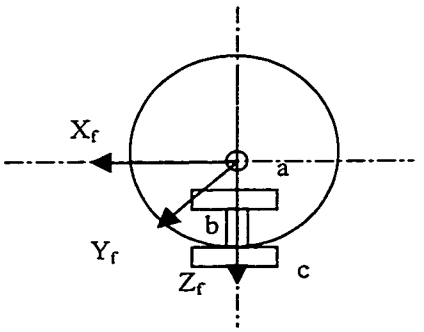

Figure 3.1.b: Front Axle

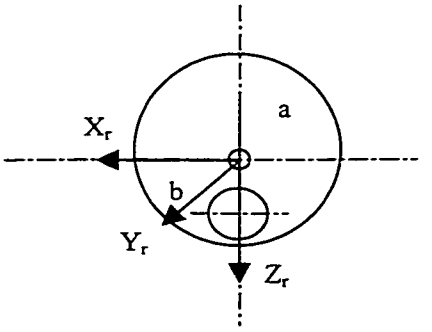

Figure 3.1.c: Rear Axle

Figure 3.1: Principle of estimating pitch moments of inertia

In doing so, the total I_{cg} for the empty bus can be expressed as:

$$I_{cg|total} = I_{cg|floor} + I_{cg|front-wall} + I_{cg|rear-wall} + I_{cg|roof} + I_{cg|side-wall} \quad (3.3)$$

And for the full bus

$$I_{cg|total} = I_{emptybus} + I_{cg|seated+standing} \quad (3.4)$$

The pitch mass moment of inertia I_{cg}, can also be evaluated by the empirical formula [29] given as:

$$I_{cg} = [(W_f + 0.4W_r)X_{11}^2 + 0.6W_r(L - X_{11})^2]/g \quad (3.5)$$

where, X_{11} is horizontal distance from bus c.g to the front axle, W_f is the front axle load, W_r is the rear axle load and W_s is the total sprung weight.

The front wheel load W_f can be expressed in terms of X_{11}, W_s and L as:

$$W_f = W_s(L - X_{11})/L \quad (3.6)$$

The rear wheel load W_r can be expressed in terms of X_{11}, W_s and L as:

$$W_r = W_s - W_f = W_s(X_{11}/L) \quad (3.7)$$

The pitch moment of inertia for the sprung mass estimated based on cubic shell assumption and the emperical relation [30] were found to be within 5%. Since no emperical relation is available for axle, the pitch moments of inertia for the axle are obtained based on simplification in terms of components and paralled axis theorem.

The pitch mass moment of inertia for the unsprung masses, are based on Figures 3.1.b and 3.1.c which show geometry of axles section. The front-axle consists of an 'I' beam as axle and two discs, whereas the rear-axle consists of a solid circular axle and two discs. The estimated inertial parameters of the candidate bus are summarized in Table 2.2 along with geometric and physical parameters for empty, half and fully loaded conditions. Table 3.1 summarizes the air springs, dampers and possible tires used for the candidate bus. The tire used in the analytical model is Michelin 305/70R22.5 XDA.

Application	Air Spring	Shock Absorber	Tire
Front Axle	1R08-036	Arvin_T712	Michelin 305/70R22.5 XDA Michelin 305/70R22.5 XZU Goodyear 305/70R22.5
Rear Axle	1R11-130	Arvin_T801	Michelin 305/70R22.5 XDA Michelin 305/70R22.5 XZU Goodyear 305/70R22.5

Table 3.1: Suspension components employed in front- and rear-axle of the candidate bus

The parameters established in this section and presented in Table 2.2 are used to carryout validation of the pitch plane model presented in chapter 2. Validations are carried out in stages starting with a free vibration analysis of the model. Free vibration analysis provides important system behavior in terms of natural frequencies, damping ratios and deflection modes of the model. Non-linear bus model incorporating nonlinear components such as air springs, dampers and the tires, is utilized for validation against road test data.

3.3 Free Vibration Analysis

Vehicle system ride performance and dynamic wheel load are strongly related to the vibration frequencies and modes of vibration, and thus dependent on the free vibration characteristics of the system.

The vehicle response is comprised of various different modes associated with the bounce, pitch, roll and lateral motions of sprung and unsprung masses. The bus model formulated in the previous chapter is therefore analyzed for its free vibration performance in the vertical and pitch modes. An eigenvalue analysis is carried out in order to

determine the natural frequencies and principal deflection modes of the bus model. For free vibration analysis all nonlinear components are linearized about their working points to facilitate the eigenvalue solution.

Free vibration analysis of pitch-plane candidate bus model comprising one sprung and two unsprung masses will provide important information regarding their bounce and pitch natural frequencies. Some of these results can be readily compared with those observed during road test of the candidate bus. The following sections present the analysis and results for undamped and damped natural frequencies and associated modes for both empty and fully loaded conditions.

3.3.1 Free-Vibration Analysis of Undamped Bus Model

Undamped free vibration analysis provides important insight on the natural frequencies associated with various dynamic modes. For this purpose, the equations of motion derived in chapter 2 are rewritten by setting all damping parameter and inputs to zero. The equations then can be represented in matrix form as:

$$[M]\{\ddot{z}\} + [K]\{z\} = \{0\} \tag{3.8}$$

Where M is the mass matrix containing six mass and inertia properties. K is the stiffness matrix containing linearized stiffness properties of suspension and tires. The eigenvalue problem for the undamped system of equation (3.8) can be formulated as [40]:

$$[A - \lambda_i I]\{\psi_i\} = \{0\} \tag{3.9}$$

where, $[A] = [M]^{-1}[K]$ is the dynamic matrix of the general eigenvalue problem, and [I] is an identity matrix. λ_i are eigenvalues, and $\{\psi_i\}$ is the eigenvector corresponding to the eigenvalue λ_i.

The eigen solution of dynamic matrix [A] is obtained using polyeig Matlab routine, which yields six pair of complex conjugate eigenvalues. The complex eigenvalue is used to obtain the natural frequencies from:

$$\omega_{ni} = \sqrt{\lambda_i} \tag{3.10}$$

where the mode i is determined from the corresponding eigenvectors.

The undamped free vibration results corresponding to unloaded and fully loaded candidate bus parameters presented in Table 2.2 are shown in Tables 3.2 and 3.3. respectively. As the results show, the highest natural frequencies correspond to these of unsprung mass pitch due to small moments of inertia and large effective pitch stiffness. The bounce natural frequency for the unsprung masses are around 9 Hz which is typical for such vehicles. The bounce and pitch natural frequencies of the sprung mass around 1Hz is due to large mass and inertia on soft suspensions. Comparison of empty and fully loaded bus natural frequencies demonstrate an increase for unsprung masses due to increase in effective stiffness, whereas there is a decrease in sprung mass natural frequencies due to increase in mass.

A comparison of natural frequencies with those of the observed during test necessitates an analysis of damped-free vibration as presented in the following subsection.

3.3.2 Damped Free-Vibration Analysis

Free vibration analysis of the six DOF pitch plane model is carried out for damped case. The equations of motion for damped free vibration are obtained by setting

DOF	f_n (Hz)
Rear-Axle pitch, θ_r	14.463
Front-Axle pitch, θ_f	10.516
Front-Axle bounce, z_f	8.9198
Rear-Axle bounce, z_r	8.5764
Bus Body bounce, z_b	1.1837
Bus Body pitch, θ_b	0.9739

Table 3.2: Natural frequencies an empty bus

DOF	f_n (Hz)
Rear-Axle pitch, θ_r	16.7
Front-Axle pitch, θ_f	12.494
Front-Axle bounce, z_f	9.0786
Rear-Axle bounce, z_r	8.744
Bus Body bounce, z_b	1.0631
Bus Body pitch, θ_b	0.7658

Table 3.3: Natural frequencies of a fully loaded bus

the inputs to zero. The equation of motion derived in chapter 2 can then be rearranged in the following form:

$$M\ddot{Z} + C\dot{Z} + KZ = 0 \tag{3.11}$$

Where $Z^T = \{Z_b, \theta_b, Z_f, \theta_f, Z_r, \theta_r\}$ are the response variables. M, C and K are 6x6 mass, damping and stiffness matrices containing masses, linearized damping and linearized stiffness parameters. Based on the equations derived in chapter 2, the elements of these matrices are presented in Appendix A. The linearized equation (3.11) can be represented in standard eigenvalue problem in matrix form as [57]:

$$[A_D - \lambda_D I]\{\psi_D\} = \{0\} \tag{3.12}$$

where the dynamic matrix is of size 12x12:

$$A_D = [M^*]^{-1}[K^*]$$

$$M^* = \begin{bmatrix} I & 0 \\ 0 & M \end{bmatrix} \qquad K^* = \begin{bmatrix} 0 & I \\ -K & -C \end{bmatrix}$$

$\{\psi_D\}^T$ is the response vector containing $\{\dot{Z}, Z\}$ that describes the mode shape.

Eigenvalue solution of the dynamic matrix $[A_D]$ is obtained using MATLAB polyeig routine which yields 12 complex conjugate eigenvalues of the form.

$$\mu_i = \alpha_i + i\beta_i$$

From the real and imaginary components of the eigenvalue, system characteristics such as natural frequency, damped natural frequency and damping ratio can be defined as:

$$\omega_{ni} = \sqrt{\alpha_i^2 + \beta_i^2} \tag{3.13}$$

$$\omega_{di} = |\beta_i| \tag{3.14}$$

$$\zeta_i = -\frac{\alpha_i}{\omega_{ni}} = \sqrt{1 - \left(\frac{\omega_{di}}{\omega_{ni}}\right)^2} \tag{3.15}$$

The computed damped eigenvalues and corresponding natural frequency, damped frequency and damping ratio for the empty bus model are shown in Table 3.4. The results corresponding to fully loaded bus are shown in Table 3.5. The frequencies obtained from undamped and damped free vibration analysis are very close to the dominent experimental frequencies observed during the tests. Furthermore, these frequencies can readily be compared with transmissibility presented later in this chapter.

From the damping ratios of different modes it is evident that for the suspension parameters used, the unsprung mass modes posseses large damping ratio, whereas, the sprung mass damping ratios are negligible. For the fully loaded case, the damping ratio is lower for unsprung mass modes and higer for the sprung mass modes. This is attributed to the fact that the effective suspension damping parameter for fully loaded bus is higher than empty case. The characteristics of the components used in the canditate bus system are utilitzed in the simulation of the pitch plane model demonstrated effectively through a frequency response analysis presented in the following subsection.

3.4 Deterministic Frequency Response Analysis

Steady state frequency response analysis for deterministic input is a highly useful tool that provides important insight in the dynamic performance of the system over a frequency range. Although highly efficient tools exist for efficient frequency response analysis of linear systems, they lack in effeciveness to predict the actual performance of a nonlinear system. Specially, if the nonlinearities are strong and amplitude of excitation is wide.

DOF	f_n (Hz)	Eigenvalue	f_d (Hz)	ξ
Front-Axle pitch, θ_f	10.516	-16.65 ± 63.944i	10.177	0.25197
Rear-Axle pitch, θ_r	14.406	-3.3503 ± 90.452i	14.396	0.037015
Bus Body pitch, θ_b	0.97614	-0.005296 ± 6.1333i	0.97614	≈ 0
Front-Axle bounce, z_f	8.9191	-2.306 ± 55.993i	8.9116	0.042869
Rear-Axle bounce, z_r	8.6015	-4.0452 ± 53.893i	8.5773	0.041148
Bus Body bounce, z_b	1.1823	-0.002837 ± 7.4288i	1.1823	≈ 0

Table 3.4: Empty bus damped natural frequencies and damping ratios

DOF	f_n (Hz)	Eigenvalue	f_d (Hz)	ξ
Front-Axle pitch, θ_f	12.494	-16.646 ± 76.718i	12.21	0.21204
Rear-Axle pitch, θ_r	16.658	-3.3637 ± 104.61i	16.65	0.032137
Bus Body pitch, θ_b	0.76559	-0.066759 ± 4.8099i	0.76552	0.013878
Front-Axle bounce, z_f	9.0783	-2.3019 ± 56.994i	9.0709	0.040356
Rear-Axle bounce, z_r	8.7626	-4.0158 ± 54.91i	8.7393	0.072938
Bus Body bounce, z_b	1.0639	-0.13894 ± 6.6832i	1.0637	0.020785

Table 3.5: Fully loaded bus damped natural frequencies and damping ratios

The pitch-plane model of the modern urban bus developed in chapter 2 posses strong nonlinearities due to suspension and tire properties. Solutions are thus obtained utilizing numerical integration tool to obtain time reponse to sinusoidal inputs. From the steady-state time response, the transmissibilities for each response variable are obtained to establish the frequency response of the pitch-plane bus model in the frequency range of 0-20Hz. The description of excitation and transmissibility reponses for bus body and axles are presented and discussed in the following subsections.

3.4.1 Sinusoidal Excitations

As discussed above, this part of the investigation deals with deterministic frequency response. For this, sinusoidal in-phase and out-of-phase excitation in the form of:

$$Z_{ti}(t) = \overline{Z}\sin\omega t \qquad \text{where, i = f, r...} \tag{3.16}$$

is applied to the front- and rear-tires where amplitude of excitation $\overline{Z}$, is 1 cm for medium level excitation and 3 cm for high level excitation. The frequency of excitation may be treated as a function of bus forward speed U for a fixed wavelength λ such that:

$$\omega = 2\pi\frac{U}{\lambda} \tag{3.17}$$

For a given velocity, therefore, the input to rear-axle can be defined with a time delay such that

$$Z_{ti}(t) = \overline{Z}\sin\omega(t+\tau) \tag{3.18}$$

Where the time delay τ is defined as a function of wheel base b, and velocity of bus U, as:

$$\tau = \frac{b}{U} \tag{3.19}$$

The above sinusoidal inputs for the front and rear tires with time delay are used to describe the motion and velocity of the tires in the equations of motion presented in chapter 2. The sinusoidal results are presented and discussed in the following subsection.

3.4.2 Response to Sinusoidal Excitations

The six differential equations of motion for the pitch plane bus model along with the inputs for front and rear tires described above are solved simultaneously in time domain. Fourth-order Runge-Kutta method with variable time step as a function of frequency is used to obtain time response for each of the masses of the system. Simulations are carried out for long enough to ensure that the response has reached its steady-state level. The steady-state peak responses are utilized to compute the transmissibility for each response. Number of simulations has been carried out at different constant forward velocity to obtain the frequency response in the range of 0 to 20 Hz.

The simulated transmissibility responses as RMS bounce acceleration ratio corresponding to empty bus parameters presented in Table 2.2 and nonlinear component models presented in chapter 2 are shown in Figures 3.2 and 3.3. Figure 3.2 presents the transmissibility responses of sprung and unsprung masses in 0-20 Hz frequency range. As shown, the bus body bounce response has a dominant frequency around 1 Hz corresponding to its bounce natural frequency, and a secondary peak around 10 Hz which corresponds to the natural frequencies of the axles. Similarly, the axles exhibit a dominant frequency around 10 Hz corresponding to their natural frequencies and a

secondary peak around 1 Hz which corresponds to sprung mass natural frequency. These natural frequencies are close to the natural frequencies for the modes established from free vibration analysis of the linearized model. The natural frequencies exhibited by the nonlinear frequency response are found to be slightly higher than those predicted by linear free vibration analysis. This can be attributed to hardening nature of the nonlinear air springs used on such velocities.

The results in Figure 3.2 further show natural frequency acceleration transmissibility ratio of 1.75 for the bus body. The natural frequency acceleration transmissibility ratio for the front- and rear-axles are found to be 3.35 and 2.6 respectively. The lower transmissibility ratio for the fornt-axle is attributed to the fact that the candidate bus posseses an effective damping ratio for the front-axle which is higher than that of rear-axle as demonstrated by damped free vibration analysis.

The RMS pitch acceleration transmissibility defined as $\frac{\ddot{\theta}_i}{\ddot{Z}_r}$, for the bus body as well as front and rear axles are shown in Figure 3.3. These results show a dominant frequency around 1 Hz corresponding to the pitch natural frequency of the bus body. The results further show highly damped peaks at frequencies greater than 10 Hz which correspond to the pitch resonance frequencies of the front-and rear-axles. These results further confirm the findings of damped free vibration analysis. As it was found, the damping ratio for pitch motion of front-axle is significantly higher than that of rear-axle which resulted in suspression of peaks for the front-axle in pitch motions.

Similar to empty bus parameters, transmissibility responses are also obtained for parameters correosponding to fully loaded bus and nonlinear components. Figures 3.4 and 3.5 present the RMS bounce and pitch acceleration ratio for the fully loaded case. As

these results show, the trends are very similar to those of empty case and conforms to the damping ratio trend observed in the damped free vibration analysis for the fully loaded case. Comparison of Figures 3.2 and 3.4 indicates that there is an increase in peak responses for all masses when the bus is fully loaded. This was predicted from damped free vibration analysis for the axles. However, for the sprung mass (bus body), both transmissibility and natural frequency found to increase for the case of fully loaded which is contrary to the trend observed from linear free vibration analysis. This behavior can be attributed to the strong nonlinearity in both suspension siffness and damping. The results presented in Figure 3.5 for the pitch acceleration transmissibility demonstrate same trend where the increase in pitch natural frequency for both axles are apparent for fully loaded case. This result further demostrates that the effective damping ratio for axle pitch motion is reduced when fully loaded condition is considered.

From the results of nonlinear deterministic response, while assessing the acceleration transmissibilities, it can be concluded that the linear free vibration analysis is more accurate for modes associated with unsprung masses. Whereas, the nonlinearity has significant influence on the modes associated with the sprung mass since the transmissibility ratio variations in linear analysis do not agree with the non-linear analysis for the sprung mass.

3.5 Random Response and Validation

Performance analysis through computer simulation on analytical models necessitates accurate characterization of model perameters, component characterization and description of excitations. The analytical model developed for this investigation

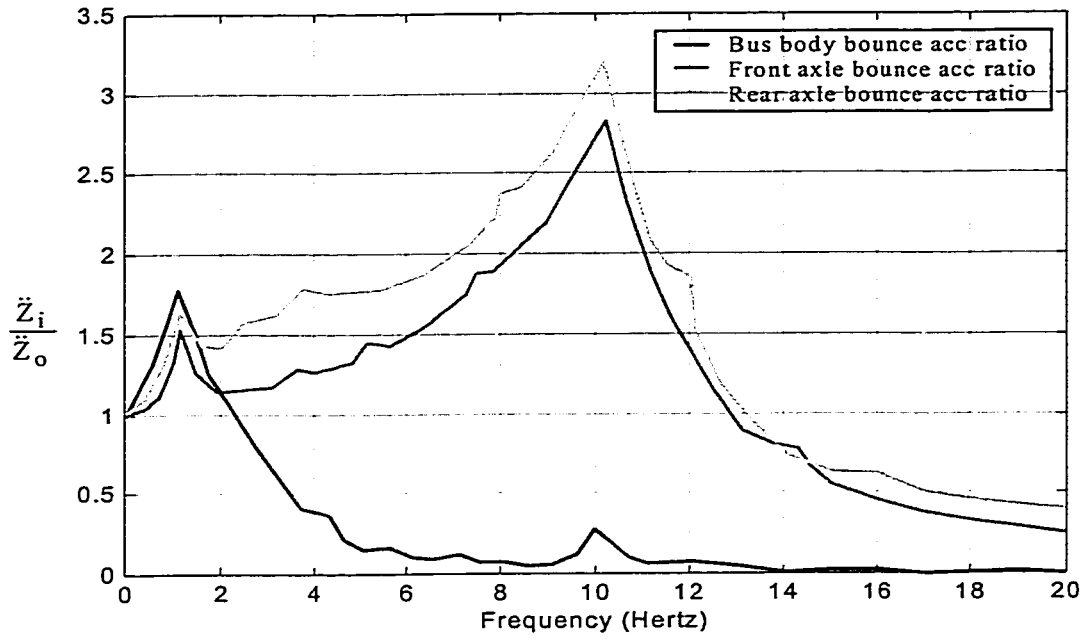

Figure 3.2: Frequency vs rms bounce acceleration ratio $\left(\frac{\ddot{Z}_i}{\ddot{Z}_o}\right)$ of empty bus body & axles

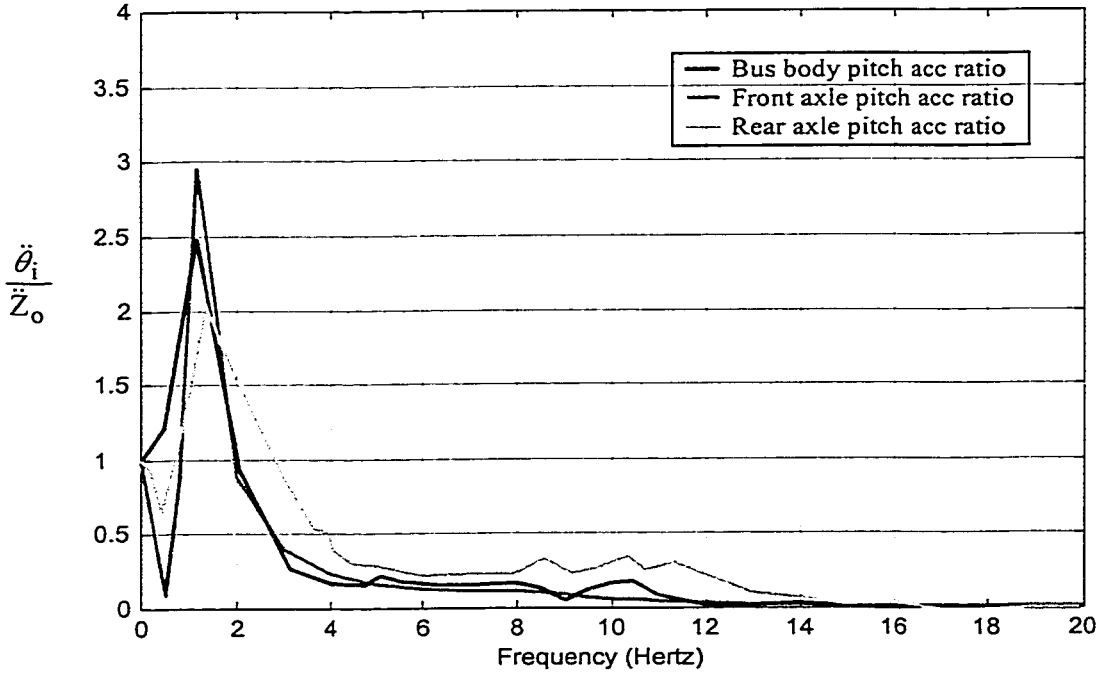

Figure 3.3: Frequency vs rms pitch acceleration ratio $\left(\frac{\ddot{\theta}_i}{\ddot{Z}_o}\right)$ of empty bus body and axles

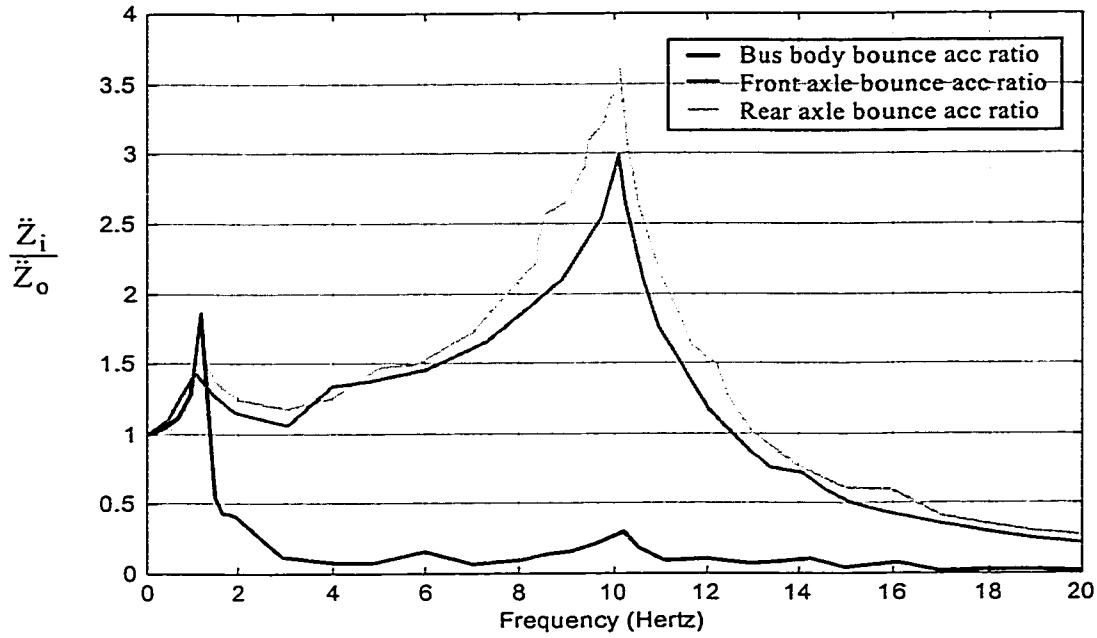

Figure 3.4: Frequency vs rms bounce acceleration ratio $\left(\frac{\ddot{Z}_i}{\ddot{Z}_o}\right)$ of full bus body and axles

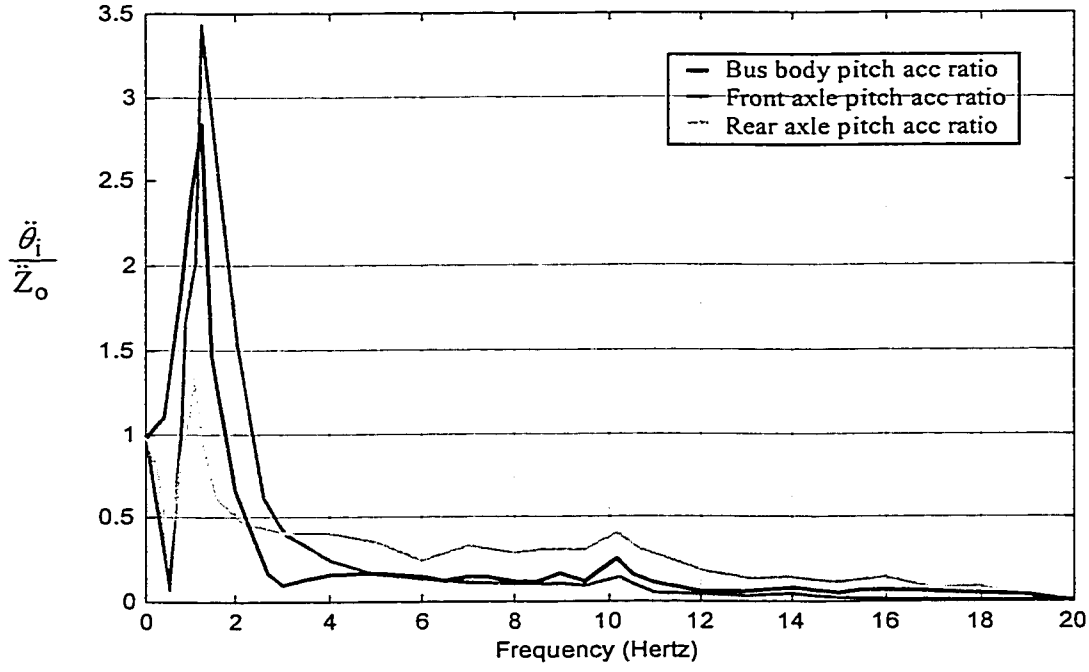

Figure 3.5: Frequency vs rms pitch acceleration ratio $\left(\frac{\ddot{\theta}_i}{\ddot{Z}_o}\right)$ of full bus body and axles

consists of number of simplifying assumptions including in-plane modeling. All efforts are however, made to include reasonably accurate component models such as air spring, suspension damping and tire characteristics as described in chapter 2.

The analyses of the pitch-plane model presented so far in this chapter, namely free vibration analysis and deterministic frequency responses provide important insight and trends on the behavior and dynamic responses. Attempts are further made to carryout a quantitative validation for responses at different locations of the bus and tire loads. Such validation, although difficult, is essential to gain confidence in the investigation and to develop reliable computer based design tools in evaluating driver and road friendliness of such vehicles. For this, experimental results available at CONCAVE research centre from a full scale modern urban bus tested on Montreal roads are utilized. The mass-inertia and component properties for the candidate bus considered in this investigation are presented earlier in the thesis and are used for analysis presented in this chapter. The following sections describe the selected road inputs, the measurement locations and the comparison of measured and simulated results for response and axle load.

3.5.1 Characterization of Road Roughness

While the roughness characteristics of highways and secondary roads have been extensively measured and analyzed [42], the roughness properties of urban roads are reported in literature. In recent investigation at CONCAVE research center, measurements were taken on six different roads in and around Montreal. Three such roads characterized as "smooth" (Roland Therrien), "rough" (Cote-Des-Neiges) and "medium rough" (Marie Victorin) are used in this investigation. The displacement power

spectral density (PSD) for the three roads established in chapter 2 are represented in Figure 2.20.

3.5.2 Measurement Locations

During the testing of candidate bus on the given roads, measurements were taken at the driver and various passenger seat locations. Tests were performed at 30, 50 and 70 km/h for empty and fully loaded conditions. The measurement locations and there positions with respect to bus center of gravity are shown in Figure 3.6. The pitch plane coordinates from these locations are summarized in Table 3.6. As shown in the table, the position coordinate for each location with respect to the centre of gravity (cg) changes with loading due to fixed location for seats and change in bus c.g. location.

3.5.3 Driver and Road Friendliness Performance under Random Road Excitation

A typical dynamic response of the pitch-plane urban bus model in terms of driver and road friendliness are obtained for candidate bus parameters. Excitations used is that of a medium rough road (Marie-Victorin) at half loaded condition. Figures 3.7 and 3.8 show the PSD of bounce acceleration, and tire force respectively. The results shown in Figure 3.17 are for the acceleration response of the driver and four passenger seats defined in Table 3.6. These results show that the seats which are farther from the center of gravity of the bus yield larger vertical acceleration due to pitching motion. Among all the locations considered, the largest acceleration level is found to be at the driver's seat around the pitch and bounce resonance frequency of the bus body.

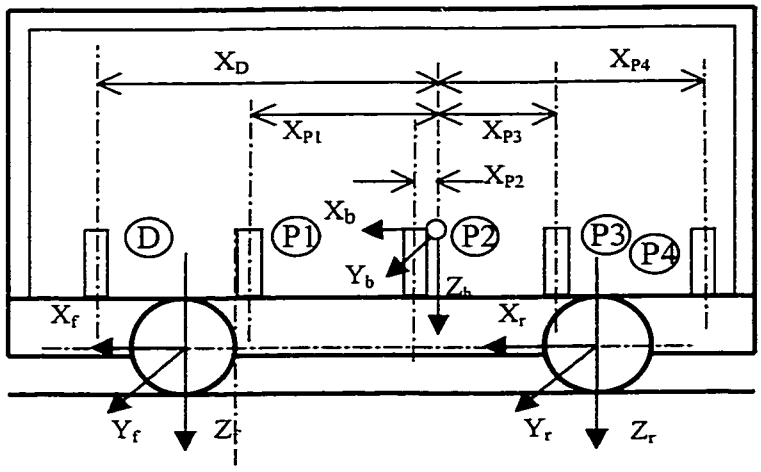

Figure 3.6: Bus body showing location of driver and passenger seats

Load	Coordinate	Driver	Passenger 1	Passenger 2	Passenger 3	Passenger 4
Empty	X (m)	6.06	2.8275	0.6177	-0.8564	-4.8342
	Z (m)	0.795	0.795	0.795	0.795	0.795
Full	X (m)	5.769	2.5365	0.3267	-1.1474	-5.1252
	Z (m)	0.7845	0.7845	0.7845	0.7845	0.7845

Table 3.6: Coordinates of driver and passengers in bus body frame of reference

These results further show that the wheel hop and its resonance frequency around 10 Hz have negligible influence on the bounce acceleration levels at the driver and passenger seats. Other results obtained but not shown indicate that rough road increases higher frequency components and so the wheel hop increases while running on rougher roads. When the speed is increased the acceleration response of the seat specially at the frequency of bus body resonance increases. Since the higher frequency components are smaller in magnitude, increasing the speed does not effect wheel hop magnitude

substantially. Similar to bounce acceleration responses, the pitch response of the analytical and experimental investigation is shown in Figure 3.12. The result shows the simulated response in comparison with the envelope of the measured response. The pitch acceleration which any seat receives is the same as for the bus body so the pitch acceleration PSD is plotted for the bus body only.

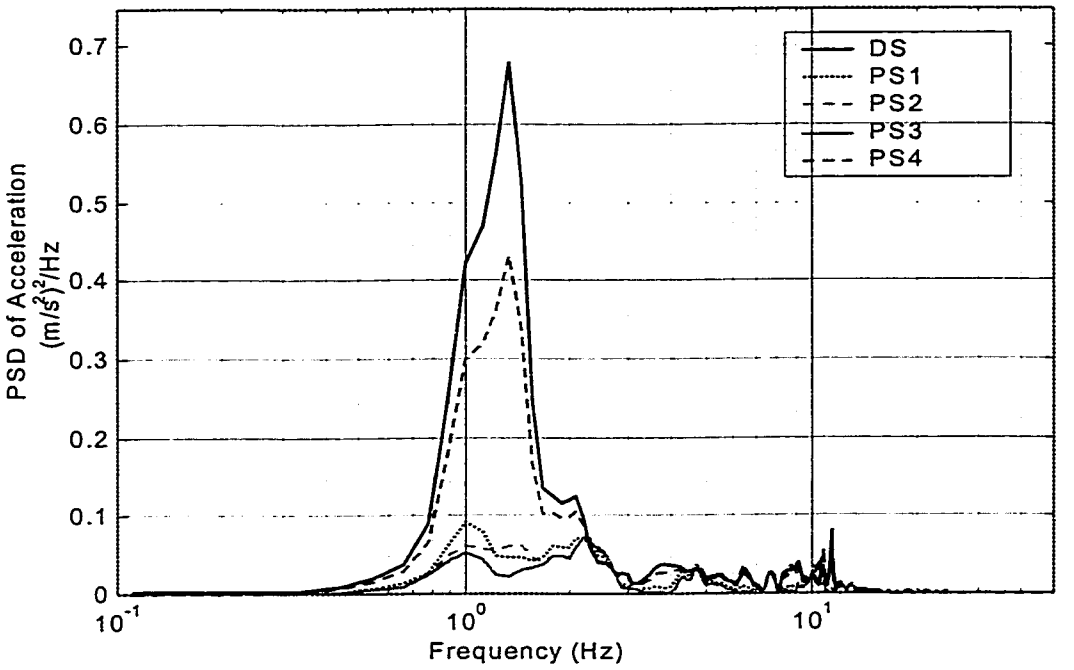

Figure 3.7: Analytical plot of frequency vs PSD of vertical acceleration at driver and four passenger seats for half loaded bus on medium rough road at 50 km/h

The simulations are then repeated for rough and smooth roads in order to obtain bounce responses at selected seat locations. The bounce and pitch responses from the simulated results are compared with those obtained experimentally and are presented in the following subsection.

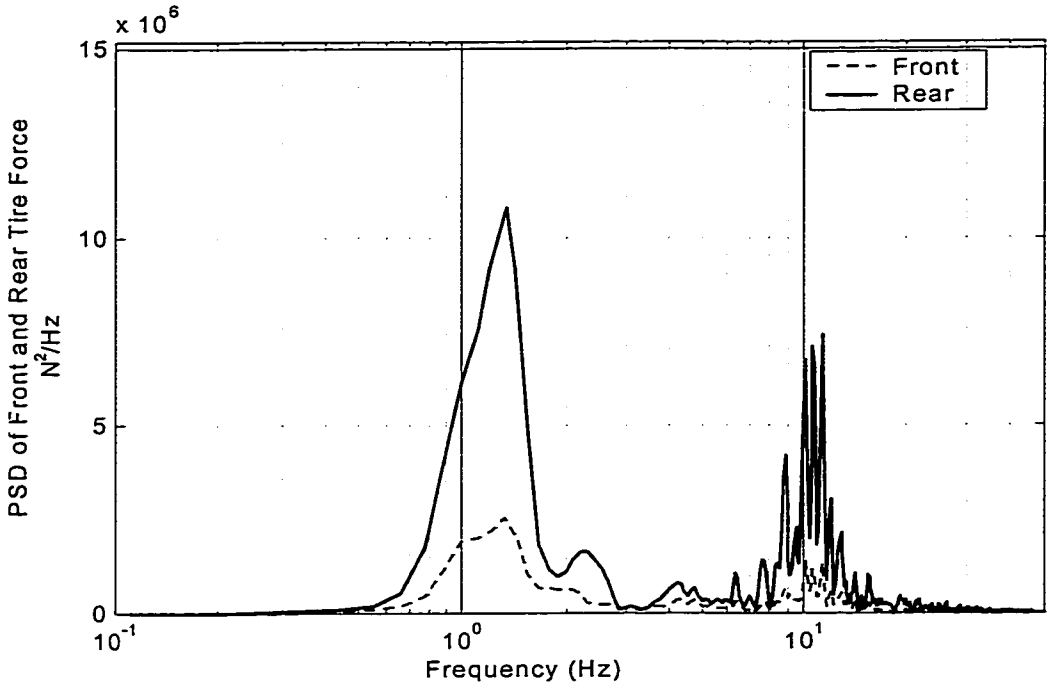

Figure 3.8: Plot of frequency vs PSD of front and rear tire force for half loaded bus at 50 km/h on medium rough road

3.5.4 Validation of Analytical Pitch-Plane Model

Simulation of the pitch-plane candidate bus model is carried out utilizing the time history of road inputs for the measured smooth and rough roads. Same input is used for front and rear axles with appropriate time delay based on bus forward speed. The responses at the driver and four passenger locations are obtained based on the bounce and pitch responses of the bus body using kinematic relations shown in Figure 3.6.

Simulations are performed at a vehicle speed of 30km/hr, 50km/hr and 70km/hr and the vertical acceleration response at the driver seat and four passenger seats location is evaluated using kinematics transformation. The PSD estimates of the resulting vertical and pitch responses are obtained using FFT (Fast Fourier Transform) technique, and compared with the measured data to examine the validity of the pitch plane model. For a

given speed and road, the measured time history was divided into four segments. The PSD for each segment was combined for the speed and road to obtain an envelope of maximum and minimum values for a test run.

Figure 3.9 presents a comparison of vertical acceleration PSD response of driver seat of the candidate bus, running at 30 km/hr, subject to rough road excitations. The result shows the simulated response along with the mean and maximum envelope of the measured response. The vertical acceleration response of the driver and passenger seats reveals trends similar to those observed from the envelopes of the measured data. The peak values occur in the vicinity of sprung and unsprung mass resonant frequencies near 1Hz and 10Hz, that are also comparable to the frequencies of predominant vertical vibrations observed from the envelope. Similar comparisons are made for locations corresponding to passenger seat 1 and 4 as presented in Figures 3.10 and 3.11, respectively. As the results show, the passenger seat responses also stay in between the maximum and mean measured acceleration at those seats in almost entire range of frequency. The main difference observed is in the wheel hop frequency, which is around 10.8 Hz for the measured data instead of around 10.0 Hz predicted by analytical model. This difference in frequency may be due to the difference between tire and suspension component characteristics of those actually fitted to the test bus and the model. In general the model response characteristics show similar frequencies of predominant vibration as those obtained experimentally. The experimental results, however, show several other peaks over the range of frequency. These are attributed to the fact that actual bus consists of numerous components with flexibility that are not included in simple model. Among various components the beaming effect of the bus body is the one which has its

fundamental resonance frequency around 6 Hz. There are also contributions due to engine and drive train vibrations, which have higher natural frequencies around or above 20 Hz.

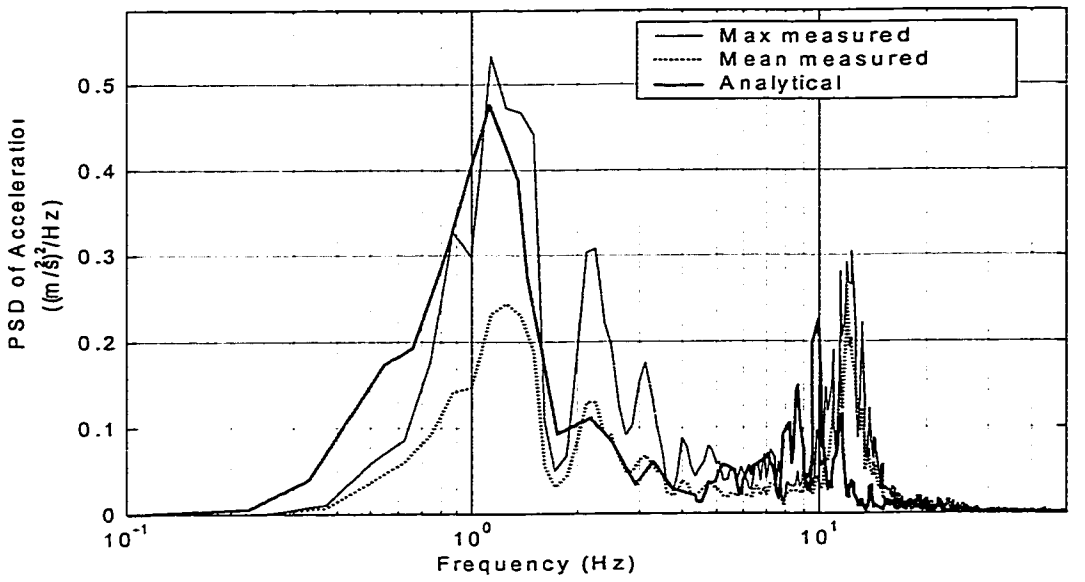

Figure 3.9: Maximum measured, mean measured and analytical plot of frequency vs PSD of vertical acceleration at driver seat for rough road at 30 km/h

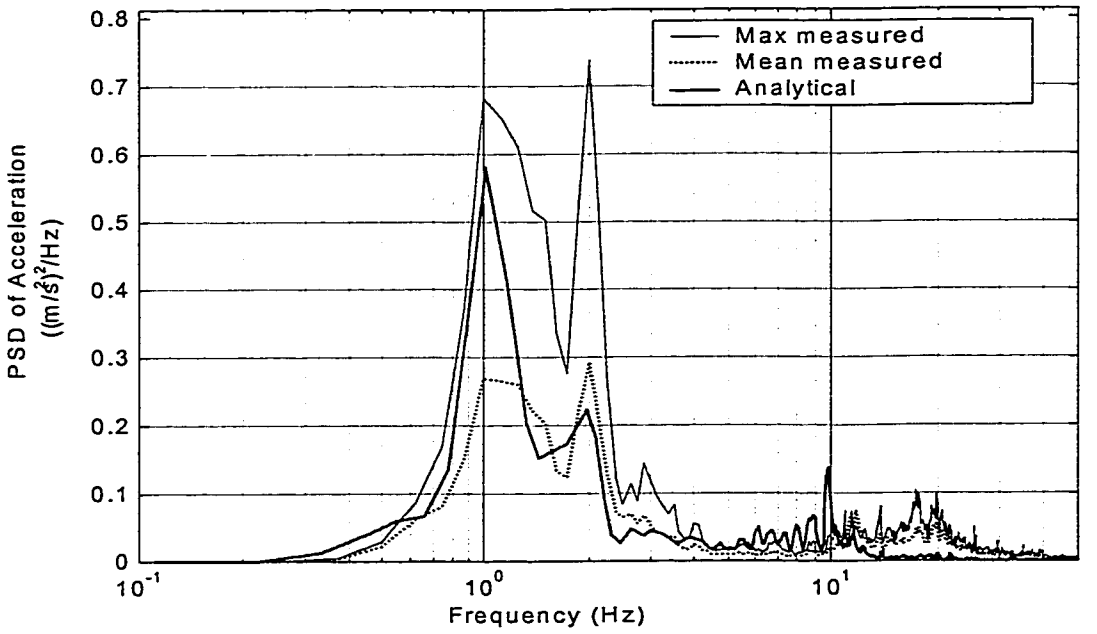

Figure 3.10: Maximum measured, mean measured and analytical plot of frequency vs PSD of vertical acceleration at passenger # 1 seat for rough road at 30 km/h

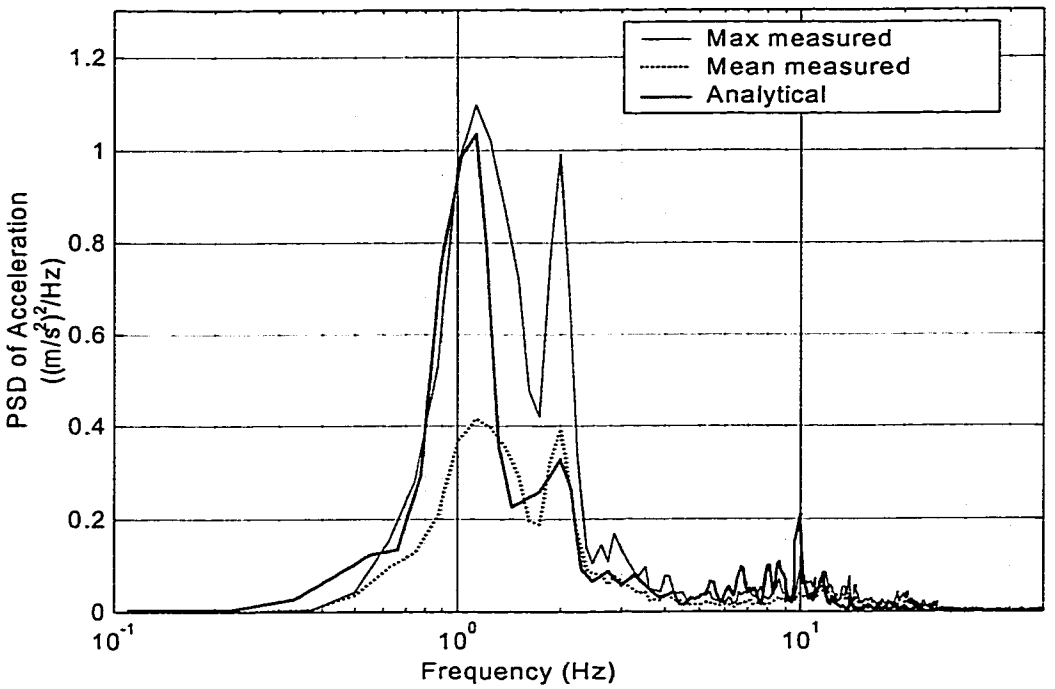

Figure 3.11: Maximum measured, mean measured and analytical plot of frequency vs PSD of vertical acceleration at passenger no 4 seat for rough road at 30 km/h

The pitch acceleration response of the driver and passenger seat shows a similar trend observed from the envelopes of the measured data. The peak values occur near 1 Hz and 10 Hz which are the sprung and unsprung mass resonant frequencies and are comparable with the measured envelope peaks. There is a slight difference in the peak near the wheel hop frequency, which shows 10.15 Hz for the measured envelope whereas it is 10.0 Hz for the simulated result. The cause of this slight difference in frequency peaks at wheel hop may be the same as for the bounce mode that is, the difference in tire and suspension component characteristics used in the model and the actual tire and suspension component specifications. The peak around 11.2 Hz is predominant in the measured envelope compared to the simulated model. This difference is due to the fact that in actual bus there are different components which, are not considered in the

mathematical model used for simulation. These component's resonance frequency peaks appear on measured frequency spectrum but not in the model.

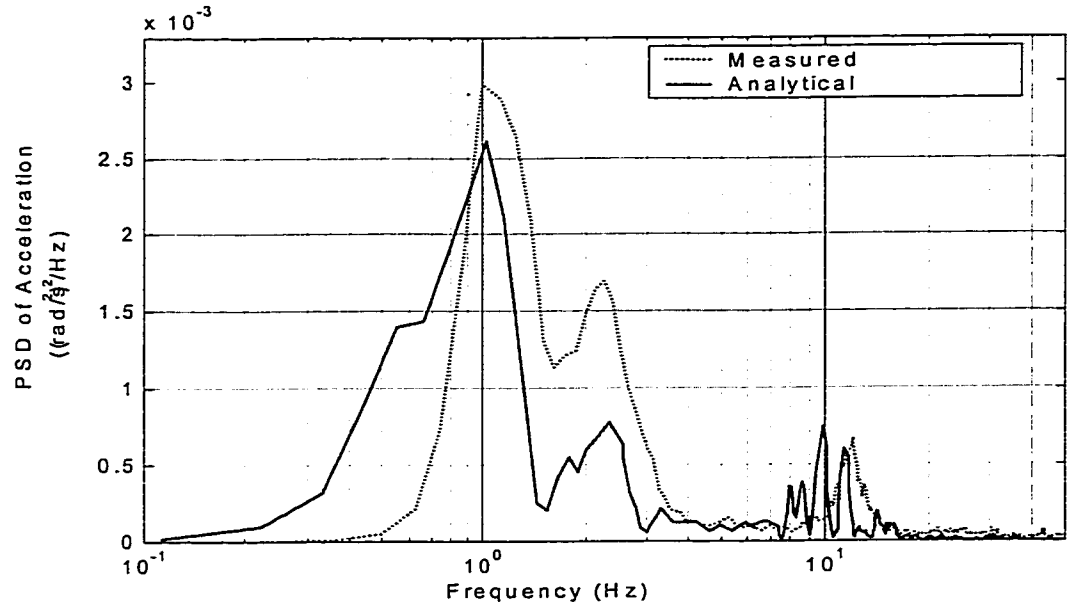

Figure 3.12: Measured and analytical plot of frequency vs PSD of bus body pitch acceleration for rough road at 30 km/h

Similar to rough road responses presented in Figures 3.9 to 3.12, Figures 3.13 to 3.16 present the comparison for smooth road at 30 km/h. It presents a comparison of vertical acceleration PSD response of driver and passenger seats of the candidate bus, running at 30 km/h subject to smooth road excitations, with mean and maximum measured data envelopes. The PSD of vertical acceleration at the driver seat for the bus running on smooth road shows the same overall trend but there is a marked difference in the peak values at sprung and unsprung mass resonance frequencies. The unsprung mass resonance frequency peak for smooth road is about one fourth of the unsprung mass resonance peak for the rough road. There is further higher reduction in the peak at sprung mass resonance (hop) frequency, which is, less than one sixth for the smooth road compared to the rough road. This reduction in the PSD peak values at sprung and

unsprung mass signifies the effect of lower displacement PSD for the smooth road. As with the measured acceleration envelopes for the rough road, other weak frequency components for the smooth road are there but the PSD is negligible. The frequency components of engine, drive train and other high and intermediate frequencies are there but they are visible in the measured envelope and not very significant in the simulated results.

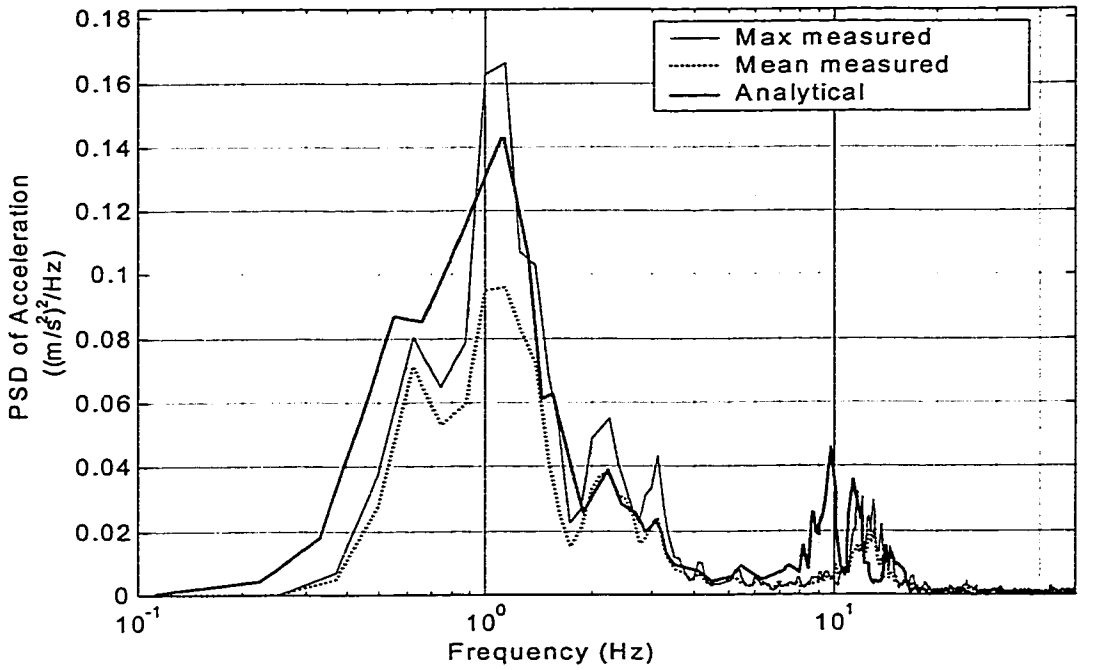

Figure 3.13: Maximum measured, mean measured and analytical plot of frequency vs PSD of vertical acceleration at driver seat for smooth road at 30 km/h

The pitch acceleration response of the bus running at 30 km/h on smooth road shows the same overall trend as it is for the rough road with a significant reduction in the peak PSD values for the bus body. The peak for the sprung mass pitch acceleration PSD for both simulated and measured responses are very close to each other both in frequency and in magnitude.

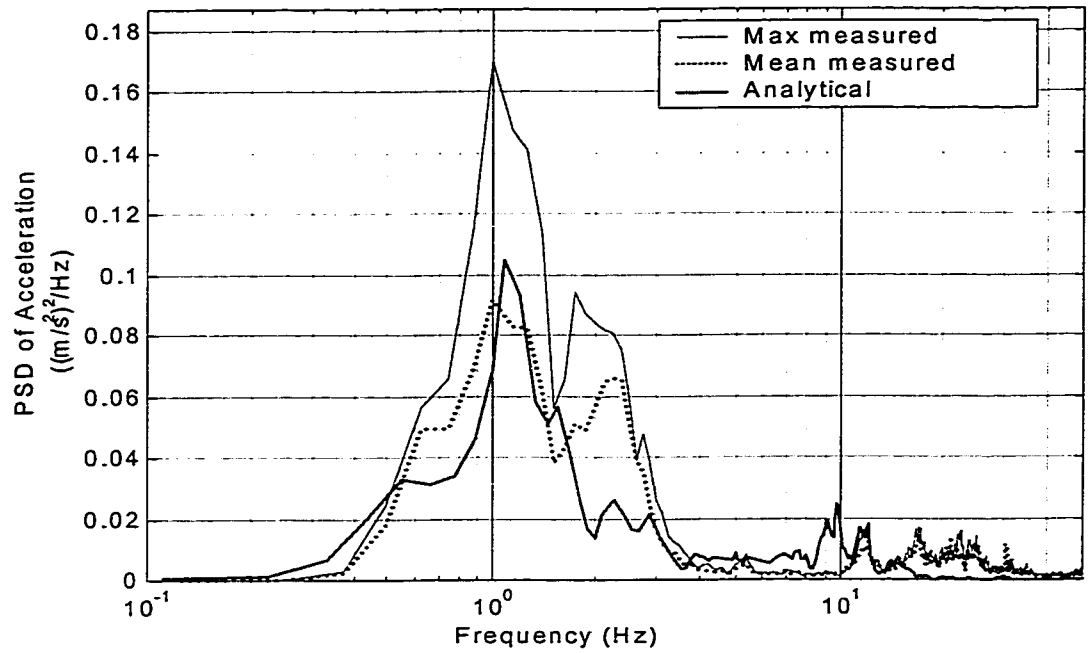

Figure 3.14: Maximum measured, mean measured and analytical plot of frequency vs PSD of vertical acceleration at passenger # 1 seat for smooth road at 30 km/h

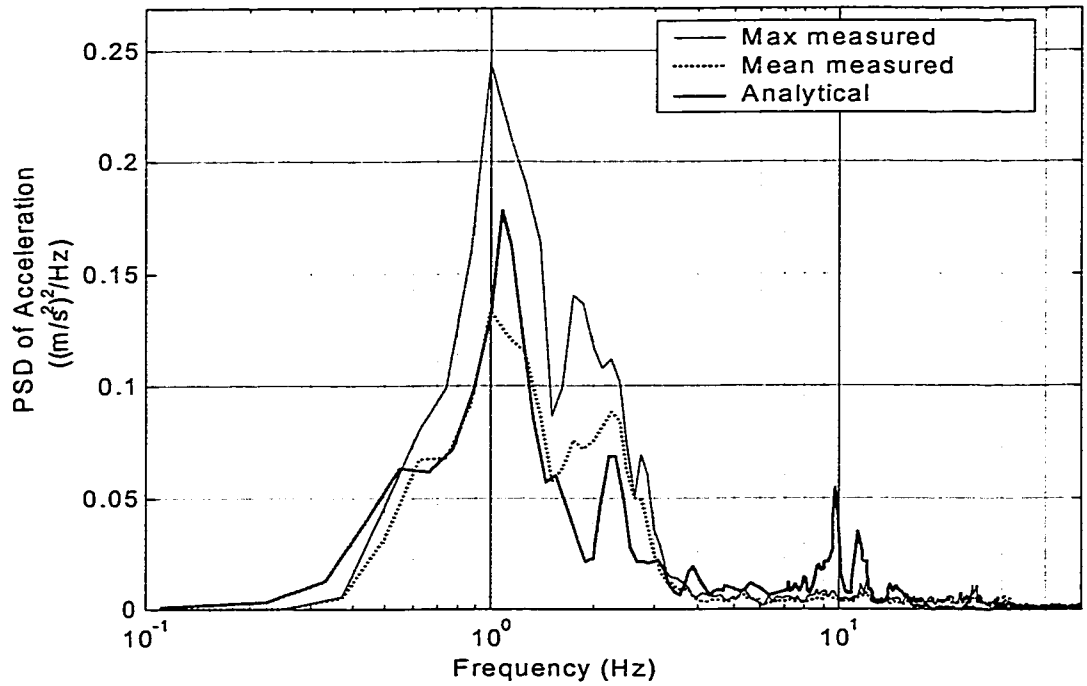

Figure 3.15: Maximum measured, mean measured and analytical plot of frequency vs PSD of vertical acceleration at passenger # 4 seat for smooth road at 30 km/h

The wheel hop frequency is close in magnitude but again there is a slight difference in the frequency, which is 10.1 Hz for the measured envelope and 10 Hz for the analytical model.

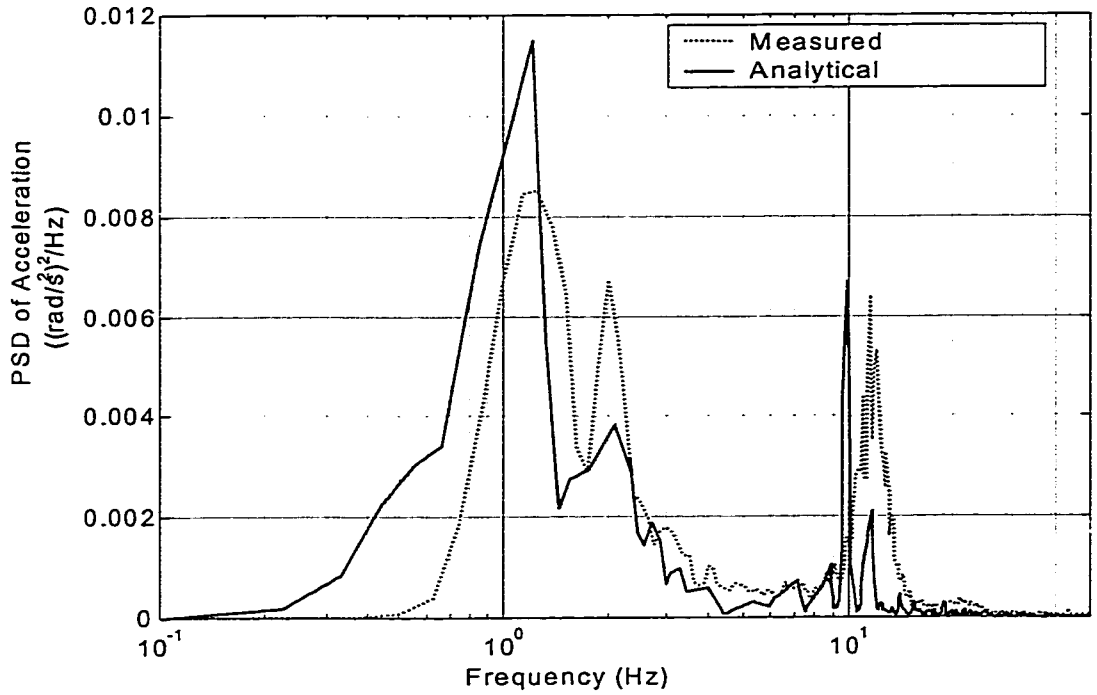

Figure 3.16: Measured and analytical plot of frequency vs PSD of bus body pitch acceleration for smooth road at 30 km/h

3.5.5 Validation of Dynamic Wheel Load Response

The pitch-plane model of urban bus developed in chapter 2 is formulated to establish driver and road friendliness. The road friendliness is a measure of dynamic load imposed on the road by such vehicles. As discussed in the introduction and literature review, urban buses are known to produce significant dynamic wheel loads on urban roads. In this section attempts are made to validate the developed pitch plane model for

its effectiveness in predicting the dynamic wheel load produced by a modern urban bus. For this, available experimental data and conditions are incorporated in the model.

In an experimental investigation, measurements were taken for the dynamic wheel load of urban buses IRC [23]. The measurements were performed on the rear wheels under excitations arising from roads and wooden plank at speeds of 35 km/h and 50 km/h. The tests were performed three times for 35 km/h speed and four times for 50 km/h speed on two different streets. These two streets which were taken for the measurement of dynamic tire forces were different than the streets which were taken for the measurement of acceleration response of the candidate bus. The inertia corrected time histories for left and right wheel forces, measured on two different streets in Montreal, were obtained in order to examine the validity of the pitch-plane model.

An examination of the experimental data reveals that there is a considerable variation in tire force in the vicinity of sprung mass resonance between the left and right wheels. These variations may be due to several reasons such as localized variations in cross-slope of the road, vehicle speed, and contributions due to directional dynamics of the vehicle. Such data for left and right wheel loads may be useful for validation of a 3-D model on a model in roll plane. In this investigation of pitch-plane model, however only rear-axle load may be evaluated.

Furthermore, actual description of the excitations that resulted in the experimental left and right wheel data is not known other than that the road was relatively smooth. Validation is therefore, attempted for qualitative trend only. Simulations are carried out to compute the rear axle load of the pitch plane model when subjected to the smooth and rough road described in chapter 2. Figure 3.17 presents the PSD of computed rear axle

tire force along with the measured forces for left and right wheels of the test vehicle at 50 km/h. These results show that although the trend is predicted very well by the pitch plane model, the magnitude of predicted force is significantly larger than the test forces specially at the wheel hop frequency.

Simulation results obtained for the smooth round input along with the test data are presented in Figure 3.18. In this case both trend and magnitude are comparable to the test forces. It is expected that the simulation results for rear axle of a pitch-plane model will predict a tire force that is in between the left and right tire forces of test vehicle. As demonstrated in this investigation of a complex model such as that of an urban bus against full scale on-road experiment is a highly difficult task. There are large number of uncertainities and variations that are possible in component characteristics, and description of excitation. Furthermore, in modeling of the system, only major components relevant to the study are considered and simplified. In this case a pitch-plane model was considered which completely ignores the roll dynamics that may be important for urban road operation.

The model however, showed remarkably good validation against experimental results available for both response and wheel loads. The objective of this investigations, however, is to evaluate the driver and road friendliness of the urban bus system. For this purpose extensive parametric study must be carried out to examine the influence of important parameters for each of these performance. It is therefore, necessary that a set of performance measures are established that can be effectively used to evaluate the system. The following subsections present the measures for performance that can be used in the parametric study presented in chapter 4.

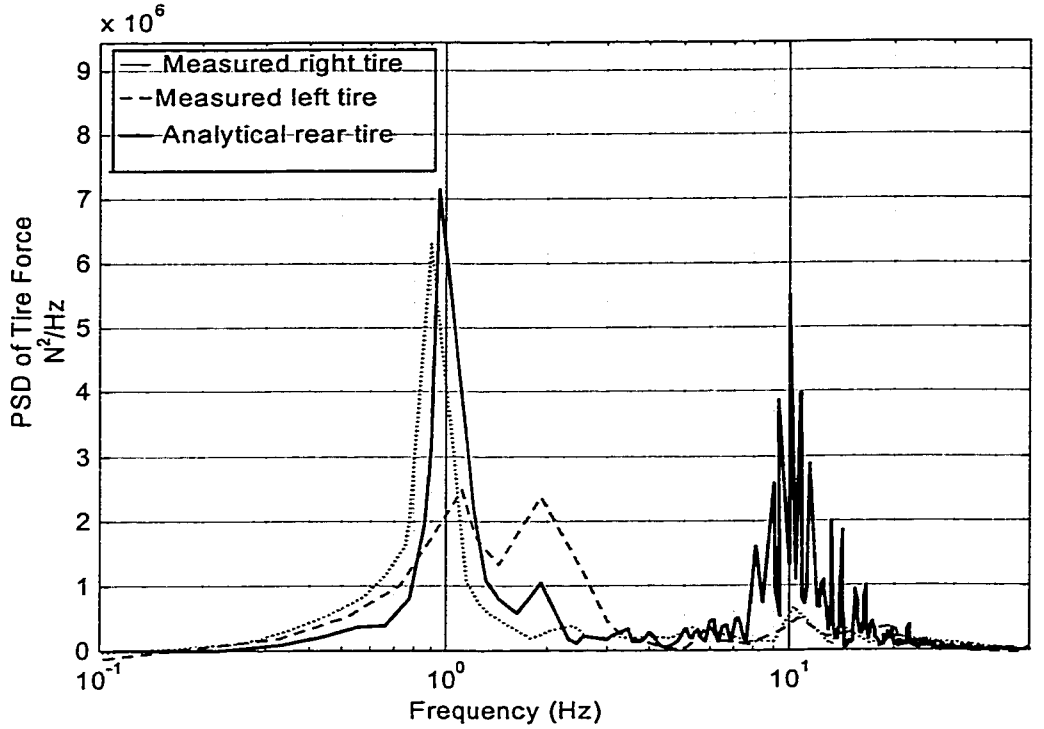

Figure 3.17: Plot of frequency vs PSD of front and rear tire force for empty bus at 50 km/h on rough road

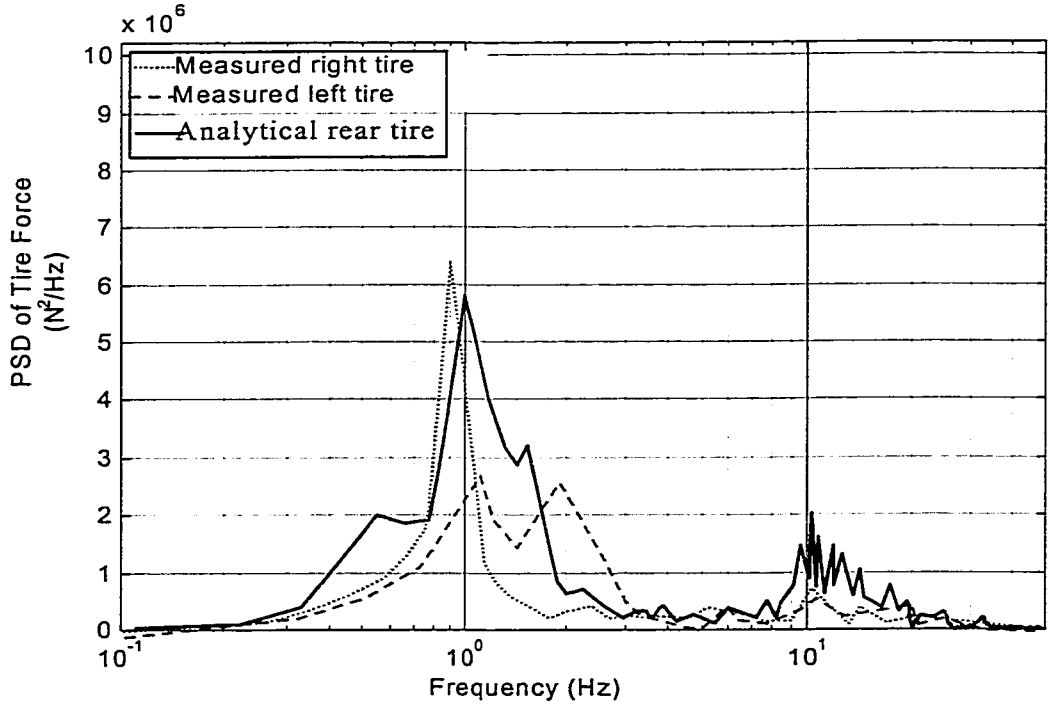

Figure 3.18: Plot of frequency vs PSD of front and rear tire force for empty bus running at 50 km/h on smooth road

3.6 Performance Measures Related to Road Friendly Bus

Vehicle generated road damage is directly related to the magnitude of the tire forces transmitted to the pavement. The tire forces transmitted to the road consist of two components a static load and the dynamic load. The static load depends on the geometry and mass distribution of the bus, and the load sharing characteristics of the suspension system. Dynamic tire forces, on the other hand, are the result of vehicle vibration caused by road roughness. The intensity of these vibrations and hence the severity of the dynamic tire forces primarily depend upon the suspension design.

Dynamic tire forces and their interaction with the pavement is a complex process. The extent of damage caused by these loads to pavements depend on the road structure and material characteristics, as well as the nature of the applied loads. Although a number of methods have been proposed to estimate the serviceability index or service lives of pavements, serious concerns have been raised on the validity of the methods [43]. In view of the complexity associated with the pavement mechanisms and lack of generally acceptabe assessment methods, the performance potentials of suspension systems are assessed in terms of the relative magnitudes of the dynamic tire loads.

Although dynamic tire forces of heavy vehicles are known to accelerate the pavement fatigue, the methods to quantify the road damaging potentials have not yet been established. Alternatively, a number of performance measures have been proposed to assess the relative agressivity of the heavy vehicles specially buses, and to assess the influence of various design and operating factors [13]. Some of these performance measures are described below.

3.6.1 Dynamic Load Coefficient (DLC)

The relative road damaging potentials of heavy vehicles, and the design and operating parameters are frequently expressed in terms of dynamic load coefficient (DLC). The DLC describes the magnitude of variations in the tire forces and is defined as

$$DLC = \frac{\text{RMS dynamic tire force}}{\text{Mean tire force}} \tag{3.20}$$

$$DLC = \frac{\sum_{i=1}^{N}(F_i - \bar{F})^2}{\bar{F}} \tag{3.21}$$

where,
$$\bar{F} = \frac{\sum_{i=1}^{N} F_i}{N} \tag{3.22}$$

F_i = Instantaneous tire force

$\bar{F}$ = Mean tire force

While there is considerable civil engineering literature concerned with theoretical and experimental studies of road damage caused by heavy vehicle loads, it is mostly based on the assumption that vehicles apply a constant (static) tire force to the road. Dynamic forces that are caused by the interaction of a heavy vehicle with road surface roughness constitute a significant portion of the total tire forces. Peak tire forces can be as much as twice their static values, and RMS levels are typically 20-30% of the static forces [43]. The road damage assessement thus necessitates appropriate considerations of the dynamic tire forces. Many studies have concluded that the DLC strongly depends on the road surface roughness, vehicle speed, vehicle configuration, geometry and mass distribution, axle loads, properties of the suspension and tires, and the vehicle vibration

modes. David Cebon [1] recommended that under normal operating conditions, the DLC of 0.1 - 0.3 are typical. Experimental studies by Sweatman [2] and Woodroofe et al [42] reported DLC value up to 0.4 for particular poor tandem suspensions. The recommended and measured values are only applicable to straight line driving.

3.6.2 Road Stress Factor (RSF)

Eisenmann [2] proposed a measure known as 'road stress factor', Φ, assuming that the road damage is related to fourth power of the instantaneous (dynamic) wheel force at a point on the road. The formulation was based upon the comprehensive study undertaken by AASHO road test [31]. Assuming that the dynamic wheel forces are Gaussian (normal distribution), Eisenmann showed that the expected value of the fourth power of the instantaneous wheel force is given by:

$$\Phi = E(1 + 6S^2 + 3S^4)\, P^4_{stat} \tag{3.23}$$

where, the dynamic load stress factor is defined as

$$\nu = 1 + 6S^2 + 3\, S^4 \tag{3.24}$$

Where, P_{stat} is the static tire force, and S is the coefficient of variation of dynamic tire force (essentially the DLC). E is the factor which depends on wheel configuration and tire-pavement contact pressure. For single (front axle) standard profile tires with 90 psi tire inflation pressure, its value is 0.84 whereas, for dual tires (rear-axle) it is 0.93 [2]. For typical highway conditions of roughness and speed, Sweatmann [2] measured the dynamic road stress factor ν in the range 1.11 to 1.46 depending on the suspension system. It is expected that suspension should rank in the same order whether the wheel loads are compared in terms of road stress factor or DLC.

$$\Phi_{95th} = (1+1.645DLC)^4 \tag{3.25}$$

Equation 3.25 is the Sweatmann road stress factor and is defined on the basis of Sweatmann's impact factor of the tire load. As pointed out earlier, Eisenmann's road stress factor formula assumes randomness of dynamic wheel loads and, therefore, underestimates the pavement damaging potential. Sweatmann [8] suggested that the severity of the dynamic loads can be better evaluated by the 95th percentile (Sweatmann) impact factor.

The RSF approach is used in a limited number of studies to estimate the pavement damage caused by dynamic tire forces and to introduce new legislation relevant to axle configuration and loads [34]. While equation 3.23 presents an attempt to mathematically characterize the road damage due to dynamic tire forces, its accuracy is subjected to considerable criticism [7,58,59], since RSF is based on inherently uncertain fourth power law. Moreover, RSF method neglects the sensitivity of the road response to variations in the speed and frequency of the applied loads and assumes that each suspension system on a vehicle does not influence the tire forces generated by other axles [34]. Nevertheless, the Eisenmann's and Sweatmann's road stress factor was considered to be appropriate for comparison of the pavement damaging potential of the same vehicle with different types of tires and different suspensions.

3.6.3 Peak Tire Force

The peak force is the maximum force transmitted to the pavement during the entire course of run in a given time history, and is given by:

$$F_{max} = Max\{F_{zij}\ ,\ i = 1,\ldots,\ N\} \tag{3.26}$$

where, F_{zij} is the instantaneous tire vertical force and N is the number of simulation points.

If the distribution of the wheel loads applied to the pavement suface by a fleet of traffic is truly random, then pavement wear caused by a wheel is directly related to its DLC. However, if the most severe dynamic loads are applied to the same pavement locations i.e. for spatially repeatable severely high load or peak loads, then pavement wear is mostly directly related to the peak dynamic wheel loads.

Cebon [15,28] suggested that road damage is governed by damage at the worst locations rather than by an average value over the total road surface, and that this worst location exists because the largest (peak) dynamic load always occur at the same locations (spatial repeatability).

3.6.4 Crest Factor

The crest factor is defined as the ratio of maximum to the mean tire force. The ratio is an indicator of the severity of tire force variation. The higher the crest factor the higher would be the maximum tire force and the lower the crest fator the lower would be the maximum tire force relative to the mean tire force. It is a relative measure which depends on mean tire force but estimates the highest transient or peak of the tire force in a single course of run. This factor is thus a clear indicator of how high the tire force go and so it also indicates the road wear and road damaging potiential. It is expressed as [5]:

$$\text{Crest Factor} = \frac{F_{T\,max}}{\bar{F}_T} \tag{3.27}$$

Crest factor is a good indicator of the road damaging potential of the bus if the dynamic loads are applied to the same pavement locations, i.e. to the spatially repeatable

loading senario. This measure doesn't have any information about the steady state behavior of the bus i.e. the mean tire force or how the tire force varies in a run and the damaging potential related to the static or the mean tire force.

3.6.5 Impact Factor

Eisenmann's road stress factor formula assumes randomness of dynamic wheel loads and therefore, underestimates the pavement damaging potential. Sweatman [5] suggested that the severity of the dynamic loads can be better evaluated by the 95th percentile impact factor, which is estimated by

$$IF_{95th} = 1 + 1.645DLC \tag{3.28}$$

and the corresponding road stress factor would be

$$\Phi_{95th} = (IF_{95th})^4 \tag{3.29}$$

3.7 Performance Measures Related to Driver Friendly Bus

The two measures used for driver friendly bus or ride comfort are absorbed power and RMS vertical acceleration. The absorbed power criterion is based on the hypothesis that ride comfort is related to energy dissipated due to internal damping in the human body. Absorbed power is determined by calculating a weighted integral of the power spectrum of acceleration in all three dimensions. The weighting functions, which are functions of frequency, are the mechanical impedance of the human body at the driver/passenger-seat interface, and are higher for frequencies to which the human body is most sensitive. The vertical seat acceleration is calculated using a ISO 2631 [41] filter.

Driver/passenger-seat dynamics are assumed not to have any effect on the dynamics of rest of the bus.

3.7.1 RMS Acceleration

The ride quality is concerned with driver and passenger comfort related to the road condition and suspension performance. The seat is also a very important element in a ride analysis since the flexibility of the seat isolates the driver from high-frequency vertical vibrations. For simplicity this study uses the driver/passenger floor location rather than driver/seat and passenger/seat interface for the evaluation of performance.

The response at driver and different passenger locations are obtained based on bus body bounce and pitch motions and kinematic relation for the location. To have an estimate of the acceleration at driver or passenger seat rms acceleration is used in this study. The rms acceleration at a location is defined as:

$$\ddot{z}_{rms} = \sqrt{\frac{\sum_{j=0}^{N} \ddot{z}_j^2}{N}} \tag{3.30}$$

where z_j is the bounce or pitch acceleration component from respective acceleration time history.

3.7.2 The Weighted rms Acceleration

The ride performance of a vehicle is assessed in terms of magnitude and frequency contents of vibration transmitted to the driver or passenger seat. The frequency to which a human driver is most fatigue sensitive for the horizontal and vertical

vibrations, lies in the range from 1 to 2 Hz and 4 to 8 Hz respectively. The human sensitivity to rotational vibration is mostly in 0.5 to 1.5 Hz frequency range [41]. The international standard (ISO-2631/1) has outlined a procedure to assess the human exposure to whole-body ride vibrations in terms of overall frequency-weighted rms acceleration at the driver/passenger seat interface [41]. The standard defines frequency-weighting W_k for vertical vibration in the 0.5-80 Hz frequency range, and W_e for the pitch vibration in the 0.1-80 Hz frequency range. The point worth mentioning here is that the seat suspension for the driver or for the passenger was assumed to be not present which will alter the actual response obtained at the driver/passenger seat interface. In the analysis of pitch plane model, accelerations are evalutated on the floor at fixed positions just undreneath the driver and the selected four passenger seats locations. In actual scenario the driver/passenger seat is above the floor with some fixture fitted to the floor or to the side wall and/or roof. This fixture will also alter the frequency response at the driver/passenger seat interface. Since these factors which can change the vibration response of driver/passenger seat, the ride performance of the bus is best assessed in terms of true rms accelerations. Two different measures are used here, based upon true and frequency-weighted rms accelerations and are thus defined as:

$$\ddot{z}_{rms} = \sqrt{\frac{1}{T}\int_0^T \ddot{z}_b^2 dt} \quad ; \quad \ddot{\theta}_{rms} = \sqrt{\frac{1}{T}\int_0^T \ddot{\theta}_b^2 dt} \tag{3.31}$$

$$\ddot{z}_{w,rms} = \sqrt{\frac{1}{T}\int_0^T \ddot{z}_{w,b}^2 dt} \quad ; \quad \ddot{\theta}_{w,rms} = \sqrt{\frac{1}{T}\int_0^T \ddot{\theta}_{w,b}^2 dt} \tag{3.32}$$

Where T is the total time of exposure, $\ddot{z}_{rms}$ and $\ddot{\theta}_{rms}$ are the true rms accelerations along the vertical and pitch axes. $\ddot{z}_b$ is the vertical acceleration of the bus body (sprung mass) and $\ddot{\theta}_b$ is the pitch acceleration of the bus body. $\ddot{z}_{w,rms}$ and $\ddot{\theta}_{w,rms}$ are the frequency-weighted rms accelerations along the vertical and pitch axes, respectively. $\ddot{z}_{w,b}$ and $\ddot{\theta}_{w,b}$ are the frequency weighted vertical and pitch accelerations, respectively. Convolution method is used to determine frequency-weighted vertical and pitch accelerations of the bus body. First the time history is passed through the band limiting and weighting filters, $H_b(s)$ and $H_w(s)$, as defined in ISO-2631 [38].

$$\ddot{z}_{w,s}(s) = \ddot{z}_s(s)H_b(s)H_w(s) \text{ and } \ddot{\theta}_{w,s}(s) = \ddot{\theta}_s(s)H_b(s)H_w(s) \tag{3.33}$$

$H_b(s)$ is composed of low-pass $H_l(s)$ and high-pass $H_h(s)$ filter functioins respectively. The weighting filter, $H_w(s)$, consists of two components $H_t(s)$ and $H_s(s)$, which are defined as; acceleraion-velocity transition and upward step transfer functions respectively.

The filter functions are,

$$H_b(s) = H_h(s)H_l(s) \text{ and } H_w(s) = H_t(s)H_s(s) \tag{3.34}$$

and

$$H_h(s) = \frac{s^2}{s^2 + \sqrt{2}\omega_1 s + \omega_1^2};\quad H_l(s) = \frac{\omega_2^2}{s^2 + \sqrt{2}\omega_1 s + \omega_1^2};\quad H_t(s) = \frac{1 + \dfrac{s}{\omega_3}}{1 + \dfrac{s}{Q_4\omega_4} + \left(\dfrac{s}{\omega_4}\right)^2}$$

$$H_s(s) = \frac{1 + \dfrac{s}{Q_5\omega_5} + \left(\dfrac{s}{\omega_5}\right)^2}{1 + \dfrac{s}{Q_5\omega_6} + \left(\dfrac{s}{\omega_6}\right)^2} x \left(\frac{\omega_5}{w_6}\right)^2 \qquad \text{for vertical vibration}$$

$H_s(s) = 1$ for pitch vibration (3.35)

The various coefficients in the transfer functions are listed in Table 3.8 below

Direction	Band-limiting		Acceleration-velocity transition			Upward step			
	f_1(Hz)	f_2(Hz)	f_3(Hz)	f_4(Hz)	Q_4	f_5(Hz)	Q_5	f_6(Hz)	Q_6
Vertical	0.4	100	12.5	12.5	0.63	2.37	0.91	3.35	0.91
Pitch	0.4	100	1.0	1.0	0.63	∞	—	∞	—

Table 3.7: Coefficients of transfer functions of the frequency weightings.

3.8 Summary

Attempts are made for quantitative and qualitative validation of the developed pitch-plane model against available experimental results with full-scale bus tested. Linearized free vibration analysis and nonlinear frequency responses are obained to get indepth understanding of dynamic behavior. Validations are carried out by comparing simulated results with those of experimentally obtained, on smooth and rough roads. The results indicate that the pitch plane model of canditate bus, subject to excitations arising from rough and smooth roads, yields trends very similar to those observed from the measured data. The following inference can be drawn from the analysis with respect to the validity of the simplified bus model. The PSD of vertical and pitch acceleration response of sprung mass shows reasonably good agreement with the envelopes of measured data. The frequencies of predominant vibration response of the models are quite close to those of the measured reponse and the trends of magnitudes of acceleration PSD are generally

comparable. The discrepancies between the analytical and the measured response is mostly because of:

a. Over simplified model representation

b. Differences in the specified and the actual operating conditions of the bus

c. Difference in component characteristics in actual bus and the model.

The PSD of dynamic tire forces, derived from the experimental and roll plane model, was used for the validation of pitch plane model. It served well only for the qualitative validation. The quantitative comparisons of magnitudes of PSD of tire forces, however, show considerable deviations between the model results and measured data. These deviations are much more obvious near wheel hop frequency whereas, the deviation near the bus body bounce resonance frequency is much less. Some of the deviations can also be attributed to the causes listed above.

Finally a number of performance measures for road and driver friendliness are outlined that are used for parametric study presented in the next chapter.

CHAPTER 4

PARAMETRIC STUDY FOR DRIVER/PASSENGER AND ROAD FRIENDLINESS

4.1 Introduction

The validated pitch-plane model of the candidate urban bus developed in chapter 3 is utilized to carryout an extensive parametric study. The primary objective here is to examine the influence of key operating and design parameters on the performance of the vehicle. Various performance measures discussed in chapter 3 for measure of ride quality and pavement load are utilized to evaluate the influence of selected parameters on different urban road conditions.

Studies conducted on commercial freight vehicles have established that gross vehicle weight, axle loads, suspension and tire properties effect the dynamic tire force most significantly [28,15]. The significant influence of suspension properties on the rms acceleration i.e the ride quality, and dynamic tire force have been performed and emphasized in many other studies. Buses and heavy vehicles have high road damaging potential due to their high tire force which initiates rutting in the road surface. Due to this high potential of road damage by excessive tire loads of heavy vehicles transmitted to the pavement, an OECD study has emphasized the need for developments in road-friendly vehicle suspension [42]. According to the study, a road friendly suspension is defined as one, which yields vehicle body bounce mode natural frequency less than 2 Hz and damping ratio of approximately 0.2.

The ride quality of bus is influenced by several parameters, such as suspension and tire properties, intertial properties and geometrical properties. For a given configuration suspension parameters that may have most influence on ride quality include suspension stiffness, damping ratio, and suspension geometry. Dynamic tire forces of heavy vehicles are strongly related to vibration modes of the vehicle associated with vertical and pitch motions of the sprung and unsprung masses. The vibration modes and thus the dynamic wheel loads are dependent upon the intertial and geometrical properties of the vehicle, and properties of the suspension and tire. The dynamic wheel loads in general, predominate in the low frequency range associated with the resonances of the sprung masses. The control of bus vibration in these frequency bands through optimal suspension design can enhance both the road friendliness and ride quality of the vehicle. Soft suspension springs are highly desirable to improve the ride quality and wheel load performance, the realization of adequate directional control and rattle space performance necessitates relatively hard suspension springs.

Some of the other parameters which may influence the performance of the bus are speed, load and road roughness. The parameters which are selected for the parametric study in this investigation can be classified as operating and design parameters. The selected operating parameters include: road roughness, tire inflation pressure, loading, and operating speed. The vehicle design parameters selected for the parametric study include front and rear damping constants, front and rear spring constant, as well as suspension geometry and position. The influence of variations in selected parameters on the driver/passenger friendliness is investigated using $\ddot{x}_{rms}$ and $\ddot{x}_{w,rms}$, $\ddot{\theta}_{rms}$ and $\ddot{\theta}_{w,rms}$, measures of acceleration response and transmissibility. The primary

performance measure used for road-friendliness of the bus is dynamic load coefficient (DLC). Sweatmans [5] road stress factor and Sweatmans impact factor, a measure of pavement damaging potential are further used to compare effect of tire and suspension properties on road friendliness performance of the bus.

4.2 Influence of Variations in Operating Parameters

The validated pitch-plane model of the candidate bus is utilized to investigate the sensitivity of performance measures to variations in operating parameters. It is a well known fact that the dynamic wheel load applied by heavy vehicles to the pavement increases significantly when vehicle speed and road roughness are increased [5]. Speed and road roughness are thus two of the most important operating parameters that must be considered in an investigation pertaining to driver- and road-friendliness of urban bus. For urban buses, other frequent variation in operational parameter include number of passengers on bus, loading and tire pressure. For the parametric study of the candidate bus model, the operational parameters considered include road roughness, tire inflation pressure, loading and operating speed. For each case, simulation results in terms of performance measures discussed in chapter 3 are obtained for the nominal candidate bus and for an increase and decrease in the parameter.

4.2.1 Road Roughness

The effect of road roughness is examined by obtaining simulated performance measures under random road excitations. As discussed in chapter 2 and 3, the road excitations are characterized with respect to its roughness. Available measured road data

characterized as smooth, medium and rough roads are utilized as input in order to evaluate the influence of road roughness on the performance measures. Table 4.1 summarizes the results in terms of various road friendliness and driver/passenger friendliness performance measures it is evident that the rear axle exhibit larger road damage potential in terms of all performance measures. A comparison of DLC between medium and rough roads indicate an increase of 100% for both front and rear tires for increased road roughness. Result shows that in terms of all performance measures, road damaging potential of the bus on rough roads increases substantially with increase in road roughness: 80 - 90% increase in road stress factor RSF, and around 20% increase in impact factor IF; and about 25 - 30% increase in crest factor and the maximum tire force when road roughness is increased from medium to rough. The vertical acceleration of the driver and all four passenger seats also increases with increase in the road roughness. The highest magnitude increment is for the middle seats of passenger no 2 and 3 which increases by 80% in rms acceleration and 85% in weighted rms acceleration. The rms and weighted rms vertical acceleration also increase for other passengers and driver location but to a lesser degree. The results indicate a 50% increase in the rms and 75% for weighted rms vertical acceleration for the driver and passenger number 4 due to roughness increased from medium to rough. The important performance measures, i.e. DLC and weighted rms accelerations that reflect the driver- and road- friendliness performance of the bus are summarized in Figure 4.1. All these results show a nearly linear trend for change in both performance with change in road roughness.

Location	Performance Measure	Road		
		Smooth	Medium Rough	Rough
Front Axle	F_{max}(kN)	75.12	91.05	113.5
	Crest Factor	1.3534	1.6794	2.0913
	DLC	0.0327	0.1089	0.2188
	RSF	0.9467	1.9327	3.4202
	IF	1.0645	1.1791	1.3599
Rear Axle	F_{max}(kN)	125.39	160.54	206.16
	Crest Factor	1.3645	1.7170	2.2102
	DLC	0.0630	0.1325	0.2647
	RSF	0.7649	2.2011	4.2445
	IF	1.0945	1.2180	1.4354
Driver	$\ddot{z}_{rms}$ (m/s^2)	0.5213	0.9654	1.4479
	$\ddot{z}_{w,rms}$ (m/s^2)	0.2314	0.4860	0.8364
	$\ddot{\theta}_{rms}$ (rad/s^2)	0.1063	0.1850	0.2783
	$\ddot{\theta}_{w,rms}$ (rad/s^2)	0.0647	0.0940	0.1375
Passenger # 1	$\ddot{z}_{rms}$ (m/s^2)	0.2134	0.5452	0.9084
	$\ddot{z}_{w,rms}$ (m/s^2)	0.1084	0.3444	0.6290
Passenger # 2	$\ddot{z}_{rms}$ (m/s^2)	0.1592	0.4981	0.8927
	$\ddot{z}_{w,rms}$ (m/s^2)	0.0968	0.3309	0.6092
Passenger # 3	$\ddot{z}_{rms}$ (m/s^2)	0.1505	0.5242	0.9422
	$\ddot{z}_{w,rms}$ (m/s^2)	0.0833	0.3259	0.6020
Passenger # 4	$\ddot{z}_{rms}$ (m/s^2)	0.4253	0.8306	1.2622
	$\ddot{z}_{w,rms}$ (m/s^2)	0.2123	0.4617	0.8008

Table 4.1: Performance variation due to the change in road roughness

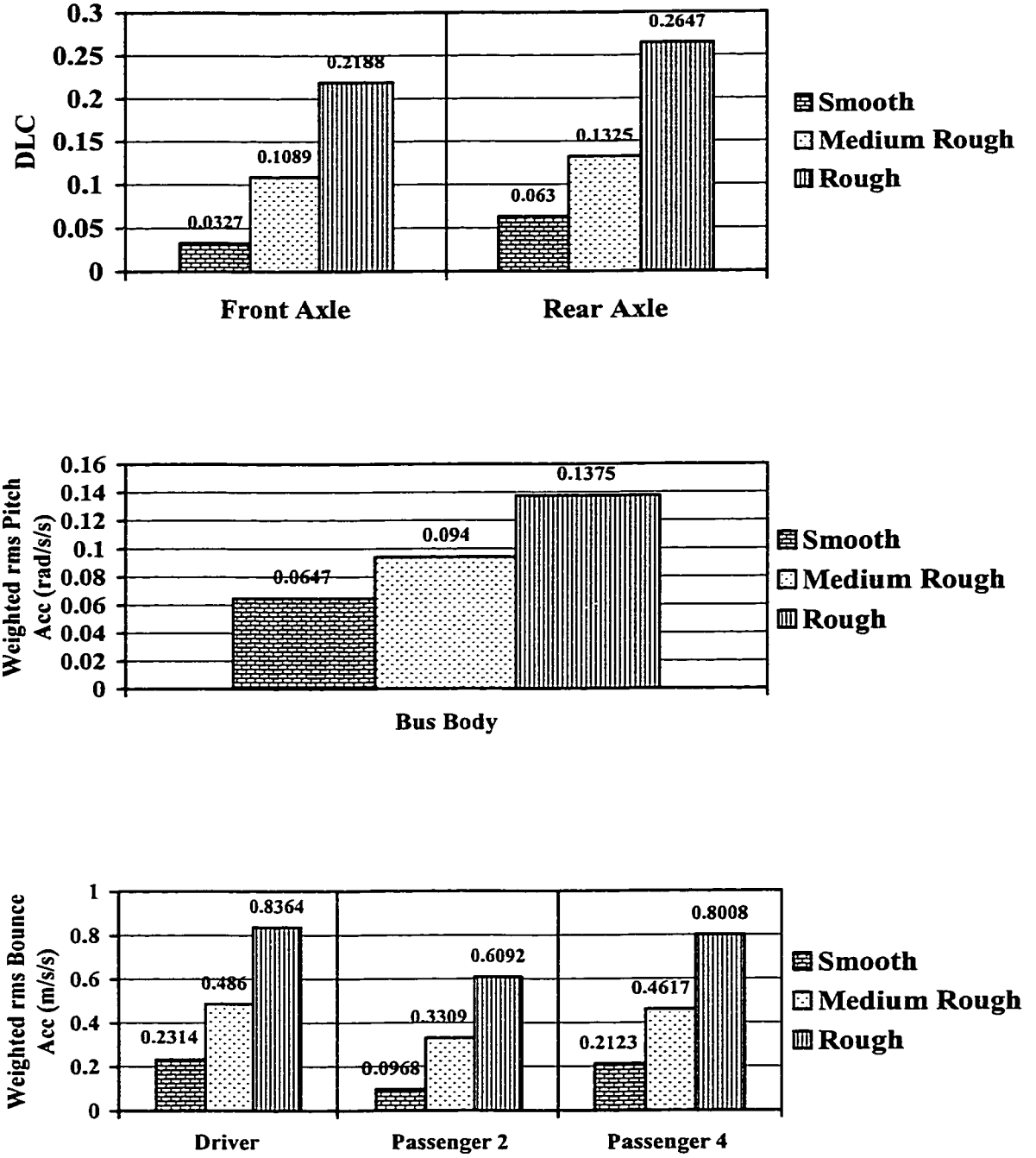

Figure 4.1: Effect of road roughness on DLC, weighted rms bounce and pitch acceleration

4.2.2 Inflation Pressure

Tire Inflation pressure is valid between 85 and 120 psi to examine its effect on the performance measures of the bus. Table 4.2 illustrates the influence of variation of tire inflation pressure on performance measures, derived from analysis of pitch plane model of the bus. The corresponding figure 4.2 shows the variation in DLC, weighted rms bounce and pitch acceleration due to this change in tire inflation pressure. The results show that, inflation pressure of the tires can significantly improve the DLC performance of the bus. The reduction in DLC is attributed to reduced vertical stiffness of tires with lower inflation pressure. The results show that the DLC can be reduced by approximately 10%, when inflation pressure is reduced from 110 psi to 85 psi. The maximum tire force increases with an increase in inflation pressure which is also a sign of higher road damaging potential. The increase of 2% for an increase in tire pressure from 110 to 120 psi and a reduction of around 3% for a reduction in tire pressure from 110 psi to 85 psi is however not very significant. The measure of ride quality in terms of weighted pitch and vertical acceleration of sprung mass also indicate an increase with increase in tire pressure. The tire inflation pressure of 85 psi leads to reductions in weighted and unweighted rms accelerations of driver and all the four passenger of the bus. The influence of the performance measures summarized in Figure 4.2 indicates a near linear trend for measures. As the result show there is 25% change in pitch response and 20% change in bounce response as a result of variation in tire pressure between 85 and 120 psi.

Location	Performance Measure	Tire Inflation Pressure		
		85 Psi	110 Psi	120 Psi
Front Axle	F_{max} (kN)	87.9	91.05	92.79
	Crest Factor	1.5534	1.6794	1.7116
	DLC	0.0982	0.1089	0.1135
	RSF	1.8206	1.9327	1.9827
	IF	1.1616	1.1791	1.1866
Rear Axle	F_{max} (kN)	156.07	160.54	163.81
	Crest Factor	1.6690	1.7170	1.7520
	DLC	0.1204	0.1325	0.1368
	RSF	2.0603	2.2011	2.2517
	IF	1.1981	1.2180	1.2250
Driver	$\ddot{z}_{rms}$ (m/s^2)	0.9395	0.9654	0.9788
	$\ddot{z}_{w,rms}$ (m/s^2)	0.4696	0.4860	0.4916
	$\ddot{\theta}_{rms}$ (rad/s^2)	0.1813	0.1850	0.1867
	$\ddot{\theta}_{w,rms}$ (rad/s^2)	0.0937	0.0939	0.0944
Passenger # 1	$\ddot{z}_{rms}$ (m/s^2)	0.5258	0.5452	0.5538
	$\ddot{z}_{w,rms}$ (m/s^2)	0.3284	0.3444	0.3493
Passenger # 2	$\ddot{z}_{rms}$ (m/s^2)	0.4808	0.4981	0.5044
	$\ddot{z}_{w,rms}$ (m/s^2)	0.3149	0.3309	0.3357
Passenger # 3	$\ddot{z}_{rms}$ (m/s^2)	0.5076	0.5242	0.5299
	$\ddot{z}_{w,rms}$ (m/s^2)	0.3100	0.3259	0.3307
Passenger # 4	$\ddot{z}_{rms}$ (m/s^2)	0.8068	0.8306	0.8427
	$\ddot{z}_{w,rms}$ (m/s^2)	0.4454	0.4617	0.4671

Table 4.2: Performance variation due to the change in tire inflation pressure

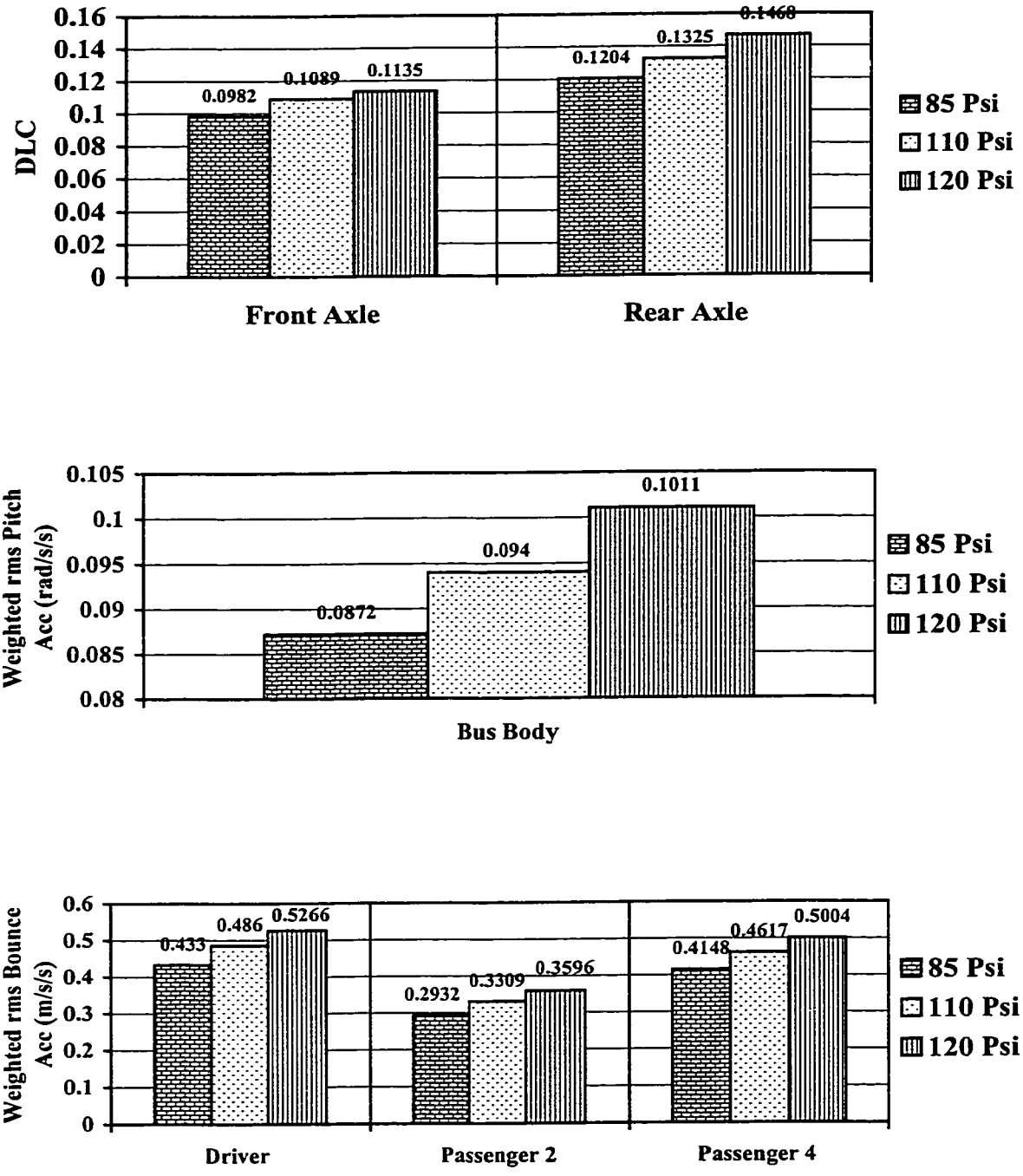

Figure 4.2: Effect of Tire Inflation Pressure on DLC, weighted rms bounce and pitch acceleration

4.2.3 Operating load

The influence of operating load on the performance measures is evaluated by considering empty, half and fully loaded bus conditions. Table 4.3 illustrates the influence of variations in the passenger load on the performance measures, derived from analysis of pitch plane model of the bus. The results show that the DLC due to both front axle and rear-axles of the bus is lowest under fully loaded condition. The DLC of the front axle tires with no passenger load is 30% higher than those obtained under half loaded condition and 13% higher than those obtained under fully load condition. These variations in the DLC are mostly attributed to its definition, the variations in the tire forces normalized by the mean load. The DLC values, therefore, decrease with increase in the static load. The peak force due to front axle is to be affected more due to loading than that of rear axle. The peak force due to front axle increase by more than 30% while the rear axle peak force increases less than 20% when empty bus is compared with fully loaded. The rms acceleration and rms weighted acceleration for the second passenger reduce 20% from empty to half loaded bus and about 12% for the half to fully loaded bus. The unweighted and weighted rms accelerations along the vertical axis also increases considerably under empty condition. The frequency weighted rms acceleration under no-load condition increases from 20% to 30% for different seat locations, compared to that obtained under fully loaded condition. Summary of the results presented indicate that both DLC and driver/passenger bounce response decreases with loading in a linear fashion. Increase in load however causes a slight (6%) decrease in the pitch acceleration of the bus body.

Location	Performance Measure	Load on the bus		
		Empty	Half	Full
Front Axle	F_{max}(kN)	78.08	91.05	103.64
	Crest Factor	1.8610	1.6794	1.5670
	DLC	0.1356	0.1089	0.0948
	RSF	2.2379	1.9327	1.7857
	IF	1.2231	1.1791	1.1560
Rear Axle	F_{max}(kN)	146.67	160.54	174.08
	Crest Factor	1.8241	1.7170	1.6383
	DLC	0.1489	0.1325	0.1209
	RSF	2.4023	2.2011	2.0664
	IF	1.2450	1.2180	1.1990
Driver	$\ddot{z}_{rms}$ (m/s^2)	1.0448	0.9654	0.9290
	$\ddot{z}_{w,rms}$ (m/s^2)	0.5469	0.4860	0.4481
	$\ddot{\theta}_{rms}$ (rad/s^2)	0.1890	0.1850	0.1831
	$\ddot{\theta}_{w,rms}$ (rad/s^2)	0.0966	0.0940	0.0912
Passenger # 1	$\ddot{z}_{rms}$ (m/s^2)	0.6359	0.5452	0.4957
	$\ddot{z}_{w,rms}$ (m/s^2)	0.4061	0.3444	0.3048
Passenger # 2	$\ddot{z}_{rms}$ (m/s^2)	0.5930	0.4981	0.4423
	$\ddot{z}_{w,rms}$ (m/s^2)	0.3122	0.2647	0.2343
Passenger # 3	$\ddot{z}_{rms}$ (m/s^2)	0.6034	0.5242	0.4763
	$\ddot{z}_{w,rms}$ (m/s^2)	0.3882	0.3259	0.2858
Passenger # 4	$\ddot{z}_{rms}$ (m/s^2)	0.8620	0.8306	0.8272
	$\ddot{z}_{w,rms}$ (m/s^2)	0.5138	0.4617	0.4297

Table 4.3: Performance variation due to the change in bus operating load

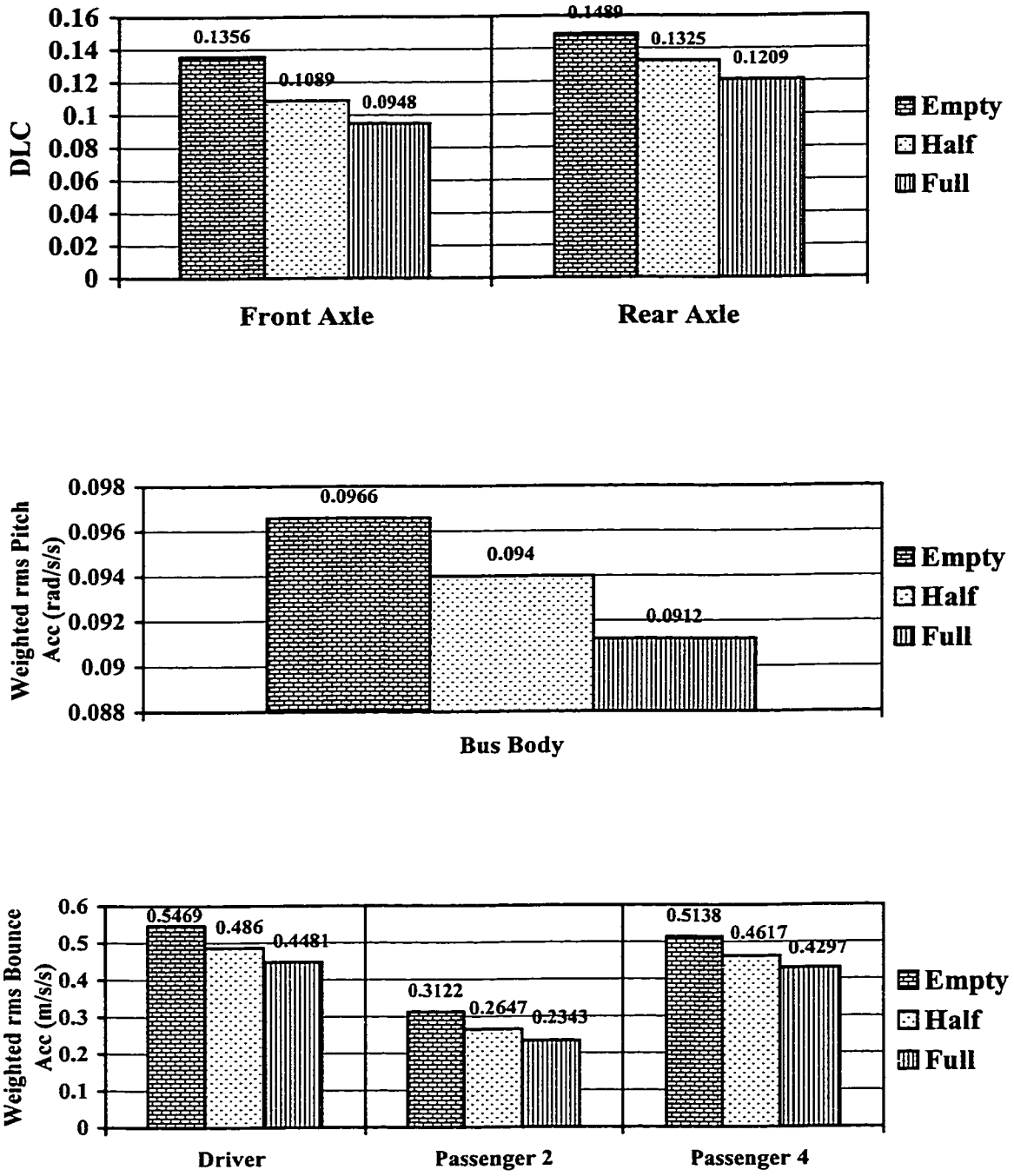

Figure 4.3: Effect of Operating Load on DLC, weighted rms bounce and pitch acceleration

4.2.4 Operating Speed

The influence of operating speed on the performance measures is evaluated by considering half loaded bus running at 30, 50 and 70 km/h speed on medium rough road. Table 4.4 illustrates in tabular form the influence of variations in the passenger load on the performance measures, derived from analysis of pitch plane model of the bus. The DLC due to front axle tires of the bus reduces 30% and increases 43% by reducing and increasing the speed respectively. The DLC due to rear-axle tires reduces 36% and increases 33% for increase and reduction in speeds respectively. This change in DLC shows that random load peaks depend on the speed of the vehicle and for the heavy axle it changes more at low speeds than at high speeds. On the other hand, for lighter axle, the change is greater at higher speeds. The increase in the road stress factor, crest factor, impact factor and maximum tire force with increase in speed indicates, higher pavement damage potential and since road stress factor increase is much prominent than the impact factor or the maximum tire force it can be inferred that the damaging potential is less for spatially repeated road excitations. The weighted rms bounce and pitch, and rms bounce and pitch acceleration reduce considerably, where pitch rms acceleration reduces 42% from medium to low speed but only increases 16% from medium to high speed, so the low speed favors the ride vibration performance. This indicates that pitching effect is less pronounced as speed goes higher specially from 50 km/h to 70 km/h. For the driver and the last passenger i.e. passenger no. 4, although the change in vertical acceleration is much more prominent , the trend is similar as seen in the rms pitch or weighted pitch acceleration or the rms or weighted rms acceleration of any other seat. These trends are clearly demonstrated by the summary of key results presented in Figure 4.4.

Location	Performance Measure	Bus Speed (km/h)		
		30	50	70
Front Axle	F_{max}(kN)	79.68	91.05	106.35
	Crest Factor	1.4673	1.6794	1.9567
	DLC	0.0764	0.1089	0.1551
	RSF	1.6060	1.9327	2.4814
	IF	1.1257	1.1791	1.2551
Rear Axle	F_{max}(kN)	146.32	160.54	188.96
	Crest Factor	1.5660	1.7170	2.0234
	DLC	0.0852	0.1325	0.1765
	RSF	1.6903	2.2011	2.7725
	IF	1.1402	1.2180	1.2904
Driver	$\ddot{z}_{rms}$ (m/s^2)	0.6701	0.9654	1.1686
	$\ddot{z}_{w,rms}$ (m/s^2)	0.3456	0.4860	0.5550
	$\ddot{\theta}_{rms}$ (rad/s^2)	0.1067	0.1850	0.2146
	$\ddot{\theta}_{w,rms}$ (rad/s^2)	0.0518	0.0940	0.0974
Passenger # 1	$\ddot{z}_{rms}$ (m/s^2)	0.4595	0.5452	0.6661
	$\ddot{z}_{w,rms}$ (m/s^2)	0.2675	0.3444	0.4082
Passenger # 2	$\ddot{z}_{rms}$ (m/s^2)	0.4259	0.4981	0.5861
	$\ddot{z}_{w,rms}$ (m/s^2)	0.2601	0.3309	0.3941
Passenger # 3	$\ddot{z}_{rms}$ (m/s^2)	0.4306	0.5242	0.6059
	$\ddot{z}_{w,rms}$ (m/s^2)	0.2574	0.3259	0.3890
Passenger # 4	$\ddot{z}_{rms}$ (m/s^2)	0.6011	0.8306	1.0107
	$\ddot{z}_{w,rms}$ (m/s^2)	0.3322	0.4617	0.5298

Table 4.4: Performance variation due to the change in bus operating speed

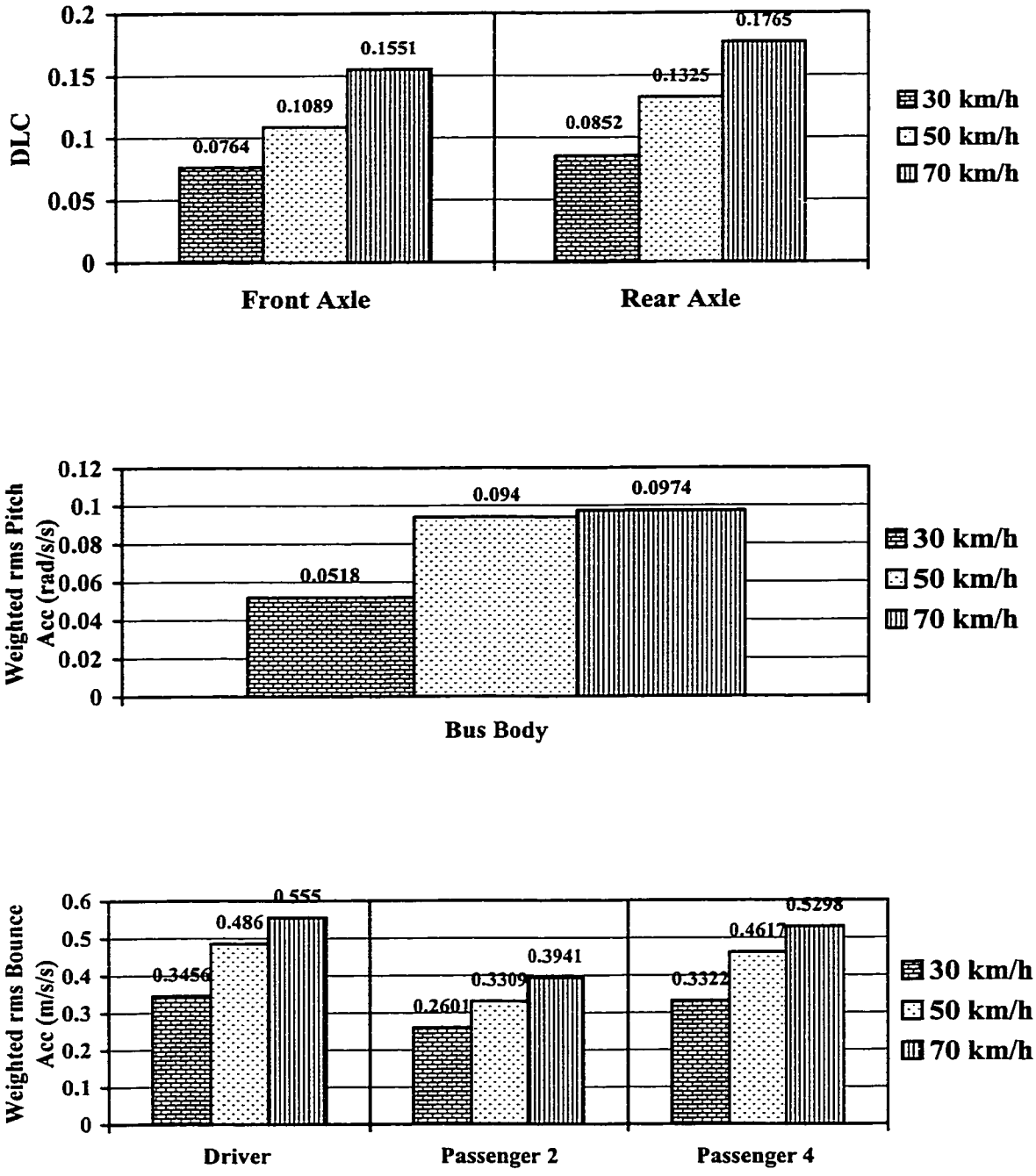

Figure 4.4: Effect of Bus speed on DLC, weighted rms bounce and pitch acceleration

4.3 Influence of Variations in Design parameters

Although dynamic tire load and ride performance of vehicles may be influenced by many design parameters, the present parametric study is limited to variations in the suspension related parameters. Vehicle suspension designers are faced with a challenge due to conflicting stiffness requirements between ride and handling performance. Similarly, damping presents a conflict between the low and high frequency performance. In this investigation, however, the influence of variation in suspension damping and stiffness are examined in view of ride quality and pavement load. There are numerous other parameters associated with suspension and vehicle system design that were considered in this investigation. This section however, presents some of these parameters which showed noticable influence on the performance of interest. These parameters include suspension geometry, ride height and wheel base. Similar to operational parameters the results generated for the above design parameters are presented in the following subsection.

4.3.1 Influence of Damper Parameter Variations

The dampers used in modern urban bus suspensions are highly nonlinear with asymmetric characteristics for compression and extension, and consists of many parameters as discussed in section 2.4.2 and are shown in an schematic in Figures 2.17 and 2.18. The influence of variations in damping properties on performance measures is investigated by varying various damping parameters of the suspension dampers. These parameters include low speed compression mode damping coefficient, C_{cl}; assymetry factor, p; bounce mode reduction factor, γ_c, rebound mode reduction factors, γ_{el} and

γ_{e2}; and transition velocity, V_e. The above mentioned parameters are varied by 25% about their nominal values. All the other simulation parameters are maintained at their nominal values (bus speed 50 km/hr, medium-rough road, half loaded bus). The influence of variations in the damper friction force was observed to be relatively small, and thus not presented in this parametric study. The pitch plane model is used to examine the variational effect of front and rear damper parameters separately.

4.3.1.1 Influence of Front Damper Parameter Variations

The influence of variations in front damper parameters on the performance measures are illustrated in Table 4.5 and Table 4.6. Table 4.5 presents the result for variation in C_{cfl}, p_f and γ_{elf} while Table 4.6 presents the results for variations in DLC weighted rms bounce and pitch acceleration. The results show that variations in front suspension damping parameters affect both the performance measures. The DLC due to tire forces on both axles decrease with increase in compression mode damping C_{cfl} and asymmetry factor p_f. The results show that the DLC due to tire forces on front axle change about 3% when C_{cfl} is increased or reduced by 25% from its nominal value. The DLC due to tire forces on front axle decreases insignificantly by an increase in asymmetry factor of 25% but DLC increases 3% if asymmetry factor is reduced by 25% of its nominal value. The DLC due to the increase or reduction in C_{cfl} on rear axle doesn't change significantly whereas, due to the change in asymmetry factor, p_f, it changes only 1% both for increase in p_f or decrease in p_f. The rms vertical acceleration for driver seat changes 10% with a change of 25% in C_{cfl}. This effect is almost the same for passenger no 1 and 2 but for passenger no 3 and 4, although the effect is not much pronounced it is

opposite, i.e. the rms vertical acceleration increases with increase in C_{cfl} and reduces with a decrement in C_{cfl}. Any change of 25% in p_f changes rms weighted vertical acceleration by 3% for passenger seats no 1, 2 and 3. The effect of these parameters on pitch acceleration is more significant. The rms pitch acceleration reduces 7% for increase in C_{cfl} of 25% and increase 6% for a reduction in C_{cfl} of 25%.

Table 4.6 shows the effect of the change in number of phases for compression as well as in extention. The first set of results in Table 4.6 shows the front damper, modeled as a two phase compression and two phase extention damper, while the second set corresponds to three extention phases and two compression phases. The effect of V_c is not substantial around the nominal value of 0.155m/s and thus has been taken as nominal value for the modified two phase compression model of the front damper. The effect of changing C_{c2f} on DLC and the ride performance of front seats including the driver is more prominent when it is 4000Ns/m. Changing it further to 8000Ns/m does not bring any substantial change. Introducing the third extention phase doesn't introduce any substantial change in the overall response of the bus. It is obvious from table 4.6 that the effect of high extention coefficient is beneficial for vibration and force isolation but the first phase high extention coefficient is enough for this effect. Any further high extention coefficient phase doesn't change the overall performance except marginally.

From the results it may be concluded that front suspension dampers with a little higher compression mode damping and low degree of asymmetry can yield considerable imporvement in the ride quality of the front seats with only slight deterioration of the rear tire DLC performance. Figures 4.5 and 4.6 illustrates these parameters in terms of DLC and weighted rms accelerations for variations in front damper parameters.

Location	Perform Measure	C_{efl}(Ns/m)			p_f			γ_{elf}		
		1480	**1972.8**	**2466**	**11.80**	**15.67**	**19.60**	**0.124**	**0.166**	**0.207**
Front Axle	F_{max}(kN)	90.959	91.05	91.131	90.53	91.05	91.98	91.04	91.05	91.06
	CF	1.6457	1.6794	1.7130	1.6701	1.6794	1.6965	1.6792	1.6794	1.6795
	DLC	0.1126	0.1089	0.1054	0.1117	0.1089	0.1086	0.1089	0.1089	0.1088
	RSF	1.9889	1.9327	1.8795	1.9636	1.9327	1.9302	1.9328	1.9327	1.9325
	IF	1.1817	1.1791	1.1768	1.1838	1.1791	1.1787	1.1791	1.1791	1.1790
Rear Axle	F_{max}(kN)	160.72	160.54	160.35	160.66	160.54	160.50	160.54	160.54	160.53
	CF	1.7244	1.7170	1.6925	1.7184	1.7170	1.7165	1.7170	1.7170	1.7169
	DLC	0.1310	0.1325	0.1339	0.1315	0.1325	0.1334	0.1325	0.1325	0.1326
	RSF	2.1903	2.2011	2.2150	2.1883	2.2011	2.2116	2.2000	2.2011	2.2014
	IF	1.2168	1.2180	1.2192	1.2163	1.2180	1.2195	1.2179	1.2180	1.2181
Driver	$\ddot{z}_{rms}$ (m/s²)	1.0693	0.9654	0.8643	0.9417	0.9654	1.0092	0.9616	0.9654	0.9686
	$\ddot{z}_{w,rms}$ (m/s²)	0.5297	0.486	0.4384	0.4783	0.4860	0.4963	0.4853	0.4860	0.4866
	$\ddot{\theta}_{rms}$ (rad/s²)	0.1964	0.185	0.1689	0.1838	0.1850	0.1869	0.1848	0.1850	0.1851
	$\ddot{\theta}_{w,rms}$ (rad/s²)	0.0997	0.094	0.0871	0.0935	0.0940	0.0953	0.0939	0.0940	0.0940
Passengr 1	$\ddot{z}_{rms}$ (m/s²)	0.5874	0.5452	0.4981	0.5167	0.5452	0.5882	0.5419	0.5452	0.5481
	$\ddot{z}_{w,rms}$ (m/s²)	0.3729	0.3444	0.3107	0.3346	0.3444	0.3554	0.3437	0.3444	0.3450
Passengr 2	$\ddot{z}_{rms}$ (m/s²)	0.5412	0.4981	0.4538	0.4711	0.4981	0.5327	0.4958	0.4981	0.5001
	$\ddot{z}_{w,rms}$ (m/s²)	0.3571	0.3309	0.2986	0.3209	0.3309	0.3419	0.3302	0.3309	0.3315
Passengr 3	$\ddot{z}_{rms}$ (m/s²)	0.5138	0.5242	0.5341	0.5538	0.5242	0.4996	0.5259	0.5242	0.5224
	$\ddot{z}_{w,rms}$ (m/s²)	0.3202	0.3259	0.3295	0.3370	0.3259	0.3159	0.3266	0.3259	0.3252
Passengr 4	$\ddot{z}_{rms}$ (m/s²)	0.8219	0.8306	0.8508	0.8744	0.8306	0.806	0.8338	0.8306	0.8269
	$\ddot{z}_{w,rms}$ (m/s²)	0.4556	0.4617	0.4707	0.4722	0.4617	0.4536	0.4623	0.4617	0.461

Table 4.5: Performance variation due to the change in front damper parameters

Location	Perform. Measure	C_{c2f} (γ_{c1f}) (Ns/m)			C_{e3f} (γ_{e2f}) (Ns/m)		
		4000	**1972.8**	**8000**	**10000**	**5126.8**	**30000**
Front Axle	F_{max}(kN)	91.51	91.05	91.65	91.13	91.05	91.21
	CF	1.7431	1.6794	1.7513	1.6798	1.6794	1.6809
	DLC	0.1042	0.1089	0.104	0.1084	0.1089	0.1086
	RSF	1.8606	1.9327	1.8592	1.9318	1.9327	1.9314
	IF	1.1742	1.1791	1.168	1.1789	1.1791	1.1784
Rear Axle	F_{max}(kN)	160.24	160.54	160.21	160.46	160.54	160.43
	CF	1.6901	1.7170	1.6885	1.7158	1.7170	1.7153
	DLC	0.1348	0.1325	0.1353	0.1332	0.1325	0.1335
	RSF	2.2035	2.2011	2.2058	2.2017	2.2011	2.2019
	IF	1.2194	1.2180	1.2198	1.2202	1.2180	1.2211
Driver	$\ddot{z}_{rms}$ (m/s^2)	0.9263	0.9654	0.9221	0.9657	0.9654	0.9658
	$\ddot{z}_{w,rms}$ (m/s^2)	0.4656	0.486	0.4629	0.487	0.486	0.487
	$\ddot{\theta}_{rms}$ (rad/s^2)	0.1789	0.185	0.1785	0.184	0.185	0.185
	$\ddot{\theta}_{w,rms}$ (rad/s^2)	0.0909	0.094	0.0906	0.0945	0.094	0.0948
Passengr1	$\ddot{z}_{rms}$ (m/s^2)	0.5212	0.5452	0.5201	0.5454	0.5452	0.5455
	$\ddot{z}_{w,rms}$ (m/s^2)	0.3307	0.3444	0.3287	0.3446	0.3444	0.3447
Passengr 2	$\ddot{z}_{rms}$ (m/s^2)	0.4826	0.4981	0.4803	0.4982	0.4981	0.4982
	$\ddot{z}_{w,rms}$ (m/s^2)	0.3257	0.3309	0.3234	0.331	0.3309	0.3311
Passengr 3	$\ddot{z}_{rms}$ (m/s^2)	0.5305	0.5242	0.5316	0.5240	0.5242	0.5239
	$\ddot{z}_{w,rms}$ (m/s^2)	0.3317	0.3259	0.3331	0.3256	0.3259	0.3255
Passengr 4	$\ddot{z}_{rms}$ (m/s^2)	0.8454	0.8306	0.8472	0.8302	0.8306	0.8301
	$\ddot{z}_{w,rms}$ (m/s^2)	0.4713	0.4617	0.4725	0.4611	0.4617	0.4610

Table 4.6: Performance variation due to the change in front damper no of phases

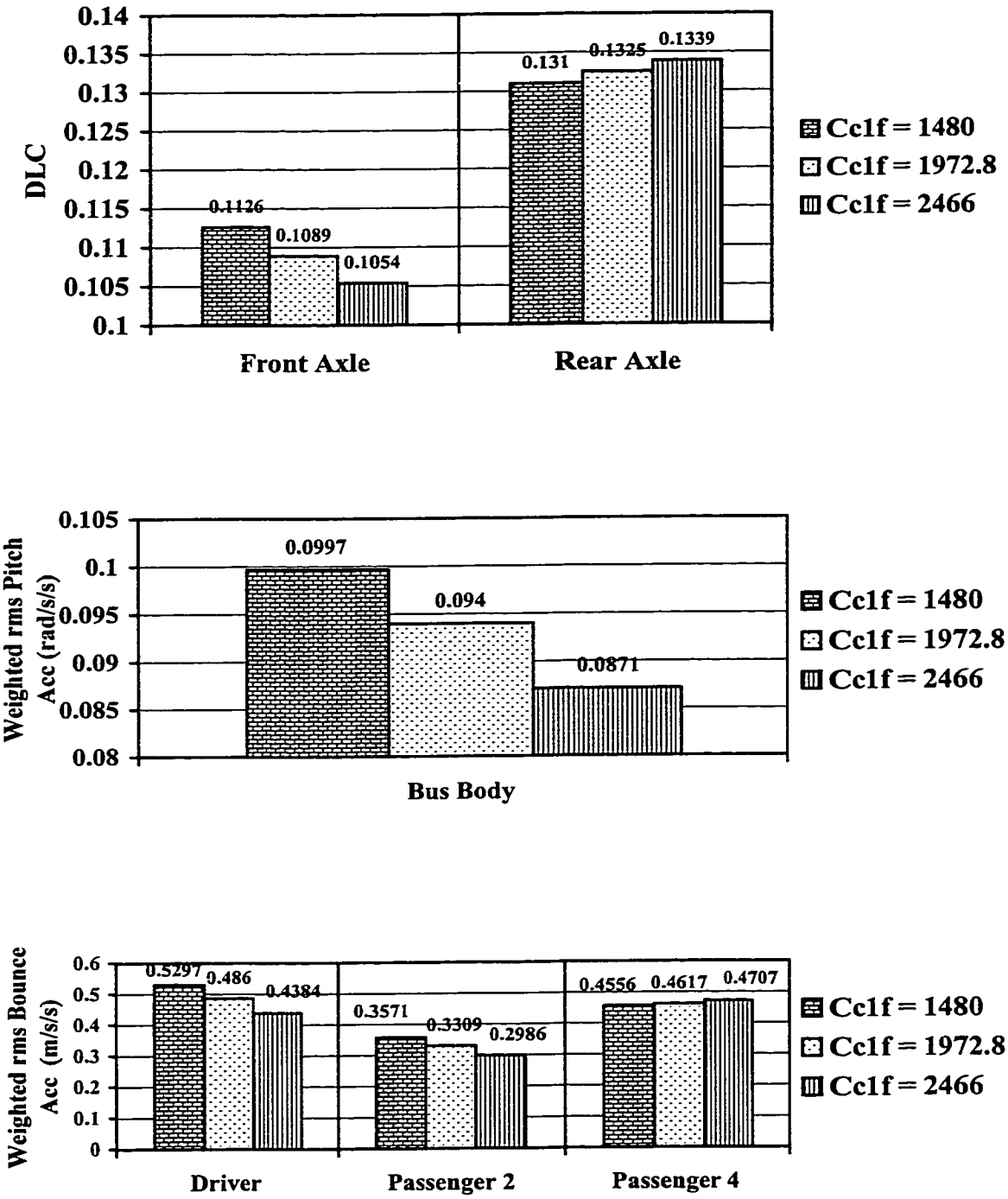

Figure 4.5a: Effect of C_{cfl} on DLC, weighted rms bounce and pitch acceleration

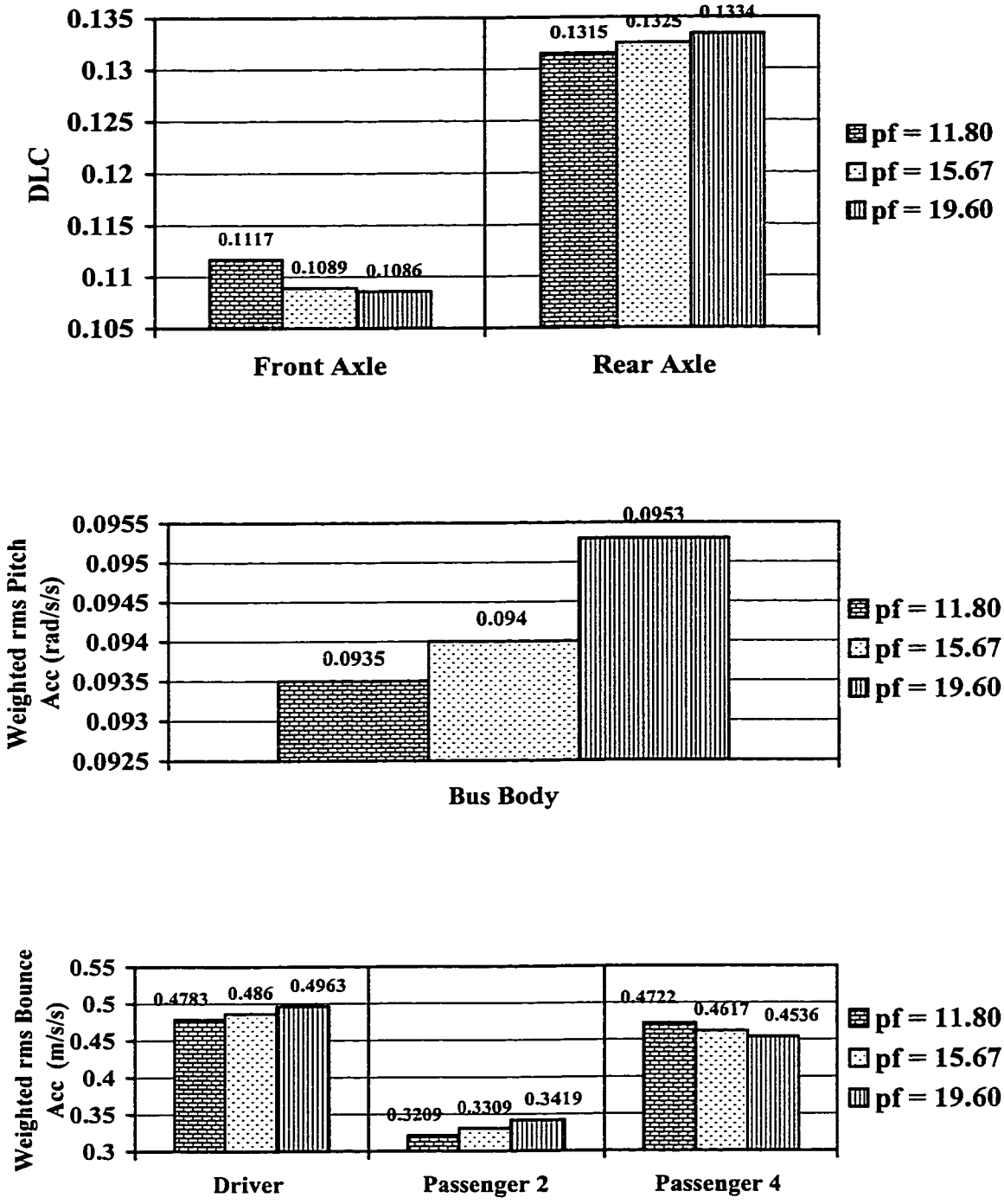

Figure 4.5b: Effect of front asymmetry ratio p_f on DLC, weighted rms bounce and pitch acceleration

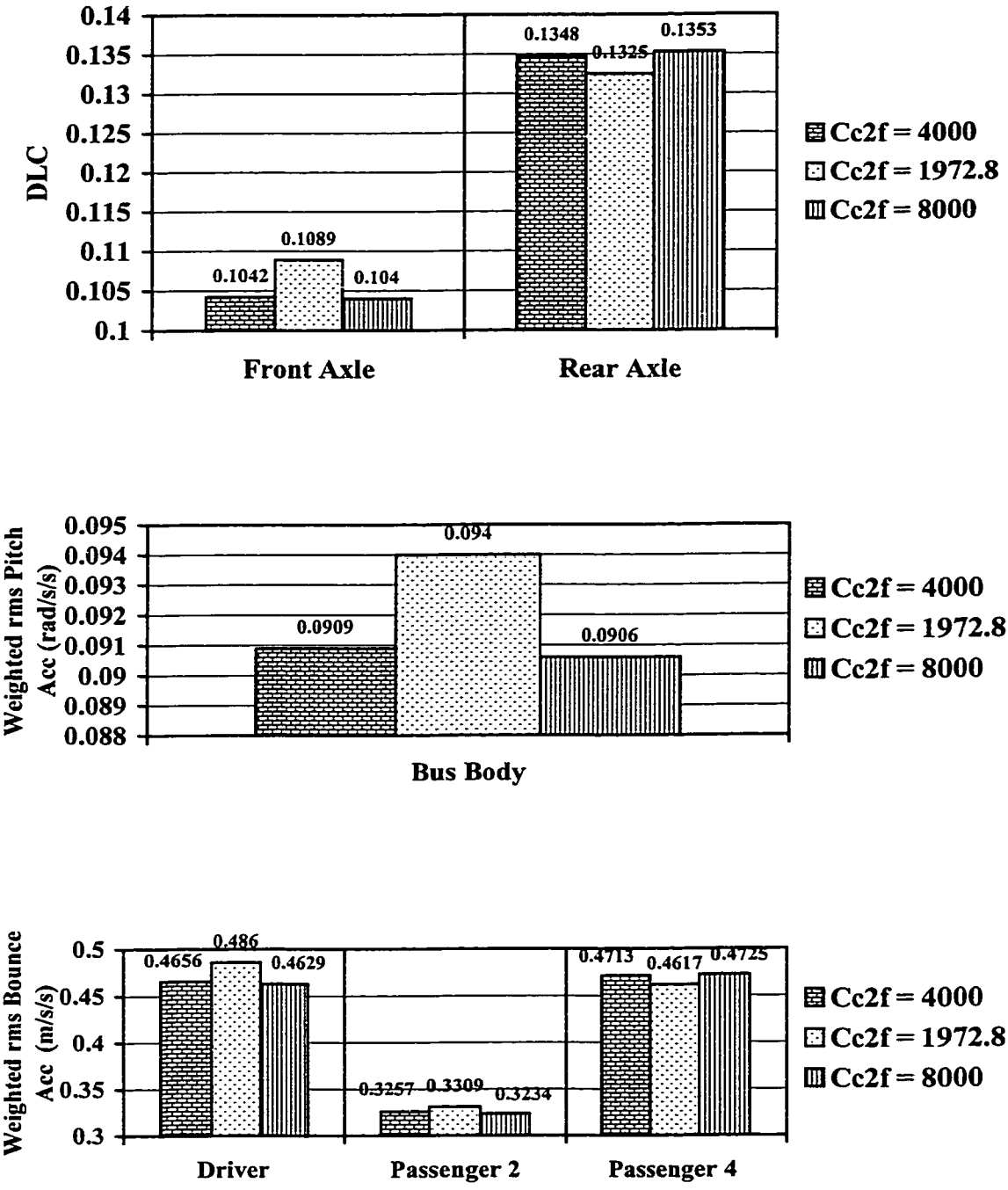

Figure 4.6a: Effect of C_{cf2} and C_{ef3} on DLC, weighted rms bounce and pitch acceleration

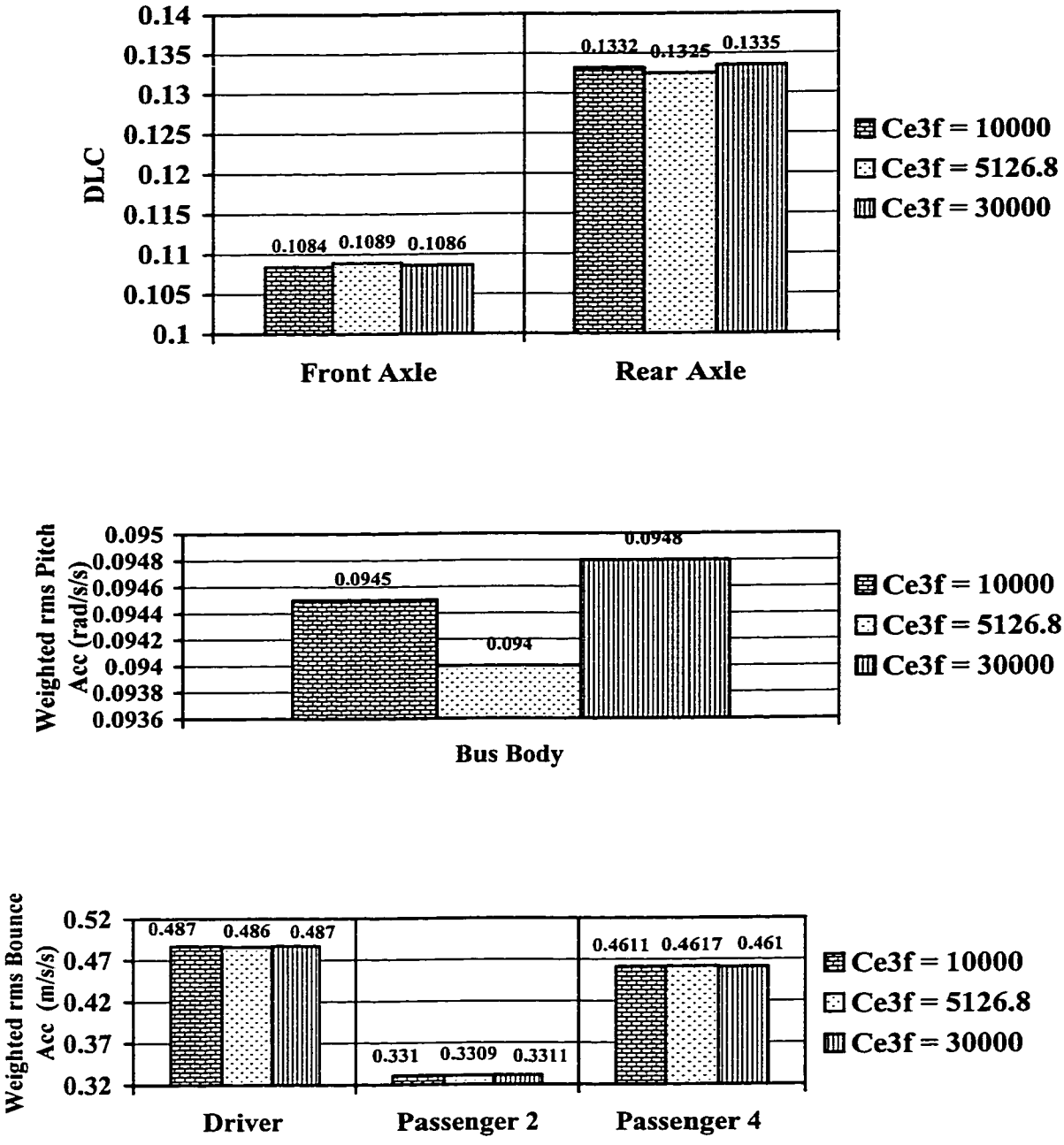

Figure 4.6b: Effect of C_{cfl} on DLC, weighted rms bounce and pitch acceleration

4.3.1.2 Influence of rear damper parameter variations

The influence of variations in the parameters of rear dampers, employed in the bus suspension, on the performance measures of the bus are illustrated in Table 4.7 and Table 4.8. The results show that variations in rear suspension damping parameters affect the performance measures of the rear suspension distinctively, whereas the change for front suspension related parameters is not significant. The DLC due to tire forces on both axles decreases only slightly with increase in compression mode damping C_{crl} and asymmetry factor p_r. The results show that the DLC due to tire forces on front axle doesn't change appreciably when C_{crl} is changed by 25% from its nominal value. Change in rear suspension damper asymmetry factor p_r of 25% affects the performace measures of rear suspension appreciably but the front suspension related measures doesn't change significantly. The effect of p_r is more pronounced when it is reduced 25% from the nominal value which increases the rear tires DLC to about 5% and increase of 25% in p_r from the nominal value decreases the DLC of rear tires by about 3%. The Sweatman's road stress factor shows the same trend with an increase of 4% for reduction of 25% in p_r and a decrease of 2% for increment in p_r of 25% in the nominal value. The rms vertical acceleration for driver or passenger 1 to passenger no 4 seats change noticeably for the rear seats such as passenger no 3 and passenger no 4. The reduction in weighted pitch acceleration by 2 - 3% for a change of 25% in p_r is observed. The reduction in rear tire DLC is accompanied by an increase in front tire DLC but this increase in front tire DLC is negligible compared to substantial gain for rear wheel DLC. The effect of rear suspension dampers rebound transition velocity is not substantial either for DLC or for vertical acceleration compared to the effect of compression mode damping coefficient.

The rear tire force DLC reduces about 1.5% for the reduction of 25% in the transition velocity whereas it reduces about 1% for 25% increase in transition velocity. The effect of transition velocity to the rms vertical acceleration or to rms weighted vertical acceleration is negligible for all seats except the seat no 2 which shows 1.7% increase in rms vertical acceleration and 2.4% in weighted rms vertical acceleration for the reduction of 25% in transition velocity.

Location	Perform. Measure	C_{crl}(Ns/m)			p_r			V_{el}(m/s)		
		468	**624.6**	**781**	**14.55**	**19.40**	**24.25**	**-0.234**	**-0.311**	**-0.389**
Front Axle	F_{max}(kN)	91.93	91.05	90.22	89.77	91.05	92.072	91.03	91.05	91.06
	CF	1.6911	1.6794	1.667	1.6558	1.6794	1.6982	1.6791	1.6794	1.6795
	DLC	0.1067	0.1089	0.1115	0.1074	0.1089	0.1102	0.1085	0.1089	0.1092
	RSF	1.9119	1.9327	1.953	1.9091	1.9327	1.9541	1.9328	1.9327	1.9331
	IF	1.1667	1.1791	1.1914	1.1673	1.1791	1.1909	1.1791	1.1791	1.1791
Rear Axle	F_{max}(kN)	158.81	160.54	162.32	157.61	160.54	162.95	160.47	160.54	160.57
	CF	1.6982	1.717	1.7356	1.6851	1.7170	1.7435	1.7162	1.7170	1.7173
	DLC	0.1362	0.1325	0.128	0.1399	0.1325	0.1280	0.1344	0.1325	0.1316
	RSF	2.2392	2.2011	2.1428	2.2954	2.2011	2.1417	2.2238	2.2011	2.1898
	IF	1.2311	1.218	1.1929	1.2302	1.2180	1.2058	1.2212	1.2180	1.2165
Driver	$\ddot{z}_{rms}$ (m/s^2)	0.9468	0.9654	0.9839	0.9143	0.9654	1.0159	0.9568	0.9654	0.9729
	$\ddot{z}_{w,rms}$ (m/s^2)	0.4768	0.486	0.4921	0.4532	0.4860	0.5234	0.4779	0.4860	0.4931
	$\ddot{\theta}_{rms}$ (rad/s^2)	0.1815	0.185	0.1874	0.1756	0.1850	0.1958	0.1829	0.1850	0.1871
	$\ddot{\theta}_{w,rms}$ (rad/s^2)	0.0927	0.094	0.0959	0.0914	0.0940	0.0970	0.0937	0.0940	0.0947
Passengr 1	$\ddot{z}_{rms}$ (m/s^2)	0.5309	0.5452	0.5526	0.5165	0.5452	0.5749	0.5403	0.5452	0.5490
	$\ddot{z}_{w,rms}$ (m/s^2)	0.3389	0.3444	0.3523	0.3154	0.3444	0.3771	0.3365	0.3444	0.3504
Passengr 2	$\ddot{z}_{rms}$ (m/s^2)	0.4895	0.4981	0.5051	0.4733	0.4981	0.5294	0.4897	0.4981	0.5033
	$\ddot{z}_{w,rms}$ (m/s^2)	0.3271	0.3309	0.3348	0.3023	0.3309	0.3631	0.3230	0.3309	0.3368
Passengr 3	$\ddot{z}_{rms}$ (m/s^2)	0.5435	0.5242	0.5056	0.5586	0.5242	0.4986	0.5306	0.5242	0.5178
	$\ddot{z}_{w,rms}$ (m/s^2)	0.3407	0.3259	0.3141	0.3581	0.3259	0.2974	0.3318	0.3259	0.3181
Passengr 4	$\ddot{z}_{rms}$ (m/s^2)	0.863	0.8306	0.797	0.8737	0.8306	0.7865	0.8366	0.8306	0.8234
	$\ddot{z}_{w,rms}$ (m/s^2)	0.4786	0.4617	0.4476	0.4983	0.4617	0.4296	0.4687	0.4617	0.4536

Table 4.7: Performance variation due to the change in rear damper parameters

Location	Perform. Measure	C_{c2r} (γ_{c1r}) (Ns/m)			C_{e3r} (γ_{e2r}) (Ns/m)		
		1500	**624.6**	**3000**	**8000**	**4580.7**	**12000**
Front Axle	F_{max}(kN)	90.94	91.05	90.90	90.97	91.05	90.97
	CF	1.6774	1.6794	1.6767	1.6779	1.6794	1.6779
	DLC	0.1092	0.1089	0.1092	0.1093	0.1089	0.1092
	RSF	1.9365	1.9327	1.9367	1.9370	1.9327	1.9368
	IF	1.1797	1.1791	1.1797	1.1797	1.1791	1.1797
Rear Axle	F_{max}(kN)	162.35	160.54	162.34	162.37	160.54	162.36
	CF	1.7382	1.7170	1.7382	1.7382	1.7170	1.7381
	DLC	0.1191	0.1325	0.1139	0.1234	0.1325	0.1234
	RSF	2.0456	2.2011	1.9878	2.0946	2.2011	2.0939
	IF	1.1959	1.2180	1.1874	1.2030	1.2180	1.2029
Driver	$\ddot{z}_{rms}$ (m/s^2)	0.9846	0.9654	0.9823	0.9643	0.9654	0.9641
	$\ddot{z}_{w,rms}$ (m/s^2)	0.4926	0.486	0.4911	0.4846	0.4860	0.4841
	$\ddot{\theta}_{rms}$ (rad/s^2)	0.1868	0.185	0.1865	0.1837	0.1850	0.1835
	$\ddot{\theta}_{w,rms}$ (rad/s^2)	0.0949	0.094	0.0947	0.0923	0.0940	0.0921
Passengr1	$\ddot{z}_{rms}$ (m/s^2)	0.5512	0.5452	0.5504	0.5364	0.5452	0.5349
	$\ddot{z}_{w,rms}$ (m/s^2)	0.3487	0.3444	0.3473	0.3404	0.3444	0.3402
Passengr 2	$\ddot{z}_{rms}$ (m/s^2)	0.5047	0.4981	0.5043	0.4953	0.4981	0.4948
	$\ddot{z}_{w,rms}$ (m/s^2)	0.3357	0.3309	0.3353	0.3285	0.3309	0.3279
Passengr 3	$\ddot{z}_{rms}$ (m/s^2)	0.5055	0.5242	0.5073	0.5344	0.5242	0.5356
	$\ddot{z}_{w,rms}$ (m/s^2)	0.3137	0.3259	0.3156	0.3462	0.3259	0.3469
Passengr 4	$\ddot{z}_{rms}$ (m/s^2)	0.8004	0.8306	0.8023	0.8339	0.8306	0.8337
	$\ddot{z}_{w,rms}$ (m/s^2)	0.4474	0.4617	0.4489	0.4662	0.4617	0.4673

Table 4.8: Performance variation due to the change in front damper no of phases

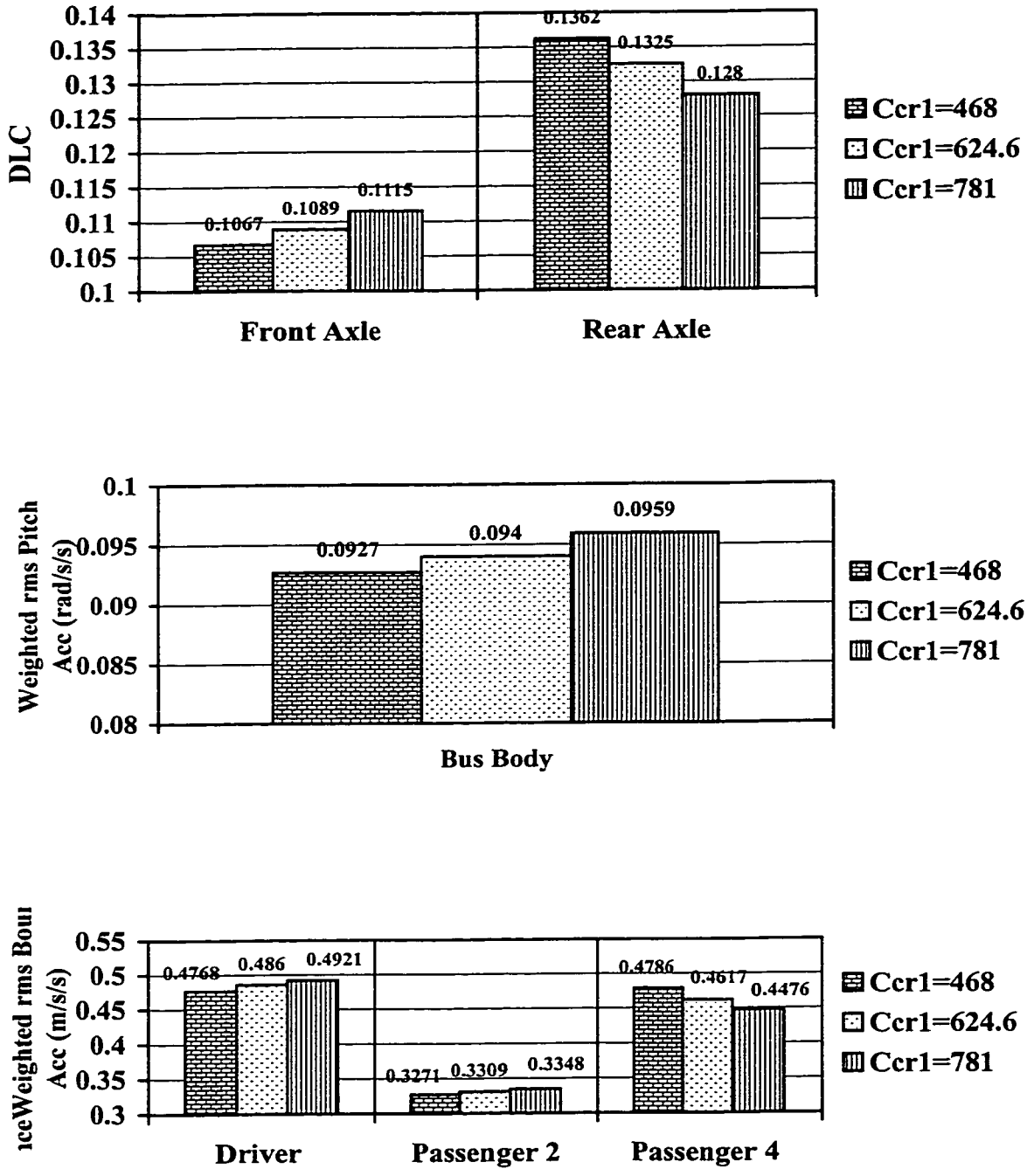

Figure 4.7a: Effect of C_{cr1} on DLC, weighted rms pitch and bounce acceleration

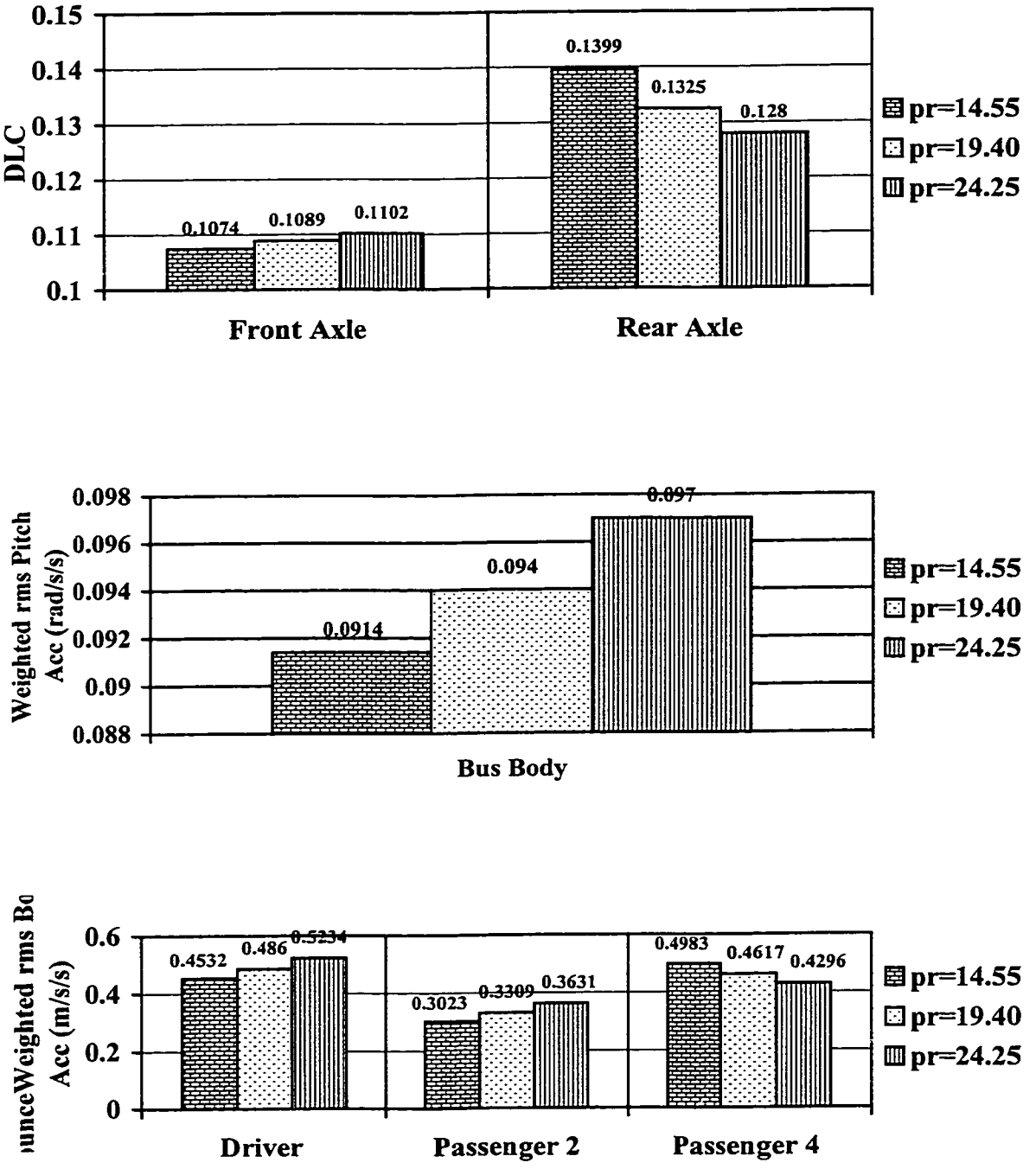

Figure 4.7b: Effect of asymmetry ratio p_r on DLC, weighted rms bounce and pitch acceleration

From the results it may be concluded that rear suspension dampers with a little higher compression mode damping and low degree of asymmetry can yield considerable improvement in the ride quality of the rear seats with only slight deterioration of the front tire DLC performance.

A reduction in the rebound damping transition velocity yields insignificant influence on the DLC, and slightly lower values of rms accelerations. It should also be noted that an increase in suspension damping tends to effectively suppress the ride vibration in the vicinity of resonant frequencies, while the magnitudes of transmitted vibration in relatively higher isolation frequency range increase. The suspension seats are known to effectively attenuate vertical vibration at frequencies above 2Hz. The suspension seat may thus provide further reductions in the rms vertical accelerations.

A 25% increase in the compression mode damping yields 5 - 10% reduction in the overall rms acceleration, while the corresponding increase in DLC is also from 1 - 2%. A higer reduction in DLC is observed by increasing the degree of assymetricity, especially for the rear dampers. While the variations in rebound mode reduction factor (γ_{el}) reveals insignificant influence on the DLC. The trends for the sensitivity of key perfomance measures due to change in rear damper parameters are further illustrated in Figure 4.8.

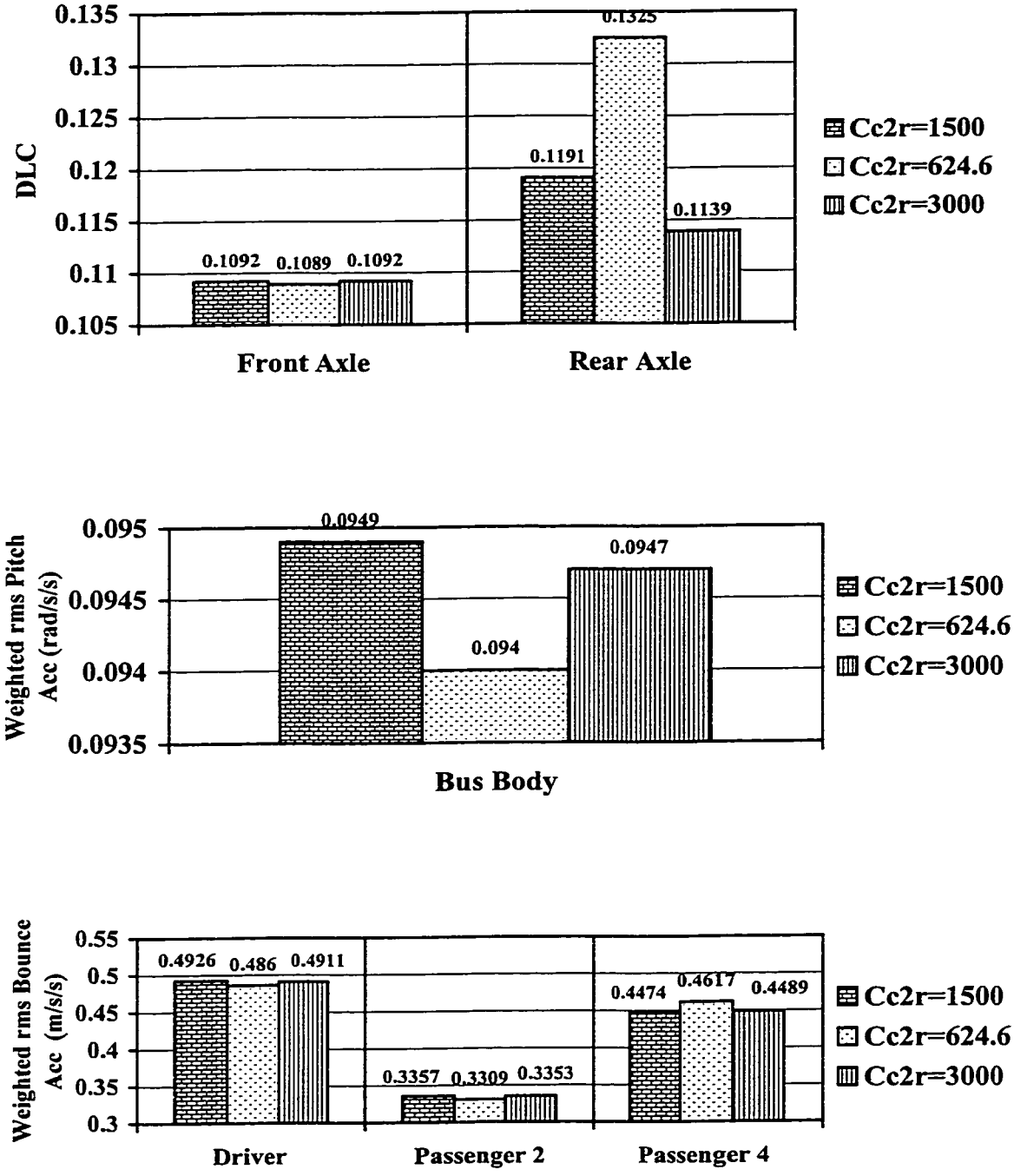

Figure 4.8a: Effect of adding second compression phase C_{c2r} (in rear dampers) on DLC, weighted rms bounce and pitch acceleration

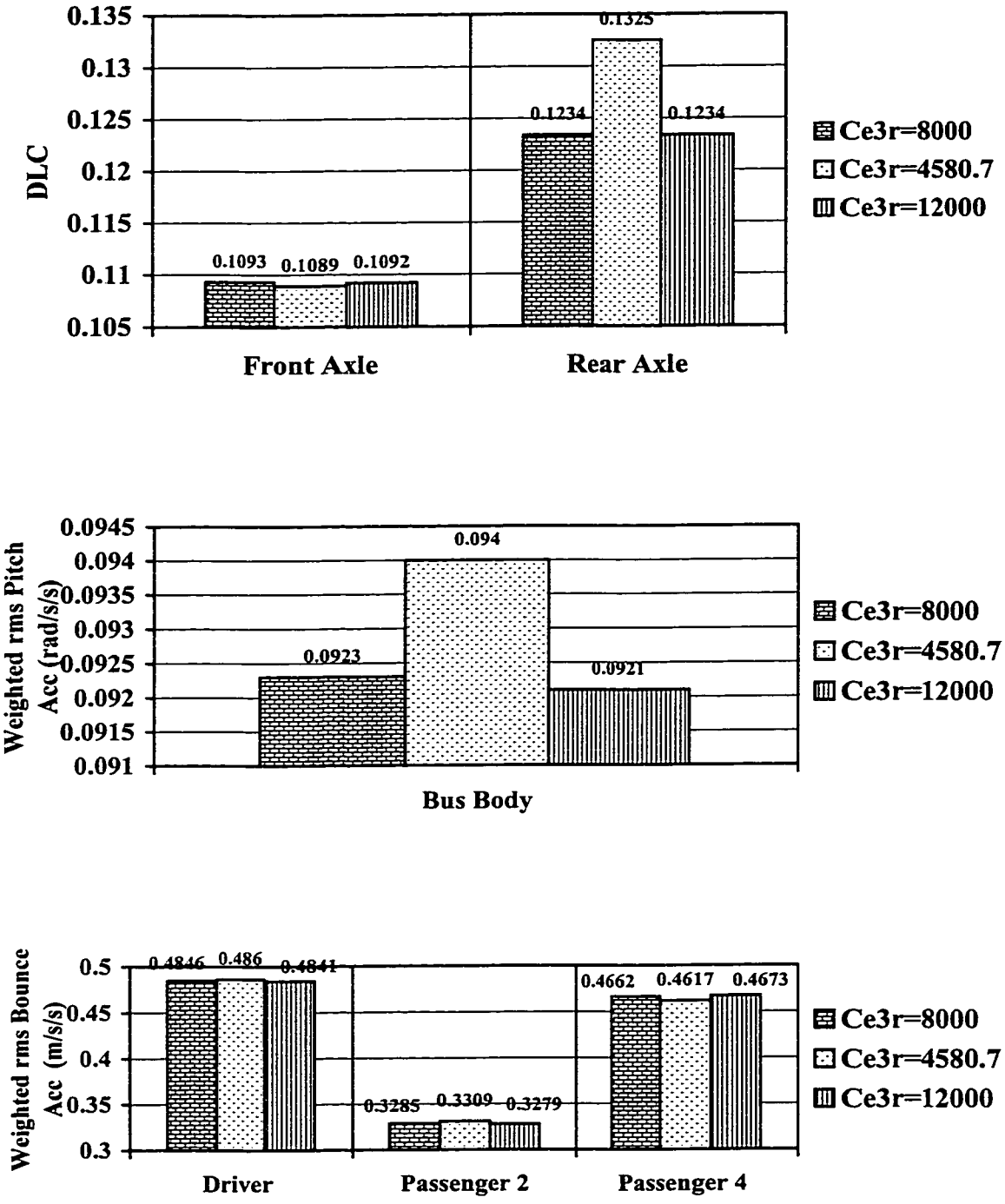

Figure 4.8b: Effect of adding third extention phase C_{e3r} on DLC, weighted rms bounce and pitch acceleration

4.3.2 Influence of Variations in Air Spring Constants

It is known that soft suspension springs can yield considerable reductions in performance measures related to ride quality and road damage potentials. On the other hand such measure poses severe constraints on the directional performance and rattle space requirements. Hard suspension springs although provide improved handling it is not desirable as it deteriorates both driver/passenger and road friendliness performances.

Modern urban bus suspension consists of air springs which provide relatively low stiffness in the ride zone, and high spring rate under extreme compressive deflections to enhance the directional performance of the vehicle. The spring rates also remain low under extreme rebound defelections. Such force-deflection characteristics of air springs are attained through design of piston geometry, which tends to influence the effective area and thus the force-deflection characteristics. The influence of variations in effective area on the performance measures is thus investigated in this study. From the measured force-deflection characteristics, it was established that the effective area is primarily related to the instantaneous bag height. As shown in section 2.4.1 the effective area was expressed as a polynomial function of dynamic deflection δ, where the area is mostly influenced by the constant coefficient k_0. The coefficient of the first order term, k_1, also revealed some contributions to the effective area in some of the candidate air bag designs.

The influence of variations in the force-deflection characteristics of air springs is investigated by varying the coefficients, k_0, and k_1, while the static ride height is maintained at the specific values. An increase in k_0 yields a direct increase in the effective area and thus a lower charge pressure may be required to achieve the desired ride height. This can also lead to relatively lower stiffness due to air spring.

4.3.2.1 Influence of Front Air Spring Parameter Variation

Table 4.9 presents the performance measures for variations in spring factors k_{of} and k_{1f}. It is clear from the results that when k_{of} is either increased or decreased 25% from its nominal value the effect is substantial in the DLC of front tire forces and the ride response of the front seats. The effect in the rear tire force DLC response as well as RSF, IF and maximum tire force is marginal. The driver is exposed around 1.5% less rms vertical acceleration when k_{of} is reduced 25% from its nominal value. Similarly when k_{of} is increased 25% there is an increase of about 1.5% in the driver rms and weighted rms vertical accelerations. Similarly the increase in rms weighted acceleration, is neglegible for the change in k_{of} for the rear passenger seats (# 3 and 4). The rms and weighted rms pitch accelerations also change only 1 - 2% for 25% change in k_{of}. The trend of change due to k_{1f} seems opposite to that of k_{of} but the magnitude is very small. Figure 4.9 therefore, only summarizes the key results corresponding to the change in k_{of}.

4.3.2.2 Influence of Rear Air Spring Parameter Variations

Similar to front spring, the rear air spring factors k_{0r} and k_{1r} are considered for their effect on the performance measures. From the results presented in Table 4.10, it is clear that when k_{0r} is either increased or decreased 25% from its nominal value the effect is substantial on performance measures. The DLC, RSF, IF and maximum tire force change insignificantly upon changing the parameter k_{0r}. The weighted rms vertical acceleration reduces 5 - 10% for a reduction of 25% in k_{0r} and the same is observed at different seats for an increase of 25% in k_{0r}. The pitch effect is almost same with 5% change both ways. Similar to front springs, the change in k_{1r} effects insignificantly on

Location	Perform. Measure	k_{of}		
		22.4	29.8	37.3
Front Axle	F_{max}(kN)	90.43	91.05	91.61
	CF	1.6791	1.6794	1.6796
	DLC	0.1112	0.1089	0.1051
	RSF	1.9483	1.9327	1.9156
	IF	1.1804	1.1791	1.1776
Rear Axle	F_{max}(kN)	160.57	160.54	160.52
	CF	1.7173	1.7170	1.7168
	DLC	0.1323	0.1325	0.1327
	RSF	2.1987	2.2011	2.2032
	IF	1.2172	1.2180	1.2189
Driver	$\ddot{z}_{rms}$ (m/s^2)	0.9524	0.9654	0.9779
	$\ddot{z}_{w,rms}$ (m/s^2)	0.4796	0.4860	0.4925
	$\ddot{\theta}_{rms}$ (rad/s^2)	0.1819	0.1850	0.188
	$\ddot{\theta}_{w,rms}$ (rad/s^2)	0.0921	0.0940	0.0958
Passengr1	$\ddot{z}_{rms}$ (m/s^2)	0.5345	0.5452	0.556
	$\ddot{z}_{w,rms}$ (m/s^2)	0.3408	0.3444	0.348
Passengr 2	$\ddot{z}_{rms}$ (m/s^2)	0.4916	0.4981	0.5046
	$\ddot{z}_{w,rms}$ (m/s^2)	0.3276	0.3309	0.3343
Passengr 3	$\ddot{z}_{rms}$ (m/s^2)	0.5185	0.5242	0.53
	$\ddot{z}_{w,rms}$ (m/s^2)	0.3227	0.3259	0.3292
Passengr 4	$\ddot{z}_{rms}$ (m/s^2)	0.8226	0.8306	0.8383
	$\ddot{z}_{w,rms}$ (m/s^2)	0.4587	0.4617	0.4656

Table 4.9: Performance variation due to the change in front air spring parameters

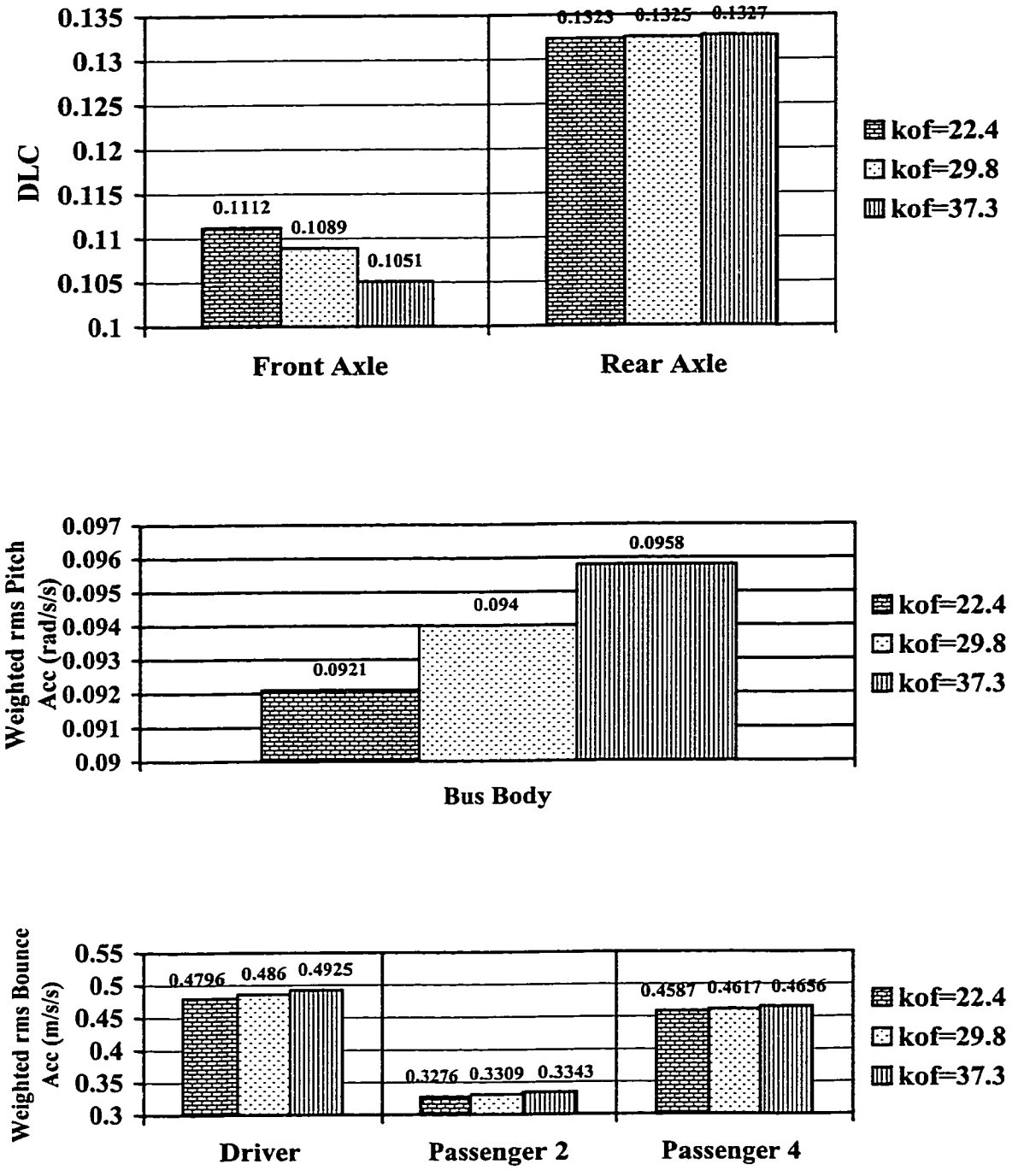

Figure 4.9: Effect of front spring stiffness k_{of} on DLC, weighted rms bounce and pitch acceleration

Location	Perform. Measure	k_{or}		
		56.90	**75.9**	**94.9**
Front Axle	F_{max}(kN)	91.819	91.05	90.09
	CF	1.6836	1.6794	1.6769
	DLC	0.108	0.1089	0.1096
	RSF	1.9208	1.9327	1.9445
	IF	1.1716	1.1791	1.1853
Rear Axle	F_{max}(kN)	158.28	160.54	162.25
	CF	1.7083	1.717	1.7232
	DLC	0.1338	0.1325	0.1317
	RSF	2.2183	2.2011	2.1876
	IF	1.2213	1.218	1.2162
Driver	$\ddot{z}_{rms}$	0.9034	0.9654	1.052
	$\ddot{z}_{w,rms}$ (m/s^2)	0.4519	0.486	0.5332
	$\ddot{\theta}_{rms}$ (rad/s^2)	0.1713	0.185	0.2038
	$\ddot{\theta}_{w,rms}$ (rad/s^2)	0.0868	0.094	0.1036
Passengr 1	$\ddot{z}_{rms}$ (m/s^2)	0.5098	0.5452	0.5947
	$\ddot{z}_{w,rms}$ (m/s^2)	0.3196	0.3444	0.3784
Passengr 2	$\ddot{z}_{rms}$ (m/s^2)	0.4611	0.4981	0.5488
	$\ddot{z}_{w,rms}$ (m/s^2)	0.3072	0.3309	0.3637
Passengr 3	$\ddot{z}_{rms}$ (m/s^2)	0.4832	0.5242	0.58
	$\ddot{z}_{w,rms}$ (m/s^2)	0.3026	0.3259	0.3582
Passengr 4	$\ddot{z}_{rms}$ (m/s^2)	0.776	0.8306	0.9066
	$\ddot{z}_{w,rms}$ (m/s^2)	0.428	0.4617	0.5079

Table 4.10: Performance variation due to the change in rear air spring parameters

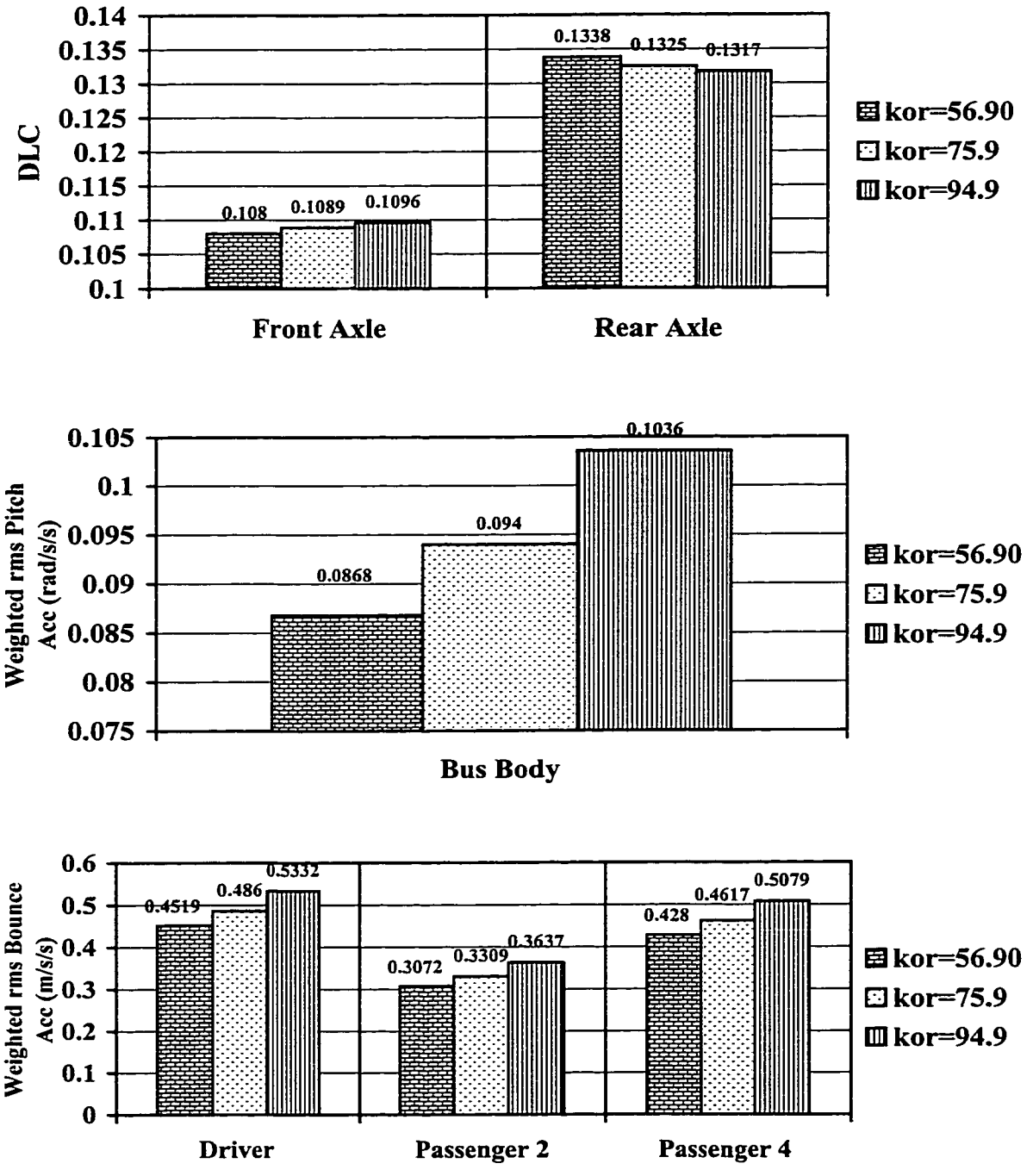

Figure 4.10: Effect of k_{or} on DLC, weighted rms bounce and pitch acceleration

ride environment related to the rms vertical acceleration at the driver/passenger seat and the dynamic tire force transmitted to the pavement. The key results, corresponding to change in k_{or} are presented in figure 4.10 to illustrate the trends.

4.4 Influence of Variations in Geometrical Parameters

There are several geometrical parameters involved in the design of bus and its suspension. Among these, the parameters such as the position of suspension along the axle, their orientation (inclination), wheel base and ride height may play a role in the driver/passenger and road friendliness performance of the bus. Simulation results for the candidate bus pitch-plane model show negligible influence for such parameters except for wheel base and ride height. This section presents the results related to the variation of these two geometric parameters

The wheel base distance is important for beaming effect, pitch plane vibration and also for the structural point of view. The change in wheel base is considered for pitch plane vibration, and performance of interest but not for the structural integrity. The ride height of the bus can be changed to certain extent by varying the static pressure in the air spring. In this case the suspension air springs will work about a new static equilibrium. Table 4.11 presents the effects of variation in wheel base and ride height. Reducing wheel base is beneficial for the ride environment but its effect is deteriorating for the road friendliness. The maximum force on front wheels increases substantially which causes premature rutting in road surface. The wheel base increment is not driver/passenger friendly although it reduces DLC but ride environment is not acceptable due to significant increase in pitch acceleration.

Change in the ride height effects the ride environment but its effect is also not very significant. If the ride height is reduced 2" from its original height than the effect is deteriorating for overall ride environment as it increases DLC, RSF and IF for the front and rear axles but the change is not very significant. On the other hand if the ride height is increased 2" from its reference height than the ride environment improves in almost every respect. The improvement is however, insignificant compared to loss of the height as it is one of the aim in designing low floor modern urban buses. The trend of the results for both wheel base and ride height are summarized in Figure 4.11a and 4.11b.

Location	Perform. Measure.	Wheel Base (m)			Ride Height		
		5.5	6.2	7.0	Ref - 2"	Ref	Ref + 2"
Front Axle	F_{max}(kN)	85.17	91.05	93.55	91.03	91.05	91.07
	CF	1.6941	1.6794	1.6655	1.6790	1.6794	1.6797
	DLC	0.1156	0.1089	0.1028	0.1092	0.1089	0.1087
	RSF	2.0069	1.9327	1.8681	1.9360	1.9327	1.9309
	IF	1.1902	1.1791	1.1691	1.1796	1.1791	1.1788
Rear Axle	F_{max}(kN)	170.62	160.54	158.05	160.45	160.54	160.61
	CF	1.7203	1.7170	1.7271	1.7161	1.7170	1.7178
	DLC	0.1299	0.1325	0.1397	0.1320	0.1325	0.1331
	RSF	2.1701	2.2011	2.1673	2.2025	2.2011	2.2002
	IF	1.2137	1.2180	1.2133	1.2182	1.2180	1.2179
Driver	$\ddot{z}_{rms}$ (m/s^2)	0.9192	0.9654	1.0242	0.9726	0.9654	0.9604
	$\ddot{z}_{w,rms}$ (m/s^2)	0.4642	0.4860	0.5127	0.4893	0.4860	0.4837
	$\ddot{\theta}_{rms}$ (rad/s^2)	0.1718	0.1850	0.1918	0.1866	0.1850	0.1837
	$\ddot{\theta}_{w,rms}$ (rad/s^2)	0.0880	0.0940	0.0980	0.0949	0.0940	0.0932
Passengr 1	$\ddot{z}_{rms}$ (m/s^2)	0.5385	0.5452	0.5653	0.5481	0.5452	0.5434
	$\ddot{z}_{w,rms}$ (m/s^2)	0.3397	0.3444	0.3501	0.3463	0.3444	0.3432
Passengr 2	$\ddot{z}_{rms}$ (m/s^2)	0.5155	0.4981	0.5132	0.5007	0.4981	0.4964
	$\ddot{z}_{w,rms}$ (m/s^2)	0.3205	0.3309	0.3403	0.3327	0.3309	0.3298
Passengr 3	$\ddot{z}_{rms}$ (m/s^2)	0.4940	0.5242	0.4931	0.5272	0.5242	0.5221
	$\ddot{z}_{w,rms}$ (m/s^2)	0.3141	0.3259	0.3412	0.3277	0.3259	0.3248
Passengr 4	$\ddot{z}_{rms}$ (m/s^2)	0.7963	0.8306	0.8809	0.8366	0.8306	0.8266
	$\ddot{z}_{w,rms}$ (m/s^2)	0.4463	0.4617	0.4798	0.4648	0.4617	0.4596

Table 4.11: Performance variation due to the change in rear geometrical parameters

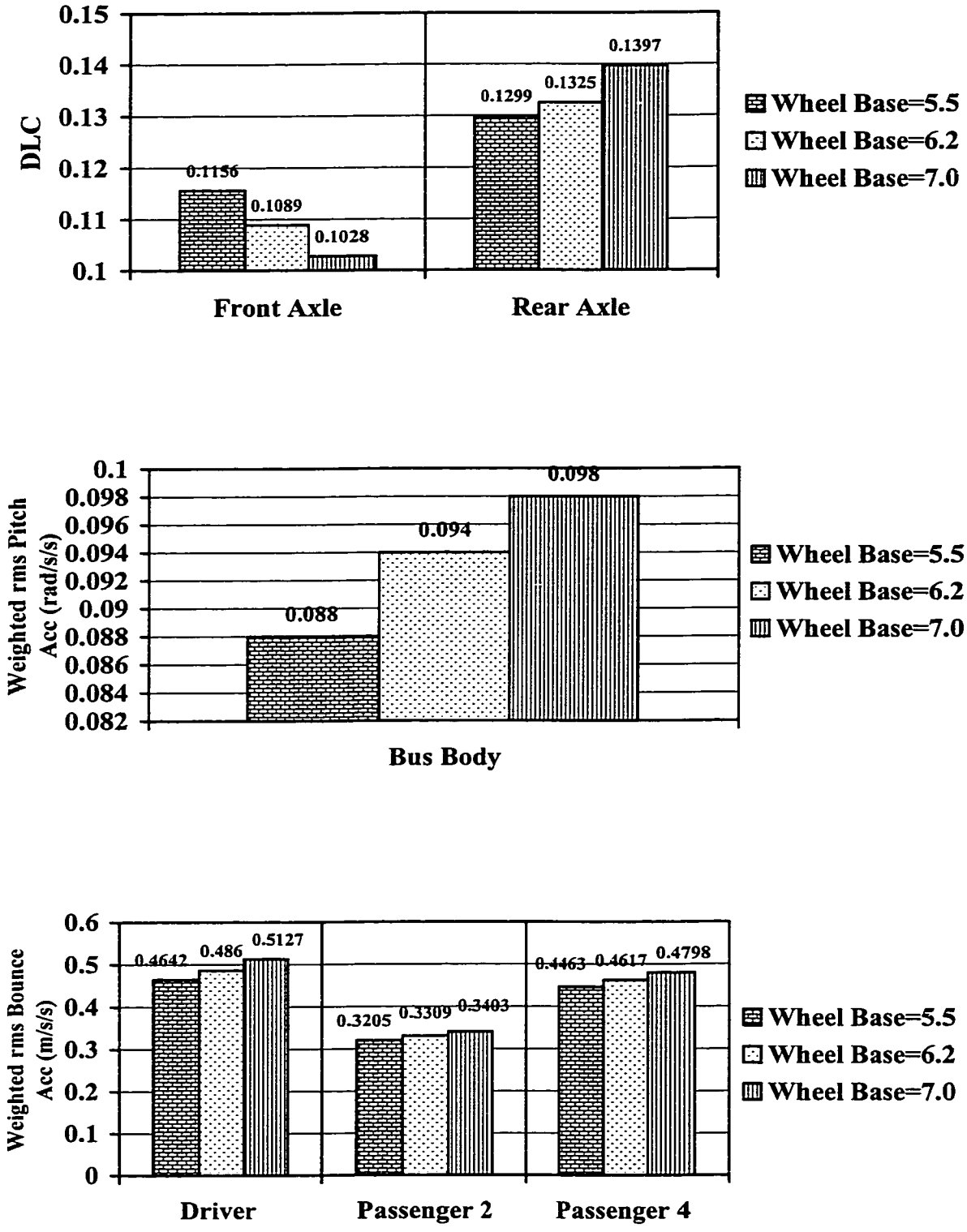

Figure 4.11a: Effect of Wheel Base on DLC, weighted rms bounce and pitch acceleration

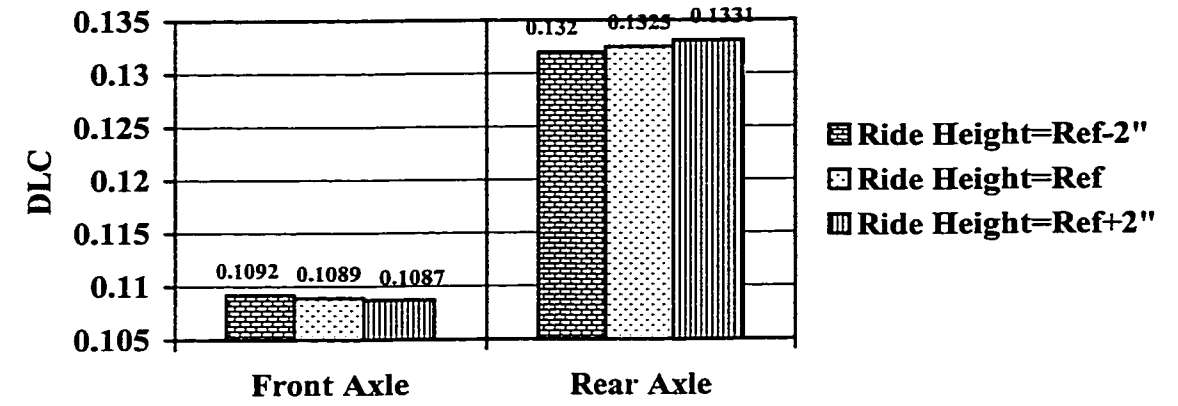

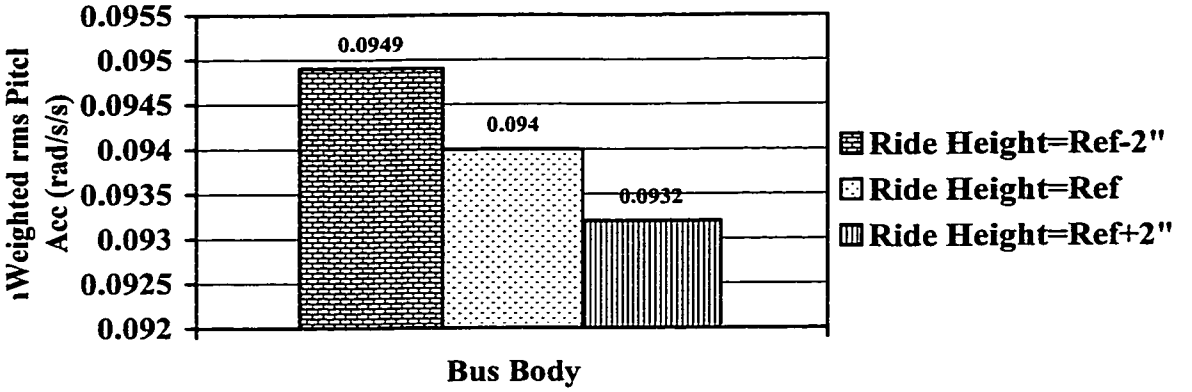

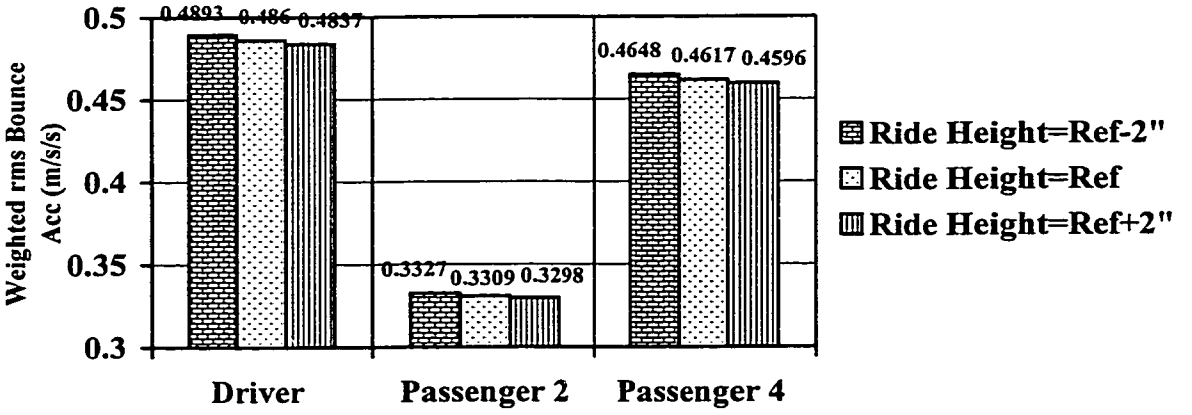

Figure 4.11b: Effect of Ride height on DLC, weighted rms bounce and pitch acceleration

CHAPTER 5

CONCLUSIONS AND RECOMMENDATIONS

5.1 Highlight of the Study

Modern urban buses operating on deteriorated urban roads are known to yield poor driver/passenger ride quality and excessive pavement load. This study is thus undertaken to examine the performance of a modern urban bus on measured urban road conditions. Due to the focus of the study on ride and pavement load, a pitch plane model of the bus with six DOF is formulated. Important components of bus related to suspension system and tire were tested in the laboratory to establish their nonlinear characteristics. Models are then developed for each of these components such that their nonlinear behavior can be simulated. Measured data from roads around Montreal was used to select three representative urban road excitations in terms of smooth, medium rough and rough roads.

The developed pitch plane model is first validated against available full scale road test data to gain confidence on both qualitative and quantitative reliability of the pitch plane model. The validated model is utilized to carryout an extensive parameteric study on the driver/passenger and road friendliness performance of the vehicle. An extensive set of performance measures were established that will reflect the performance of the bus for ride quality of driver/passenger as well as road damage potential due to dynamic tire loads. The performance of the bus for variation in several operating and design

parameters were obtained to establish criterion for improved bus design. Important conclusions drawn from the parametric study are highlighted in the following.

5.2 Specific Conclusion

The ride quality of the bus and pavement damaging potentials of the wheels are investigated for excitations arising from smooth, medium rough and rough roads. The rms and weighted rms vertical acceleration are selected to assess the driver/passenger of the bus. DLC, peak force, RSF etc. are used to assess the pavement load performance. The performance of the bus is investigated for various operating and design conditions. The results of the parametric study are summarized as follows.

- The driver is subjected to considerably higher whole body vibrations attributed to higher pitch motion at the driver seat compared to seats in the middle of the bus.
- The ride quality of the bus deteriorates considerably with increase in road roughness, vehicle speed and reduction in bus load. The bus running at 30km/hr on smooth road and full load yields best ride quality.
- The tire inflation pressure also effects the ride quality of the bus considerably. The higher the tire inflation pressure the higher is the road damage potential and ride vibration at driver/passenger seat. There are however, limitations to minimum tire pressure that can be used due to other factors such as traction and rolling resistance since bus load vary widely over a short period of time, an adaptive system to maintain minimum pressure would be an ideal solution.
- The damper asymmetricity for the front and rear dampers plays crucial role in the vibration isolation for driver and passenger seats. There is a reduction in weighted

rms vertical acceleration and respective DLC by adding a second compression phase in front and rear dampers. Increasing the second phase damping coefficient improves overall ride and dynamic load performance but above the optimum value it proves deteriorating for the perfomance. For both front and rear dampers the dual compression phase damper is thus better than the single compression phase dampers which are installed in the candidate bus design.

- Introduction of one more rebound phase in the dampers was found to have insignificant influence on the performance measure.
- The spring area k_0 can be an effective parameter to reduce the overall rms vibration at the driver/passenger seats without effecting the road damaging potential of the tire forces substantially. Its effect is more prominent for the farthest seats such as the driver and passenger no 4. The higher terms of the air spring area k_1, k_2... are not effective to change ride quality of the bus either seen from road friendliness or driver/passenger friendliness point of view.
- The position and orientation (inclination) of the suspension dampers are found to have insignificant influence on the performance measures of the pitch plane model.
- The front springs are placed side by side along the length close to each other which has a diminishing effect on the pitch motion of the axle. Reduction of this distance has a considerably large effect specially on DLC and also on RSF, IF and the maximum front tire force. Although the rms vertical vibration also reduces by reducing the distance between the two front springs but the effect of front tire force DLC is more deteriorating to the road friendliness of the bus.

- The horizontal distance between the pair of springs for front and rear axles is not a sensitive parameter for the ride performance of the bus. Its increment has almost no effect whereas its reduction is little better for the rear axle pitch vibration.
- Reducing the ride height increases the DLC, road damage potential and overall vibration at driver/passenger seat. The higher the bus the less is its DLC, road damage potential and the rms vibration at driver/passenger seats but since the effect is not substantial and also it deteriorates the roll and handling performance of the bus change in the ride height is not recommendable.
- The effect of wheel base variation is also significant. Increment in wheel base is not beneficial whether for ride or the dynamic load performance of the bus. Reducing the wheel base improves overall ride environment of the bus but on the other hand the load shift from rear to front is undesirable as it can promote rutting. Since this load shift due to reduction in wheel base is substantial it is therefore not recommended.

5.3 Recommendations for Future Work

Present research work resulted in a computer simulation model which has been validated using the field test data. The potential usefulness of the computer model can be further enhanced upon consideration of the following:

- Due to significant cross-level variations in urban roads, a 3-D model of urban bus should be studied. The model developed in this study can be extended to include roll which also effects the ride performance of a vehicle.
- From the field test experience it was found that the drive train of the vehicle, directly installed on the chassis frame, rear end on the back of passenger number 4 seat,

imposes vibrations in the higher frequency bands. The eccentric engine placement is another factor which may cause unequal higher frequency vibrations among right and left side of the bus. It is thus recommended to incorporate the drive-train components and their mounts in the model. Such a model can provide significant information related to the influence of drive-train vibration on the overall ride quality.

- The urban bus with excessive vehicle weight transmits considerably large dynamic loads to the pavements. Suspension dampers assymetricity and nonlinearities are important factors in optimizing driver/passenger ride comfort and road friendliness. The proposed two-step (phase) compression damper is better studied in detail with a three dimensional model. It is thus recommended to undertake a comprehensive three dimensional model study with optimization carried out on performance measures related to characteristics of the dampers.
- In the present investigation the seats are taken as rigidly attached to the bus floor. In practice there exists flexibilities associated with mounts and cushion on seats. Such flexibilities can be incorporated in the model to obtain better estimate of ride quality.

REFERENCES

1. Rauhut, J. B., Roberts F.L., Kennedy T.W., "Response and Distress Models for Pavement Studies", TRR 641 pp 7-14 1979.

2. Pell, P. S.. "Pavement Materials"., Proc 6th Int. Conf. On the Structural Design of Asphalt Pavements, Vol II pp 35-70, July 1987.

3. Gillespie, T. D., et al., "Effects of Heavy Vehicle Characteristics on Pavement Response and Performance". Transportation Research Board, NCHRP Report 1 - 25 (1) 1992.

4. Lin, Wen Kan et al., "Dynamic wheel/pavement force sensitivity to variations in heavy vehicle parameters, speed and road roughness", Heavy Vehicle Systems, Int. J. of vehicle design, 1(2), 1994, pp139-155.

5. Kulakowski B. T. et al., "A Study of Dynamic Wheel Loads Conducted Using A Four-Post Road Simulator, Road Transport Technology-4, Proceedings of the fourth international symposium on heavy vehicle weights and dimensions, 1995, pp301-307.

6. Sharp R.S. and Crolla D.A. "Road Vehicle Suspension System Design A review", Vehicle System Dynamics, 16, 1987, pp. 167-192.

7. Gibby, Reed et al., "Local urban transit bus impact on pavements", J. of Transportation Engineering, May-June 1996, pp 215-217.

8. Sweatman, P.F., "A study of dynamic wheel forces in axle group suspensions for heavy vehicles", ARRB Special Report, 127, 1987.

9. Muluka V. G., Rakehja S., Haseganu E. M., "Reduction of Dynamic Pavement Loads of Heavy Vehicles Through Optimal Suspension Damping and Axle Vibration Absorber", SAE Paper 962148, 1996.

10. Heath, A. N. and Goods, M. C., "Heavy vehicle design parameters and dynamic pavement loading", Australian Road Research, vol. 15 no. 4, 1985.

11. A. Hac, Adaptive Control of Vehicle Suspension, Vehicle System Dynamics, 16 (1987), pp. 57-74.

12. Oeslati, F,. et. al. "Investigation of a limited-state active suspension for articulated heavy vehicles", SAE Truck and Bus Meeting. Sept. 1995.

13. Woodrooffe J., "Heavy Truck Suspension Damper Performance for Improved Road Friendliness and Ride Quality", SAE paper 952636, 1995.

14. Boileau, P.E. and Boutin, J (1992), "'Whole body vibration exposure in urban Buses", Proceeding CSME forum SCGM 1992, 'Transport 1992+', 4th June, Concordia University, Vol. 1, pp. 332-337.

15. D. Cebon, "Vehicle Generated Road Damage: a Review, "Vehicle System Dynamics, 18 (1989), pp. 107-150.

16. Hedrick, K. et al., "Determination of road stress factor for buses", US DOT Report, 1985.

17. Osama Hudaidi et al., "Nova low-floor bus building vibration and dynamic pavement loads study", NRC Report, B-5502.1, March 1998.

18. Rakheja, S. et al., "Ride vibrations of articulated vehicles and significance of secondary suspension", SAE 1989 Noise and Vibration Conf., SAE Pub. No. P-222, 1989, pp 139-147.

19. Dixon, J. C., "Tyres, suspension and handling", Cambridge University Press, 1991.

20. Margolis D. L., Edeal D., "Towards an Understanding of "Beaming" in Large Trucks", SAE paper 902285, 1990.

21. Smith A. R., "Frame Beaming, Fifth Wheel Location Special Body Mounting and Loading Problems", SAE paper 650179, 1965.

22. Rakheja S., Ahmed A. K. W., "Simulation of Non-Linear Variable Dampers Using Energy Similarity", Engineering Computations, Vol. 8, 333-344, 1991.

23. Kenis W. J., et. al., "Calibration of a Mathematical Vehicle Dynamic Model", Road Transport Technology-4, Proceedings of the fourth international symposium on heavy vehicle weights and dimensions, 1991, pp221-233.

24. Sujatha C., Phaskara Rao P. V., Narayanan S., "Whole-body vibration exposure in Indian buses", Heavy Vehicle System, Int. Journal of Vehicle Design, Vol. No. 2, 1995.

25. Cebon, David, "Interaction between heavy vehicles and roads", SAE Publication, SP951, 1992.

26. Urban Bus Optimal Passive Suspension Study, Phase 1 "Development of Optimal Suspension Characteristics Through Systematic Study of Reduced Models" Prepared by Concave Research Center, Concordia University, 1999.

27. Elmadany M. M., "A Procedure for Optimization of Truck Suspensions", Vehicle System Dynamics, 16 (1987), pp. 297-312.

28. Cebon D. "Examination of the Road Damage Caused by Three Articulated Vehicles. Proceedings 10th IAVSD Symposium on the Dynamics of the Vehicles on Roads and Tracks, Swets and Zeitlingers, Prague.

29. Robson, J. D., "Road Surface roughness and vehicle response", Int. Journal of Vehicle design, 1(1), 1979, pp 175-183.

30. Boileau, P.E. et. al., Caraterisation de l'environnement vibratoire dans differentes categories de vehicules", unpublished report IRSST, 1998

31. Barak P., "Magic Numbers in design of Suspension for passengers Cars", SAE Paper 911921, 1991.

32. Janeway R. N. "A practical Approach to Truck Ride Instrumentation and Evaluation - A Summary", SAE paper 660140, 1966.

33. Ghoneim H., Metwalli S. M., "Optimum Vehicle Suspension with a Damped Absorber", The ASME paper 83-DET-42, 1983.

34. E. N. Thrower, "A Parametric Study of a Fatigue Prediction Model for bituminous Road Pavement", TRRL Report LR892, 1979.

35. Dohi M., Maruyama Y., "Ride Comfort Optimization for Commercial Trucks", SAE paper 902266, 1990.

36. Butkunas A. A., "Power Spectral Density and Ride Evaluation", SAE paper 660138, 1966.

37. Oueslati F., Sankar S., "Optimization of a Tractor-Semitrailer Passive Suspension Using Covariance Analysis Technique", SAE paper 942304, 1994.

38. Alain Dulac, "An investigation of Ride and Handling Performance of passive and combined Active and Passive bus suspension", M.Eng Thesis, Concordia University, Montreal, Quebec, 1993.

39. D. B. Van Deussen, "Human Response to Vehicle Vibration", SAE Trans., Vol. 77, No. 1, pp. 328-345, 1968.

40. D. E. Goldmann, "A review of Subjective Responses to Vibratory Motion of the Human Body in the Frequency Range 1 to 10 cps", Naval Med. Res. Institute, Report No. 4, March 1948.

41. International Standard ISO 2631-1 Part-1: General requirement, "Mechanical Vibration and shock, Evaluation of human exposure to whole-body vibration", 1997 (E).

42. OECD, "Dynamic loading of Pavements", OECD Report, 1992.

43. Baum J. M., Bannett and T. G. Carne, "Truck Ride Improvement Using Analytical and Optimization Methods", SAE paper 770609, 1977.

44. G. K. Misoi and R. M. Carson, "Corrugation of Unmetalled Roads, Part 1: Vehicle Dynamics", proceedings of the ImeckE Vol. 203, 1989, pp. 205-214.

45. N. C. Jackson, "Pavement Performance-A State DOT Perspective", SAE Special Publication SP 765, paper number 881843 Nov. 1988.

46. J. P. Mahoney, "The relationship Between Axle Configurations, Wheel Loads and Pavement Structure", SAE Special Publication SP 765, paper number 881844, Nov 1988.

47. Wang K., "Dynamic Analysis of a tracked snowplowing vehicle and assessment of ride quality", August 1998.

48. Le Fevre W. F., "The Highway Truck Ride Problem", SAE paper 650177, 1965.

49. Afonso, M.F.R, "Ride Dynamic Analysis of Tracked Vehicles," M.Eng. Thesis, Concordia University, Montreal, Quebec, 1989.

50. Huhatala, M., "Field Test to Compare Tires". FHWA Load Equivalence workshop, Washington, Washington D.C., 1988.

51. A Factbook of the Mechanical Properties of the Components for Single-Unit and Articulated Heavy Trucks, National Highway Traffic Safety Administration, Final report, Dec 1986.

52. Anil Dhir, M. F. R., "Ride Dynamic of High Mobility Wheeled/Tracked off-Road Vehicles: Computer Simulation with Field Validation" M.Eng Thesis, Concordia University, Montreal, Quebec, 1993.

53. Damien, T. M. et. al., "Pavement profiling various pavements: Ottawa/Smith Falls", John Emery Geotechnical Engineering Report, 1992.

54. Throwes E.N., "A parametric Study of Fatigue Prediction Model for Bituminous Road Pavements", TRRRL Report LR 892,1979.

55. Anil Dhir, Seshadri Sankar, "Analytical Track Models for Ride Dynamic Simulation of Tracked Vehicles" J. of Terramechanics, Vol. 31, No. 2, pp 107-138, 1994.

56. Smith C. C., McGehee D. Y., Healey A. J., "The Prediction of Passenger Riding Comfort from Acceleration Data", Transactions of the ASME, Vol. 100, March 1978.

57. Thomson W. T. and Dahleh M. D., "Theory of vibration with applications", Fifth edition, Prentice Hall, 1998.

58. R.R. Addis and R.A. Whitmarsh, "Relative Damaging Power of Wheel Loads in Mixed Traffic", Transport and Road Research Laboratory, Laboratory Report LR979, 1981.

59. D.F. Kinder and M.G Lay, "Review of the Fourth Power Law", ARRB, Internal Report AIR000-248, 1988.

APPENDIX 'A'

Equations of motion of Pitch-Plane model of the bus

Six coupled second order differential equations describing the ride dynamic behavior of the candidate urban bus are expressed in the following matrix form:

$$M\ddot{Z} + C\dot{Z} + KZ = K_t Z_t + C_t \dot{Z}_t$$

where,

M Mass matrix

C Damping coefficient matrix

K Stiffness matrix

C_t Tire damping coefficient matrix

K_t Tire Stiffness matrix

$$\ddot{Z} = \begin{bmatrix} \ddot{z}_b \\ \ddot{\theta}_b \\ \ddot{z}_f \\ \ddot{\theta}_f \\ \ddot{z}_r \\ \ddot{\theta}_r \end{bmatrix} \qquad \dot{Z} = \begin{bmatrix} \dot{z}_b \\ \dot{\theta}_b \\ \dot{z}_f \\ \dot{\theta}_f \\ \dot{z}_r \\ \dot{\theta}_r \end{bmatrix} \qquad Z = \begin{bmatrix} z_b \\ \theta_b \\ z_f \\ \theta_f \\ z_r \\ \theta_r \end{bmatrix} \qquad Z_t = \begin{bmatrix} z_{tf} \\ z_{tr} \end{bmatrix} \qquad \dot{Z}_t = \begin{bmatrix} \dot{z}_{tf} \\ \dot{z}_{tr} \end{bmatrix}$$

and

$$K_t = 2. \begin{bmatrix} 0 & 0 \\ 0 & 0 \\ K_{tf} & 0 \\ 0 & 0 \\ 0 & 2.K_{tr} \\ 0 & 0 \end{bmatrix}, \qquad C_t = 2. \begin{bmatrix} 0 & 0 \\ 0 & 0 \\ C_{tf} & 0 \\ 0 & 0 \\ 0 & 2.C_{tr} \\ 0 & 0 \end{bmatrix}$$

Let a $= \sin\alpha$; $b = \sin^2\alpha$; $c = \cos\alpha$; and $\alpha = 1.5182$ rad;

$$
C = 2.\begin{bmatrix}
C_{af}b + C_{ar1} + C_{ar2} & C_{af}[l_{bfo}a - (h_{bcg} - h_{bd})c]a - l_{br1}C_{ar1} - l_{br2c}C_{ar2} & \cdots \\
C_{af}a\left[l_{bfo}a - c(h_{bcg} - h_{bd})\right] - C_{ar1}l_{br1} - C_{ar2}l_{br2c} & C_{af}(l_{bfo}\sin\alpha - (h_{bcg} - h_{bd})\cos\alpha)^2 + l_{br1}^2 C_{ar1} + l_{br2c}C_{ar2} & \cdots \\
-C_{af}b & -C_{af}(l_{bfo}a - (h_{bcg} - h_{bd})c)a & \cdots \\
-aC_{af}(al_{afo} + c(h_{af} - h_{fcg})) & -C_{af}(l_{bfo}a - (h_{bcg} - h_{bd})c)(al_{afo} + c(h_{af} - h_{fcg})) & \cdots \\
-C_{ar1} - C_{ar2} & l_{br1}C_{ar1} + l_{br2c}C_{ar2} & \cdots \\
-l_{ar1}C_{ar1} + l_{ar2c}C_{ar2} & l_{ar1}l_{br1}C_{ar1} - l_{ar2c}l_{br2c}C_{ar2} & \cdots
\end{bmatrix}
$$

$$
\begin{bmatrix}
\cdots & C_{af}b & -aC_{af}[l_{afo}a + (h_{af} - h_{fcg})c] & \cdots \\
\cdots & C_{af}a\left[l_{bfo}a - c(h_{bcg} - h_{bd})\right] & -C_{af}\left[al_{afo} + (h_{af} - h_{fcg})c\right]^2\left[al_{bfo} - c(h_{bcg} - h_{bd})\right] & \cdots \\
\cdots & C_{af}b + C_{tf} & -C_{af}(l_{afo}a + (h_{af} - h_{fcg})c)a & \cdots \\
\cdots & C_{af}a(l_{afo}a + c(h_{af} - h_{fcg})) & C_{af}(l_{afo}a + (h_{af} - h_{fcg})c)^2 & \cdots \\
\cdots & 0 & 0 & \cdots \\
\cdots & 0 & 0 & \cdots
\end{bmatrix}
$$

$$
\begin{bmatrix}
\cdots & -C_{ar1} - C_{ar2} & -C_{ar1}l_{ar1} + C_{ar2}l_{ar2} \\
\cdots & C_{ar1}l_{br1} + C_{ar2}l_{br2c} & C_{ar1}l_{ar1}l_{br1} - l_{ar2c}l_{br2c}C_{ar2} \\
\cdots & 0 & 0 \\
\cdots & 0 & 0 \\
\cdots & C_{ar1} + C_{ar2} + 2C_{tr} & l_{ar1}C_{ar1} - l_{ar2}C_{ar2} \\
\cdots & C_{ar1}l_{ar1} - C_{ar2}l_{ar2c} & l_{ar1}^2 C_{ar1} + l_{ar2c}^2 C_{ar2}
\end{bmatrix}
$$

$$K = 2.\begin{bmatrix} K_{af1}+K_{af2}+K_{ar1}+K_{ar2} & K_{af1}l_{bf1}+K_{af2}l_{bf2}-K_{ar1}l_{br1}-K_{ar2}l_{br2k} & \cdots \\ K_{af1}l_{bf1}+K_{af2}l_{bf2}-K_{ar1}l_{br1}-K_{ar2}l_{br2k} & K_{af1}l_{bf1}^2+K_{af2}l_{bf2}^2+K_{ar1}l_{br1}^2+K_{ar2}l_{br2k}^2 & \cdots \\ -K_{af1}-K_{af2} & -K_{af1}l_{bf1}-K_{af2}l_{bf2} & \cdots \\ K_{af1}l_{af1}-K_{af2}l_{af2} & K_{af1}l_{af1}l_{bf1}-K_{af2}l_{af2}l_{bf2} & \cdots \\ -K_{ar1}-K_{ar2} & K_{ar1}l_{br1}+K_{ar2}l_{br2k} & \cdots \\ -K_{ar1}l_{ar1}+K_{ar2}l_{ar2k} & K_{ar1}l_{ar1}l_{br1}-K_{ar2}l_{ar2k}l_{br2k} & \cdots \end{bmatrix}$$

$$\begin{bmatrix} \cdots & -K_{af1}-K_{af2} & K_{af1}l_{af1}-K_{af2}l_{af2} & -K_{ar1}-K_{ar2} & -l_{ar1}K_{ar1}+l_{ar2}K_{ar2} \\ \cdots & -K_{af1}l_{af1}l_{bf1}-K_{af2}l_{af2}l_{bf2} & K_{af1}l_{af1}l_{bf1}-K_{af2}l_{af2}l_{bf2} & K_{ar1}l_{br1}+K_{ar2}l_{br2} & K_{ar1}l_{ar1}l_{br1}-K_{ar2}l_{ar2}l_{br2} \\ \cdots & K_{af1}+K_{af2}+K_{tf} & -K_{af1}l_{af1}+K_{af2}l_{af2} & 0 & 0 \\ \cdots & -l_{af1}K_{af1}+K_{af2}l_{af2} & K_{af1}l_{af1}^2+K_{af2}l_{af2}^2 & 0 & 0 \\ \cdots & 0 & 0 & K_{ar1}+K_{ar2}+2K_{tr} & K_{ar1}l_{ar1}-K_{ar2}l_{ar2} \\ \cdots & 0 & 0 & K_{ar1}l_{ar1}-K_{ar2}l_{ar2} & K_{ar1}l_{ar1}^2+K_{ar2}l_{ar2}^2 \end{bmatrix}$$

$$M = \begin{bmatrix} m_b & 0 & 0 & 0 & 0 & 0 \\ 0 & I_b & 0 & 0 & 0 & 0 \\ 0 & 0 & m_f & 0 & 0 & 0 \\ 0 & 0 & 0 & I_f & 0 & 0 \\ 0 & 0 & 0 & 0 & m_r & 0 \\ 0 & 0 & 0 & 0 & 0 & I_r \end{bmatrix}$$